Integrating Demand-Side Resources into the Electric Grid: Economic and Environmental Considerations

Submitted in partial fulfillment of the requirements for

the degree of

Doctor of Philosophy

in

Engineering and Public Policy

Michael J. Fisher

B.S., Economics, University of Pennsylvania
B.A.S., Systems Engineering, University of Pennsylvania

Carnegie Mellon University
Pittsburgh, PA

December, 2017

Acknowledgements

I want to thank Jay Apt, my advisor and committee chair, who has provided years of careful guidance, well-timed encouragement, and just the right amount of prodding. I also want to thank the members of my committee – Granger Morgan, Jay Whitacre, and Mario Berges have provided invaluable advice in the completion of this dissertation.

Most of all I would like to thank my wife, Molly, for her support and my sons Aaron and Eli for the motivation to finish this dissertation in a timely manner.

This work was supported in part by grants from the Richard King Mellon Foundation, the Electric Power Research Institute, and the Carnegie Mellon Electricity Industry Center. This research was also supported in part by Carnegie Mellon's Pugh Fellowship. Portions of this research used the Extreme Science and Engineering Discovery Environment (XSEDE), which is supported by National Science Foundation grant number ACI-1053575.

Abstract

Demand-side resources are taking an increasingly prominent role in providing essential grid services once provided by thermal power plants. This thesis considers the economic feasibility and environmental effects of integrating demand-side resources into the electric grid with consideration given to the diversity of market and environmental conditions that can affect their behavior.

Chapter 2 explores the private economics and system-level carbon dioxide reduction when using demand response for spinning reserve. Steady end uses like lighting are more than twice as profitable as seasonal end uses because spinning reserve is needed year-round. Avoided carbon emission damages from using demand response instead of fossil fuel generation for spinning reserve are sufficient to justify incentives for demand response resources.

Chapter 3 quantifies the system-level net emissions rate and private economics of behind-the-meter energy storage. Net emission rates are lower than marginal emission rates for power plants and in-line with estimates of net emission rates from grid-level storage. The economics are favorable for many buildings in regions with high demand charges like California and New York, even without subsidies. Future penetration into regions with average charges like Pennsylvania will depend greatly on installation cost reductions and wholesale prices for ancillary services.

Chapter 4 outlines a novel econometric model to quantify potential revenues from energy storage that reduces demand charges. The model is based on a novel predictive metric that is derived from the building's load profile. Normalized revenue estimates are independent of the

power capacity of the battery holding other performance characteristics equal, which can be used to calculate the profit-maximizing storage size.

Chapter 5 analyzes the economic feasibility of flow batteries in the commercial and industrial market. Flow batteries at a 4-hour duration must be less expensive on a dollar per installed kWh basis, often by 20-30%, to break even with shorter duration li-ion or lead-acid despite allowing for deeper depth of discharge and superior cycle life. These results are robust to assumptions of tariff rates, battery round-trip efficiencies, amount of solar generation and whether the battery can participate in the wholesale energy and ancillary services markets.

Table of Contents

List of Tables

List of Figures

Chapter 1: Overview and Motivation

Advances in information technology at the turn of the 21st century have hastened the rise of distributed, small electric resources by allowing for real-time control. At the same time, technological and logistical advancements in manufacturing provided by a globalizing economy have made many of these resources cost effective even at small scale; for example, solar panels and electrochemical batteries have recently seen significant cost declines [1,2]. Many utilities, such as those in New York [3], Illinois [4], and California [5], anticipate a time in the future where their role is redefined to act primarily as a gatekeeper for consumers to transact with one another.

These demand-side resources, so called for their typical location on the customer side of the utility meter, are taking an increasingly prominent role in providing essential grid services once provided by thermal power plants. In some regions of the U.S., peaking capacity and even fast-response services like spinning reserve and frequency regulation are routinely provided by demand-side resources. Recognizing the benefits of resource diversity both in terms of economics and reliability, the federal government has policies in place to encourage demand-side resources in both the retail and wholesale electricity market. The Energy Policy Act of 2005 specifically instructed the Secretary of Energy to quantify the national benefits of demand response (DR) and make recommendations for increasing DR penetration [6]. The Federal Energy Regulatory Commission (FERC) has instituted orders 745 [7] and 755 [8] that encourage wholesale market participation of demand response and energy storage, respectively, by regulating how these resources are compensated. Many states have also legislated goals for demand-side resources. Energy storage mandates have been set in California [9], New York [10], and Massachusetts [11].

However, policies and regulation may not affect all resources in the same way, especially within the fragmented market design of the U.S. electricity system. Different geographical regions, end-uses, and technologies may behave differently under the same regulatory scheme. The research discussed in this thesis considers the economic feasibility and environmental effects of integrating demand-side resources with consideration given to the diversity of market and environmental conditions that can affect their behavior.

Chapter 2 explores the private economics and system-level carbon dioxide reduction when using demand response for spinning reserve. Demand response (DR) for spinning reserve may be appropriate for customers whose operational constraints preclude participation in energy and capacity DR programs. Using data from California, I examine the business case across multiple customer end uses and business segments. With average annual revenue of ~$35/kW, steady end uses (e.g., lighting) are more than twice as profitable as seasonal end uses (e.g., cooling) because spinning reserve is needed year-round. Total costs for participation would need to be under $250/kW for many end uses and business segments to have payback periods less than 5 years, which is plausible given equipment cost data from California's Automated Demand Response programs. Avoided carbon emission damages from using DR instead of fossil fuel generation for spinning reserve could justify incentives for DR resources.

Chapter 3 quantifies the system-level net emissions rate and private economics of behind-the-meter energy storage. Behind-the-meter (BTM) electric storage can help customers reduce energy and demand charges, as well as provide grid services like spinning reserve and frequency regulation. I analyze BTM storage without co-located generation under different tariff conditions, battery characteristics, and ownership scenarios using metered load for several hundred commercial and industrial customers. Net emission rates are lower than marginal

emission rates for power plants and in-line with estimates of emission rates from grid-level storage. Emission rates are driven primarily by energy losses, not by the difference between marginal emission rates during battery charging and discharging. Economics are favorable for many buildings in regions with high demand charges like California and New York, even without subsidies. Future penetration into regions with average charges (e.g. Pennsylvania) will depend greatly on installation cost reductions and wholesale prices for ancillary services.

Chapter 4 outlines a novel econometric model to quantify potential revenues from energy storage reducing customer demand charges. The model is intended for utilities and other third-party storage providers who do not have the computing or human resources to build a complicated optimization model. The model is based on a novel predictive metric that is derived from the building's load profile. While my model is easier to implement, it is somewhat less accurate than an optimization model, and I quantify this added uncertainty. During model fitting, I discovered that the revenue estimates generated are independent of the power capacity of the battery if the maximum power-to-energy ratio of the storage is held constant. This effect can be used to calculate the profit-maximizing storage size, which I explore in a case study.

Finally, Chapter 5 analyzes the economic feasibility of flow batteries in the commercial and industrial market. Advanced lead-acid, lithium-ion, and flow batteries have a wide range of performance characteristics, so I investigate their effect on profitability across many commercial building and solar load profiles while applying different retail and wholesale market conditions. My analysis indicates that flow batteries are uncompetitive with li-ion and lead-acid batteries in the commercial and industrial market. Flow batteries at a 4-hour duration must be less expensive on a dollar per installed kWh basis, often by 20-30%, to break even with shorter duration li-ion or lead-acid despite allowing for deeper depth of discharge and superior cycle life. My results are

robust to assumptions of tariff rates, battery round-trip efficiencies, amount of solar generation and whether the battery can participate in the wholesale energy and ancillary services markets.

References

[1] B. Nykvist, M. Nilsson, Rapidly falling costs of battery packs for electric vehicles, Nat. Clim. Chang. 5 (2015) 329–332. doi:10.1038/nclimate2564.

[2] R. Fu, D. Chung, T. Lowder, D. Feldman, K. Ardani, R. Margolis, U.S. Solar Photovoltaic System Cost Benchmark: Q1 2016, Golden, CO, 2016. http://www.nrel.gov/docs/fy16osti/66532.pdf.

[3] NY DPS - Reforming the Energy Vision, (2017). http://www3.dps.ny.gov/W/PSCWeb.nsf/All/CC4F2EFA3A23551585257DEA007DCFE2?OpenDocument (accessed March 7, 2017).

[4] R. Walton, Illinois launches "NextGrid" utility of the future study, (2017). http://www.utilitydive.com/news/illinois-launches-nextgrid-utility-of-the-future-study/438716/ (accessed February 7, 2017).

[5] J. St. John, Southern California Edison's Grand Software Plan Is a System of Systems at the Grid Edge, (2016). https://www.greentechmedia.com/articles/read/Southern-California-Edisons-Grand-Software-Plan-is-a-System-of-Systems-at (accessed March 7, 2017).

[6] US DOE, Benefits of Demand Response in Electricity Markets and Recommendations for Achieving Them, 2006. https://emp.lbl.gov/sites/all/files/report-lbnl-1252d.pdf.

[7] Demand Response Compensation in Organized Wholesale Energy Markets, 2011. https://www.ferc.gov/EventCalendar/Files/20110315105757-RM10-17-000.pdf.

[8] Frequency Regulation Compensation in the Organized Wholesale Power Markets, 2011. https://www.ferc.gov/whats-new/comm-meet/2011/102011/E-28.pdf.

[9] Decision Adopting Energy Storage Procurement Framework and Design Program, CPUC, 2013. http://docs.cpuc.ca.gov/PublishedDocs/Published/G000/M078/K912/78912194.PDF.

[10] J. Spector, New York State Lawmakers Pass Energy Storage Target, Await Governor's Signature, Greentech Media. (2017). https://www.greentechmedia.com/articles/read/new-york-state-lawmakers-pass-energy-storage-target (accessed July 13, 2017).

[11] Energy Storage Initiative (ESI), Massachusetts Energy Environ. Aff. (2017). http://www.mass.gov/eea/energy-utilities-clean-tech/renewable-energy/energy-storage-initiative/ (accessed July 13, 2017).

Chapter 2: The Economics of Commercial Demand Response for Spinning Reserve

Abstract

Demand response (DR) for spinning reserve may be appropriate for customers whose operational constraints preclude participation in energy and capacity DR programs. We investigate the private business case of an aggregator providing spinning reserve in California across customer end uses and business segments. Revenues are calculated using end use level hourly load profiles. With average annual revenue of ~$35/kW, steady end uses (e.g., lighting) are more than twice as profitable as seasonal end uses (e.g., cooling) because spinning reserve is needed year-round. Business segments with longer operating hours, such as groceries or lodging, have more revenue potential. Total costs for participation would need to be under $250/kW for many end uses and business segments to have payback periods less than 5 years, which is plausible given equipment cost data from California's Automated Demand Response programs. Avoided carbon emission damages from using DR instead of fossil fuel generation for spinning reserve could justify incentives for DR resources.

This paper was published as Fisher, M.; Apt, J.; Sowell, F. The economics of commercial demand response for spinning reserve. *Energy Systems*. 2017, DOI: 10.1007/s12667-017-0236-x.

2.1 Introduction

Load that can respond to price or reliability signals, referred to as "demand response" (DR), lowers energy demand during periods of high prices or the need for generation capacity during periods of high load [1]; grid operators are now exploring the use of DR for ancillary services [2-5].

One ancillary service is spinning reserve. This type of reserve is also referred to as synchronous reserve and is often considered under the umbrella of contingency reserves, which include spinning and non-spinning reserve. Spinning reserves have traditionally been generators running at idle power and synchronized to the phase of the 50 or 60 Hz grid; they are able to provide rapid increases in power in response to an unexpected contingency event (e.g., loss of a transmission line or generating facility) [6]. The operational requirements vary across jurisdictions, but generally require the ability to increase generation in a short time, typically 10 minutes [7], and to maintain that response for a minimum amount of time (typically 30 to 60 minutes) [8].

The intrinsic characteristics of DR are a natural match to the requirements of spinning reserve resources. Load resources can provide higher ramp rates [3,9] at lower costs [10] than traditional generation. Furthermore, a large number of loads that are individually less reliable than a generator may provide aggregate reliability in excess of that provided by a few large generators [2,3]. The timescale on which spinning reserve operates is well served by DR because the average event lasts only 10-20 minutes [3]. Moreover, this short period is attractive to DR participants because it avoids customer fatigue and business operations changes required by the 1 to 8 hour interruptions [11] seen in energy or capacity events.

Wholesale markets in the US Mid-Atlantic, New York, Texas, and the Mid-West all allow DR to participate in spinning reserve markets. However, current Western Electricity Coordinating Council's (WECC) rules implicitly prevent the California Independent System Operator (CAISO) from allowing DR in the spinning reserve market, but this is a purely regulatory barrier. WECC rules require immediate and automatic response to system frequency to participate in spinning reserve [12] while DR typically requires a signal from an outside operator to initiate response. For our analysis we assume this barrier is removed and regulators permit DR in the wholesale environment.

The open question is whether market prices are sufficient to attract participation given time-varying resource availability and the magnitude of implementation costs. Previous studies have examined the use of DR for ancillary services and the economics of participation. Kirby [2] and Mathieu et al. [13] consider residential air-conditioning loads in New York and California, respectively. They characterized resource size and calculated potential revenue assuming time-invariant resource availability. MacDonald et al. [14] reviewed market clearing prices and participation requirements across the U.S., though they do not discuss potential resource revenue and assume the demand resource is time-invariant. MacDonald et al. [15] examined commercial building HVAC and lighting loads but did not discuss implementation costs or match time-varying resource availability with market clearing prices. Ma et al. [16] and Hummon et al. [17] examined the market dynamics of the western interconnection using unit commitment and economic dispatch models with increased flexible demand resources for energy and ancillary services. They did not consider the costs to enable DR for these services.

To our knowledge, no previous research has compared the costs and potential revenues of using DR for ancillary services while capturing the time-varying nature of resource availability

across many end uses and customer segments. The 2009 PG&E Participating Load Pilot [18] implemented DR for non-spinning reserve, and thus faced the true operational costs and potential revenues, but included only 3 participants in the study. We take a more comprehensive view using data from over 2,700 buildings in California. We examine the economics across geographic regions, building segments, and end uses within California using econometric models. California is used as an example because its varied load types and competitive market operations provide an ideal environment in which to examine the business case for DR and because the results may influence DR policy in WECC. We examine DR for commercial load, which represents approximately 50% of California's load [19]. This work adds to the existing literature by determining which commercial demand response applications are both profitable and significant to the grid, and making a first-order estimate of their environmental consequences.

We focus on the case where DR participates solely in spinning reserve (not in energy or capacity). Customers may want to participate only in spinning reserve because of the low frequency and short duration of events. Indeed, customers accounting for approximately 50% of the MW signed up through the California Automated Demand Response program participate in a voluntary energy reduction program [20]. This suggests that these customers do not find the mandatory energy curtailment required by capacity events attractive. This work does not discuss frequency regulation (another ancillary service) because this application of commercial DR remains largely in its infancy [9] and the installation costs are highly scenario specific.

There is a growing body of literature on the optimal control of demand-side resources in market and microgrid environments [21]. Here we assume the control algorithms and equipment

are sufficient to achieve the load reductions determined by our models and instead focus our analysis on the resource and the economics.

We find that steady end uses (e.g., lighting) are better able to make a profit than are seasonal end uses (e.g., cooling) because, unlike a capacity resource, spinning reserve is needed throughout the year. Payback periods of 5 years or less are plausible in certain niche applications given data on equipment costs, but longer paybacks for many resources may discourage widespread participation. Therefore, we investigate if the damages from carbon emissions avoided by procuring DR in spinning reserve are sufficient to justify monetary incentives to encourage greater DR participation.

Section 2 describes our methods and data used to characterize the implementation costs and calculate potential revenue. Section 3 presents and discusses the results of our analysis. Section 4 estimates avoided carbon emissions damages by using DR for spinning reserve and Section 5 presents our conclusions.

2.2 Methods and Data

We consider a DR aggregator who contracts with individual facilities to procure DR. These facilities receive compensation for agreeing to reduce load when called upon. In turn, the aggregator sells the cumulative DR capability to a utility or grid operator. We take the perspective of an aggregator, not an individual facility owner, because aggregators are more likely than individual facilities to have the resources necessary for sophisticated forecasting models and the complex administrative requirements necessary to participate in these markets.

Aggregators are most likely to target large commercial participants. Overhead costs are lower for these customers as administrative and marketing costs often scale per customer rather

than per kW. Large customers are also more likely to participate in DR programs [22] and have the internal building controls required for automated response.

Aggregators earn revenue based on the market clearing price and magnitude of load response, and incur costs to enable spinning reserve in participant facilities. Revenue is calculated by matching hourly DR resource availability with market clearing prices across geographic zones, building segments, and end uses. Detailed cost data are not available at the end-use or business segment level; we therefore treat costs parametrically to determine the level at which acceptable payback periods are achieved. We compare these cost levels to general cost estimates from the literature and from a cost database for an automated DR program in California.

We do not model the effects of a call for spinning reserve on energy cost. This eliminates the uncertainty inherent in modelling events with probabilistic frequency and duration. A first-order analysis shows that we are ignoring less than $5/kW-yr in potential revenue gains from energy reductions, which would not affect the conclusions of our work. Consider the case of an end use with no energy rebound after a spinning reserve event (e.g. lighting). End uses with energy rebound (e.g. cooling) will have less change in their total energy consumption. Assuming a fairly large number of events (30), long-duration events (1 hour), large energy reductions during all events (normalized value of 1 kW), and an average energy cost of $0.15/kWh, we can calculate that in this "worst-case" scenario we would be ignoring $4.50/kW-year of decreased energy costs.

2.2.1 Potential Revenue Across End Uses, Business Segments, and Geographic Location

To calculate potential revenue, we gathered hourly commercial load data that have been standardized to typical weather conditions and disaggregated by geographic zone, business

segment, and end use. Using models of these profiles, we created new profiles specifically for the period 2011-2013. Normalized hourly profiles were then matched with hourly market clearing prices to calculate potential revenue.

By using normalized load profiles to represent DR resource availability, we assume that DR resource availability for reserves is proportional to the load of that particular end use at that particular time. For energy or capacity events, which can last from 1 to 8 hours in California [11], this may not be an appropriate assumption. Commercial customers may not want a portion of their electrical service interrupted for that period of time due to operational constraints. However, spinning reserve events typically last for only 10-20 minutes, and thus customers can shed larger percentages of their load without suffering major interruptions to business operations. Data from PJM, the only region to publish hourly market clearing resource amounts for DR in spinning reserve, support this assumption (see Appendix A for discussion of this topic).

2.2.1.1 Load Disaggregation

One of the only large scale studies to quantify end use level demand across a broad geographic area is the 2006 California Commercial End Use Survey (CEUS) [23]. The CEUS collected metered data from a stratified sample of approximately 2,700 buildings in order to create hourly end use level load profiles. The sample was stratified across 12 geographic zones and 12 building segments (Table 2-1). For each building in the survey, a simulation model that disaggregates whole-facility load into 13 end uses was built in a DOE-2.2 energy simulation environment. Simulation results were calibrated to actual consumption and weather data to ensure the model was accurate. Once calibrated, the building model was run on a new standardized weather set meant to represent a typical weather year in California. Buildings within each sample strata were aggregated to produce weighted average hourly profiles. 1,872

unique hourly profiles were created across all geographic zones, building segments, and end uses.

Table 2-1: Building Segments and End Uses in CEUS

Building Segments	
College	School
Grocery	Restaurant
Health	Small Office
Lodging	Large Office
Miscellaneous	Refrigerated Warehouse
Retail	Un-refrigerated Warehouse
End-Uses	
Heating	Interior Lighting
Cooling	Exterior Lighting
Ventilation	Miscellaneous
Refrigeration	Office Equipment
Hot Water	Motors
Cooking	Process
	Air Compressor

Certain end uses from CEUS were removed from our consideration because they are not appropriate for spinning reserve. For example, exterior lighting is not a good candidate for spinning reserve because reducing exterior lighting at night may violate building codes. This left 981 profiles. The list of removed end uses and business segments (along with a reason for removal) is contained in Table 2-2.

Table 2-2: End Uses / Segments Removed in this Study

End-Uses Removed	**Reason for Removal**
Exterior Lighting	Code issues
Process	Business process constraints
Cooking	Business process constraints
Office Equipment	Business process constraints
Miscellaneous	Unknown resource type
Segments Removed	**Reason for Removal**
Small Office	Does not match cost data

2.2.1.2 Load Modelling

To convert the standardized profiles from CEUS to 2011-2013 profiles, we first separated end uses into weather and non-weather dependent categories. Non weather-dependent end uses were converted using a day-matching method. Consumption values for each hour of the day in each month were averaged, treating weekdays and weekends separately. While heating would normally be considered a weather-dependent end use, regression modelling was not successful in capturing the variation of heating profiles. Therefore, the day-matching method was used for all heating profiles.

Regression models with ARMA errors were used for weather-dependent end uses (cooling and ventilation). Via 10-fold cross-validation, we explored over 20 model specifications. The final model (Equation 1) showed the lowest average out-of-sample error across all cooling and ventilation profiles. We also investigated using lagged weather variables. Due to thermal mass, buildings often show a lagged response to outdoor temperature and humidity conditions. However, current weather conditions showed better out-of-sample prediction error than lagged weather conditions for the standardized CEUS load profiles. We believe this is an artifact of the modeling process used in the CEUS project and does not reflect what one would find if raw metered data was used.

All models exhibited significant autocorrelation in the residuals. To facilitate more accurate prediction, we chose to model the error using time-series (ARMA) parameters. A necessary condition for parameter estimation using time-series models is homoscedasticity. However, a plot of the residuals for most load profiles revealed two distinct periods during the year for which residual variance was uneven (summer vs. winter). We thus split the annual standardized models into three periods: the first winter period (Jan-Apr), summer (May-October), and last winter

period (Nov-Dec). The selection of periods for boundary months (e.g. April) was performed by examining how closely the residual variance of the month compares to other months when it was included in the winter or summer model.

The same ARMA model specification for the error term was used across all load profiles because it was successful in removing most of the autocorrelation in residuals across load profiles. We attempted to include parameters at other lags but often found that they did not reduce the Bayesian Information Criteria (BIC) and/or the coefficient estimates were not statistically significant.

$$\ln(kW_t) = \alpha + \sum_{d=Wkdy}^{Wknd} \sum_{h=1}^{24} \begin{bmatrix} \beta_{Temp}^{d,h} \mathrm{I}^d \mathrm{I}^h Temp_t \\ +\beta_{Temp^2}^{d,h} \mathrm{I}^d \mathrm{I}^h Temp_t^2 \\ +\beta_{T.RH}^{d,h} \mathrm{I}^d \mathrm{I}^h Temp_t RelH_t \end{bmatrix} + \eta_t \quad (1)$$

where:

$$(1 - \phi_1 \mathrm{B}^1 - \phi_{24} \mathrm{B}^{24})\eta_t = (1 + \theta_1 \mathrm{B}^1)\epsilon_t$$

Table 2-3: Equation 1 Variable Descriptions

Variable	Description
kW_t	Average kilowatt consumption in hour of the year t
I^d,I^h	Indicator variables for day type d (weekday/weekend) and hour of day h
$Temp_t$	Temperature (°F) in hour t
$RelH_t$	Relative humidity in hour t
$\boldsymbol{\beta}_{\boldsymbol{x}}^{\boldsymbol{d,h}}$	Regression coefficient for day type d and hour of day h for weather variable x (Temp, Temp^2, or Temp*RelH)
η_t	Error in hour t unexplained by exogenous weather variables
B	Backshift operator
$\boldsymbol{\theta}_i$	Coefficient for moving average term of lag i
$\boldsymbol{\phi}_i$	Coefficient for autoregressive term of lag i
$\boldsymbol{\varepsilon}_t$	Unexplained error in time t

Once the model coefficients were estimated for each load profile, predicting the 2011-2013 hypothetical load profiles was a 2-step process. Coefficients for exogenous weather variables were multiplied against actual hourly 2011-2013 weather data to form the base of the prediction. Next, 5,000 separate ARMA simulations were conducted using the time-series coefficients from each of the three period models (the length of the simulations was tailored for the period of the year). The simulated error at each time-step was independent and identically distributed (i.i.d.) and randomly drawn from a normal distribution with variance equal to the residual variance of the model. All simulations used a burn-in period of 50,000 iterations. The average path of the 5,000 simulations was added to the predictions from the exogenous variables to form the overall predicted load profile.

In using load data captured in 2002 to infer load profiles for 2011-2013, we assume the shape of the end use load profiles has not changed over time. Load shapes could change due to shifts in equipment stock (e.g. higher saturations of more efficient equipment) and equipment use patterns. However, commercial load has not grown in California since 2005 [19]. Load growth is not a perfect measure of changes in end use load profiles, but the authors believe it is reflective of a load environment that is in steady-state.

2.2.1.3 Normalization and Revenue Potential

Normalization of the load profiles was necessary to express our results in a standardized measure of size (per kW). Profiles were normalized to the average load during the top 50 hours in each year by temperature, which closely mirrors the method used to calculate peak kW for incentive payments in California's AutoDR program. Equation 2 displays the normalization calculation for each hour t in the profile.

$$kW_{norm,t} = \frac{kW_t}{average\left(\sum kW_{50\ hrs,2011}, \sum kW_{50\ hrs,2012}, \sum kW_{50\ hrs,2013}\right)} \quad (2)$$

The calculation of revenue was completed by matching the hourly normalized resource availability with the day-ahead market clearing price in that hour. Market clearing prices for spinning reserve are not the same across the entire CAISO region. CAISO has established separate procurement requirements for operating reserves in areas "north of path 26" (NP26) and "south of path 26" (SP26) to ensure that contingencies can be mitigated even in the case of congestion on the Path 26 transmission line. The Path 26 transmission line in central California roughly delineates the boundary between SCE and PG&E. This area is a bottleneck for power trying to flow between northern and southern California. Variations in generation mix and transmission network topology among the two regions lead to price differences. Prices for NP26 and SP26 were matched with the different forecasting zones from the CEUS. Table 2-4 details how the load forecasting zones (FCZ) were mapped to ancillary service zones (ACZ).

Table 2-4: Forecasting Zone Mapping to Ancillary Service Zone Partitions

FCZ in Service Zone "CAISO"	FCZ in Service Zone "SP26"
FCZ 1	FCZ 7
2	8
3	9
4	10
5	13
6	

In making this calculation we assume perfect forecasting of resource availability, which would tend to increase our revenue numbers. However, this did not affect the final conclusions of the study. We also assume that load resources are price-takers that do not affect the market clearing price. While ancillary service participants are worried that markets will saturate quickly and prices will collapse [24], as long as some traditional generation remains in the spinning

reserve market prices may not decrease significantly due to the payment of lost opportunity costs of energy production [5].

2.2.2 Costs

An aggregator would incur a number of costs in setting up a spinning reserve portfolio, including equipment installation for controls and automated response, telemetry for monitoring loads, equipment maintenance, participant incentives, program administration, forecasting, and CAISO administrative fees. The communications architecture of such a system in described in Figure 2-1. These expenditures would also allow participation in capacity/energy DR programs, or frequency regulation markets as control devices advance in sophistication, though in our analysis we assume end users face business constraints that prevent them from participating in energy/capacity programs.

Unfortunately, detailed cost information for this type of system across many types of loads/businesses does not exist. The closest program for which information is publicly available is PG&E's Participating Load Pilot [18]. It had only 3 participants and much of the cost for the program was spent on one-time startup costs. We were able to obtain generalized cost information for DR equipment installation (described in the next section) but cannot tie the data to specific end-uses or business types. Therefore, we treat the costs an aggregator would incur as a parametric variable in our results, reporting ranges that would provide a sufficient payback on invested capital. We use the generalized cost information on equipment installation to provide context for the reported cost ranges.

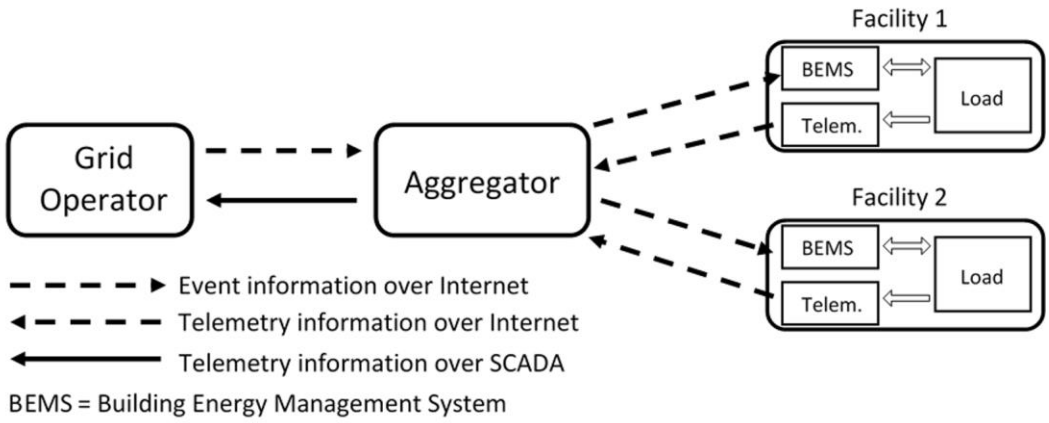

Figure 2-1: System communication architecture for loads participating in spinning reserve. Communication from the grid operator to the aggregator, and to and from the aggregator and the facility can take place over secure internet connections. Telemetry reporting from the aggregator to the grid operator must take place via a more demanding Supervisory Control and Data Acquisition (SCADA) protocol. Communication architecture design based on the OpenADR 2.0 standard (OpenADR Alliance 2014). Telemetry architecture from [25].

2.2.2.1 Equipment Cost for Event Communication and Automated Response

In order for DR to provide spinning reserve within the required 10 minutes, automated response is necessary. Personal notifications (email or phone) and manual changes to equipment operating parameters cannot guarantee 10-minute response. Automated response can be enabled by pre-programming DR strategies into control equipment so the response is implemented without human intervention.

California investor-owned utilities provide incentives for the installation and programming of such equipment through the Automated Demand Response (AutoDR) program. Salient features of the California AutoDR program are:

1. Designed for commercial/industrial customers with peak load >200 kW.

2. Requires participation in utility energy or capacity DR programs.

3. Incentives are capped at the minimum of 100% of total project cost or $300/kW of load response. These are one-time payments (not annual).

4. The amount of load response must be proven through a test event or actual performance history from energy or capacity events.

Incentive data were collected from Pacific Gas & Electric (PG&E) and Southern California Edison (SCE). Project-level incentive information from San Diego Gas & Electric and Sacramento Municipal Utility District was not available. See Appendix A for more information on the treatment of incentive data. Figure 2-2 displays the combined SCE and PG&E incentive information. The mean cost is approximately $180/kW.

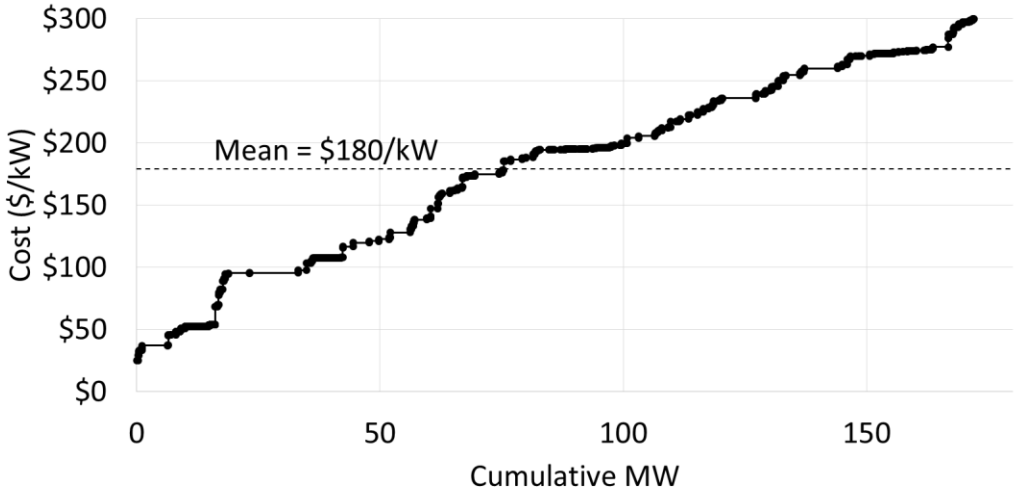

Figure 2-2: Incentives provided to install communications equipment, program and commission DR strategies. Note: incentive data includes commercial and industrial customers. Industrial customers could not be removed because the project database lacked identifying information. We do not believe that removing industrial customers would significantly affect the cost distribution as large projects were evenly spread across higher and lower $/kW values.

We assume participating commercial buildings have a building energy management system (BEMS) that can communicate with end use level equipment. The market share of BEMS in

California commercial buildings is approximately 60% for buildings with an average demand of 200kW [22].

An aggregator would also have to install telemetry at a participating building because it is required for participation in spinning reserve markets. Telemetry allows the grid operator to obtain real-time information on load characteristics, such as real and reactive power. Energy and capacity DR programs do not rely on telemetry for measurement and verification of load reductions – they use interval meter data that are already captured for billing purposes.

For small distributed resources like DR, the cost of telemetry is a significant obstacle to participation in ancillary service markets. Estimates of the cost of telemetry for a large commercial building are approximately $50,000-$80,000 [25]. Given the average load response in the AutoDR program, this cost would translate to over $200/kW. However, new designs have the potential to provide telemetry at much lower cost. Early tests show large commercial buildings could be outfitted with telemetry at an approximate cost of $50/kW of controlled load [25] or ¼ of the current cost estimate. We use the $50/kW estimate to provide context for our results.

2.3 Results

We find end uses with relatively constant load profiles throughout the year, such as lighting or refrigeration, are better suited for spinning reserve than seasonal end uses like cooling and heating. This is counter to the intuition behind traditional capacity-based DR programs that focus on seasonal end uses because they are highly correlated with the system peak demand. Spinning reserve, however, is needed at all times and is therefore best served by resources which are

available at all times. Figure 2-3 shows the results by end use and building segment combinations across all of the forecasting zones.

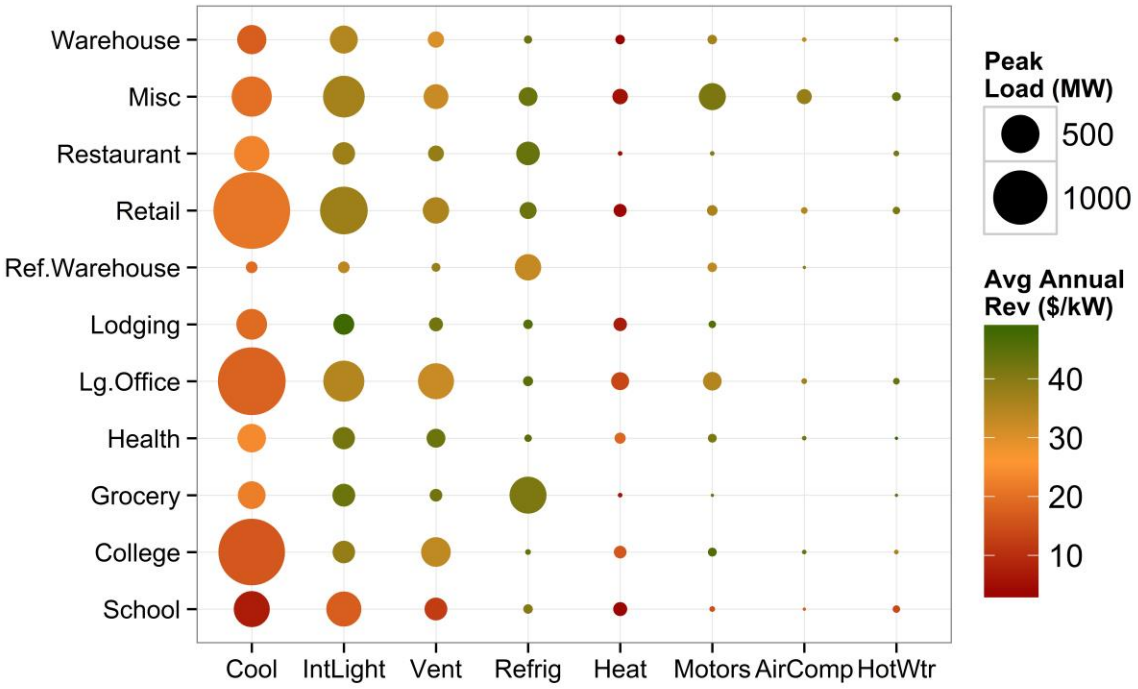

Figure 2-3: Average annual revenue for end use / building segment combinations. The area of the dot represents the total peak load for that combination across all forecasting zones. The shading of the dot corresponds to the average annual revenue potential. Average annual revenue is calculated as a weighted average across all zones, weighted by peak load.

While cooling is the largest end use by peak load in California, it nevertheless has very low revenue potential because of its seasonal nature. Interior lighting is a large end use and is well suited for spinning reserve, especially in building segments that operate on continuous schedules such as lodging. The school and college segments which have lower seasonal loads during capacity strained periods do especially poorly.

These revenue figures are next used to determine the maximum allowable cost at which an aggregator would find the simple payback of their investment to be 5 years or less. Simple payback can be calculated as the ratio of costs to annual revenue. The 5 year simple payback

threshold is important because many companies use simple payback as a metric for energy decisions and most of these companies use a threshold of 5 years or less [26]. Figure 2-4 shows the distribution of these maximum costs across (a) end uses and (b) business segments. When viewing the figure, if the reader imagines that the true cost to an aggregator was $200/kW, any point on a distribution below $200/kW would have a payback greater than 5 years. In general, higher maximum allowable costs represent those end uses / business segments that have higher revenue. The horizontal lines spanning the graphic show the low and high end of the cost distribution for communication and control equipment discussed in Section 2.2.2.

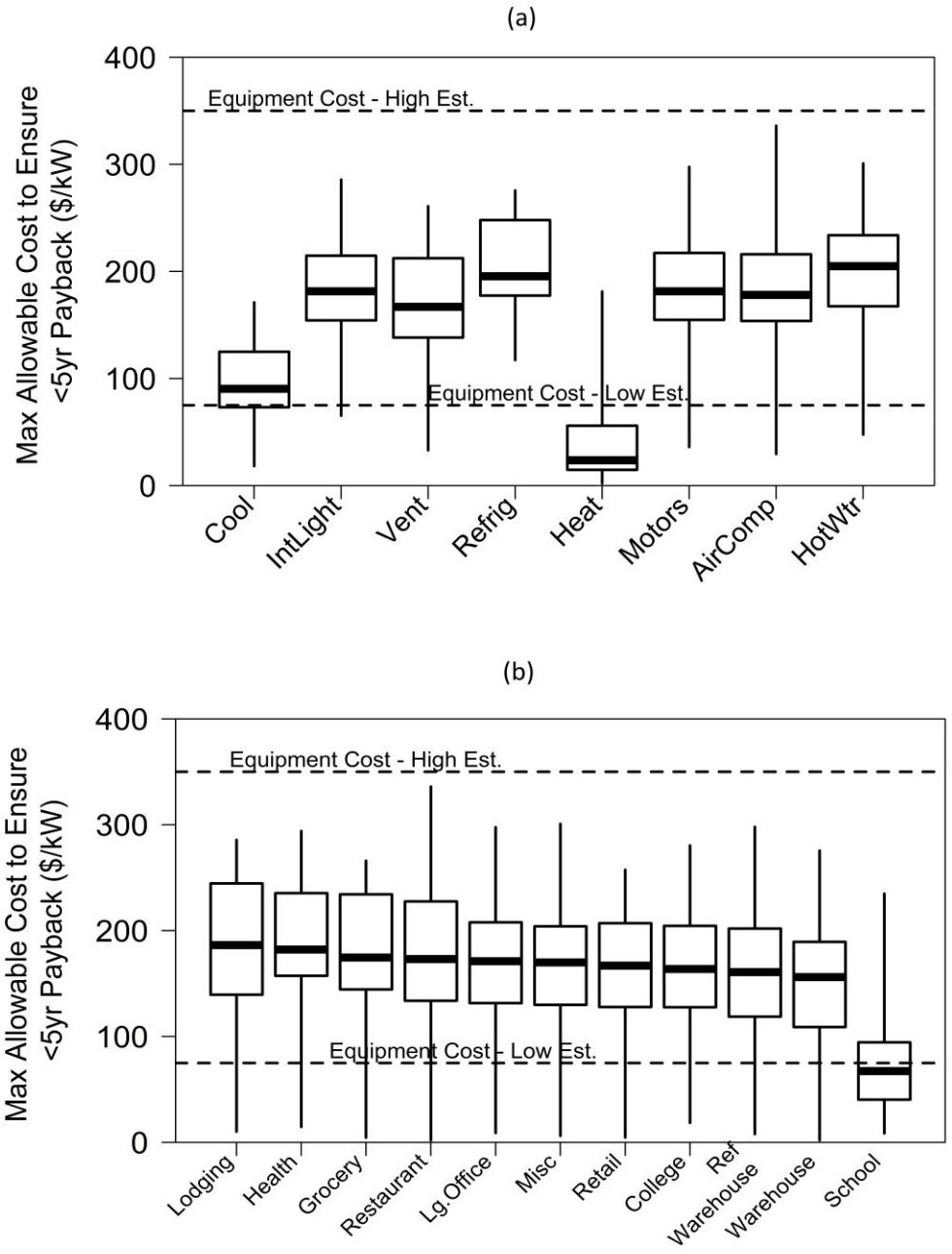

Figure 2-4: Distribution of maximum allowable costs ($/kW) incurred by an aggregator to keep payback periods under 5 years across (a) end uses and (b) business segments. Higher maximum allowable costs represent end uses / segments that have higher revenue. Horizontal lines spanning the figure represent the low and high estimate of equipment installation costs, including control equipment and telemetry (ignores other types of costs like participant incentives). Each combination of geographic zone, business segment and end use represents a single point within each distribution. The heavy horizontal line in the middle of each box marks the median. The range of the box represents the interquartile range. The whiskers extend to the extremes of the distribution.

For the majority of potential participants, total costs incurred by the aggregator would need to be below $250/kW to achieve a payback of 5 years or less, though the highest cost for any end use to achieve the 5 year threshold is $340/kW. The median cost for a 5 year payback across all end uses excluding cooling and heating is $173/kW. These are plausible maximum cost values given the distribution of equipment installation costs, though we should remind the reader that this does not include many other costs an aggregator would face (e.g., participant incentives). Thus we find that the business case probably exists to provide spinning reserve from pooled DR resources, though the aggregator would need to be selective in targeting participants.

We do not find important differences in revenue potential across geographic zones. The largest driver of difference across zones is the market price for spinning reserve; southern California (below the Path 26 transmission line) often has higher prices than northern California. Figure 2-5 shows price duration curves for northern and southern California.

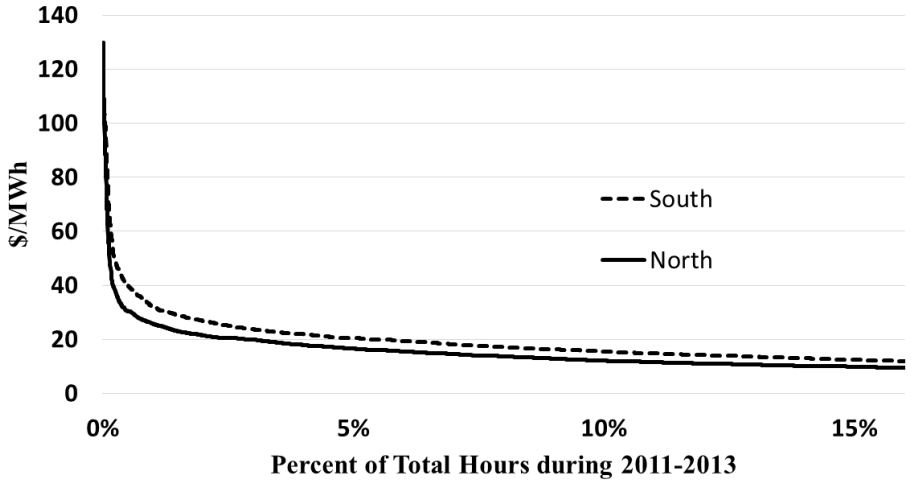

Figure 2-5: Partial price duration curves for California spinning reserve prices from 2011-2013. Prices are often higher in the southern California zone (below the Path 26 transmission line). Horizontal axis abbreviated for clarity.

2.4 Policy Implications – Avoided Carbon Emissions

We have shown that aggregators will have to be selective in targeting potential DR participants, possibly leaving a large amount of DR on the sidelines of the market. However, providing incentives to DR would improve economics and encourage participation. We now consider if such an incentive is justified by a market failure not currently captured in spinning reserve clearing prices: the damages associated with carbon dioxide (CO2) emissions from fossil fuel power generation. California already considers the social cost of carbon in their cost effectiveness tests for utility energy efficiency and DR programs [27].

To our knowledge, there has been no detailed study of the emissions avoided from DR participation in electricity markets for either energy or ancillary services. Studies of avoided emissions in reserve markets have mostly focused on renewable energy [28] or pumped hydroelectric power [29]. The most rigorous approach to this problem would make use of a dispatch model of the California grid to understand the quantity and type of fossil fuel power plants offset from DR and the duration of offset. Here we instead make a first-order estimate.

The procurement of spinning reserve is fundamentally an option to produce power, not an actual call for power. Marginal changes in the fuel mix of reserves that do not change the overall energy dispatch will not displace emissions, as nothing has physically changed on the grid. However, if enough DR is procured to offset the reserve provided by an entire plant, that plant can shut down. This assumes that the marginal plant used for reserves is online only because of the need to provide reserve. We adjust for this assumption in our calculations. The emissions saved would be the difference between the reduction from turning off the partly-loaded reserve plant and the increase of the base load plant that is now making up for the energy generation of the reserve plant.

To calculate emissions savings, it is thus important to understand the fuel types that typically provide spinning reserve and base load. The 2013 CAISO Annual Report on Market Issues and Performance [30] reports that hydro supplies approximately half of the spinning reserve in a typical year. Natural gas and imports supply approximately a quarter of this reserve each. Droughts and changing climate patterns, however, may reduce the potential for high-elevation hydropower production in California in the future [31]. Reduced hydropower energy production is typically offset by natural gas in California [32]. We assume that reduced spinning reserve from hydropower is also offset by natural gas.

Natural gas plants represent the majority of the available dispatchable generation in CAISO, hence the energy production from plants providing reserve that are offset by DR is likely assumed by other natural gas generation. We assume that all natural gas generation is performed by combined-cycle (NGCC) plants. In reality, some spinning reserve is provided by natural gas combustion turbines (NGCTs). NGCTs have higher heat rates than NGCC plants. Thus, ignoring NGCTs likely underestimates carbon savings. In this analysis, we focus just on the emissions and associated damages from CO2 and not from criteria pollutants (e.g., sulfur dioxide, nitrogen oxide, particulate matter). This first-order analysis does not consider the emissions savings during actual spinning reserve events, only the savings from a different economic dispatch of generation resources. However, criteria pollutant emissions savings during spinning reserve events may be significant. Nitrogen oxide ramping emissions from simple-cycle natural gas combustion turbines can be significantly higher than steady state emissions [34]. Thus during a spinning reserve event, demand response can offset much higher emissions from ramping natural gas plants than it does under normal dispatch conditions.

Social damages from CO2 are orders of magnitude larger than damages from criteria pollutants for natural gas plants. Assuming damages of $37 per tonne of CO2 [35] and emissions of 0.375 tonne of CO2 / MWh [36] for natural gas plants, we calculate damages of ~$14/MWh. From [37], we find damages from criteria pollutants emitted from natural gas plants on the order of $0.05/MWh.

The relationship between CO2 output and power generation is nearly linear for a NGCC plant [33], thus marginally unloading one plant and reloading another of the same type saves no CO2. But if one plant is able to be fully shut down, the CO2 saved is equal to the no-load emissions of that plant. To make a first-order estimate of the annual CO2 saved from procuring DR for spinning reserve we use Equation 3. The input assumptions are presented in Table 2-5. Total reserve was divided by the idle generating capacity of an average plant in order to calculate the number of plants shut down by procuring DR. We assume that there is enough DR to offset the reserve of natural gas plants that provide half the average annual spinning reserve requirement. This corresponds to a future scenario where the proportion of reserves provided by natural gas has increased due to falling hydro reserves.

$$Annual\ CO_2\ Savings = \frac{Total\ Reserve}{Idle} * Carbon_{no_{load}} * \%Reserve * 8{,}760 \quad (3)$$

Table 2-5: Variable Descriptions and Assumed Values for Equation 3

Variable (Units)	Description	Assumed Value	Range	
			Low Savings Scenario	High Savings Scenario
Total Reserve (MW)	The total MW of spinning reserve in CAISO offset by DR	500 MW (approx. half of average spin requirement)	250 MW[a]	750MW[b]
Idle (MW)	The amount of spinning reserve provided by each natural gas plant (idle generating capacity)	50 MW[c] (approx. 10-min ramp capability for 200MW combined-cycle turbine)	100MW[d]	40MW[e]
$Carbon_{no\_load}$ (Tonnes CO_2 / hr)	CO_2 emissions at no load	17.5 tonnes [33]	14 tonnes[f]	21 tonnes[g]
%Reserve (Unitless)	Percent of annual hours that system dispatch is reserve-constrained[h]	77%[i]	74%[j]	80%[k]
8,760 (Hours)	Number of hours in a year			

[a] Scenario where DR displaces current reserves from natural gas (~25% of requirement)
[b] Scenario where DR displaces current reserves from natural gas and hydro (~75% of requirement)
[c] Ramp rate of 2.5%/min [28]
[d] Ramp rate of 5%/min [38]
[e] Ramp rate of 2%/min (lower end of ramp rates shown in [34] Figure 4-13)
[f] 5% quantile of the true intercept of [33] Figure S4
[g] 95% quantile of the true intercept of [33] Figure S4
[h] Reserve-constrained means that the system dispatch was different from a hypothetical scenario where reserves are not required. Alternatively, a dispatch is *not* reserve-constrained if the removal of the reserve constraints from the system optimization problem does not change the overall dispatch. Reserve-constrained periods are those in which increased DR procurement would cause marginal reserve plants to shut down.
[i] Calculated from the average number of hours that spinning reserve prices are above the minimum value from 2011-2013. A reserve price at the minimum value reflects a system which is not reserve-constrained.
[j] Calculated from the low annual number of hours that spinning reserve prices are above the minimum value from 2011-2013.
[k] Calculated from the high annual number of hours that spinning reserve prices are above the minimum value from 2011-2013.

We estimate annual carbon savings at approximately one million metric tons (0.2 x 106 – 2.8 x 106 tonnes for the low and high scenarios, respectively). Avoided damages associated with carbon emission savings were calculated using two different values of carbon: (1) the social cost of carbon (SCC) computed by the United States government for emissions year 2010 under the

average 3% discount rate scenario ($37 in 2014 dollars) [35], and (2) the average 2014 market price for carbon under California's cap and trade system set up under AB32 ($12) [39]. The annual results are shown in Figure 2-6 relative to the up-front capital required to install telemetry on DR resources.

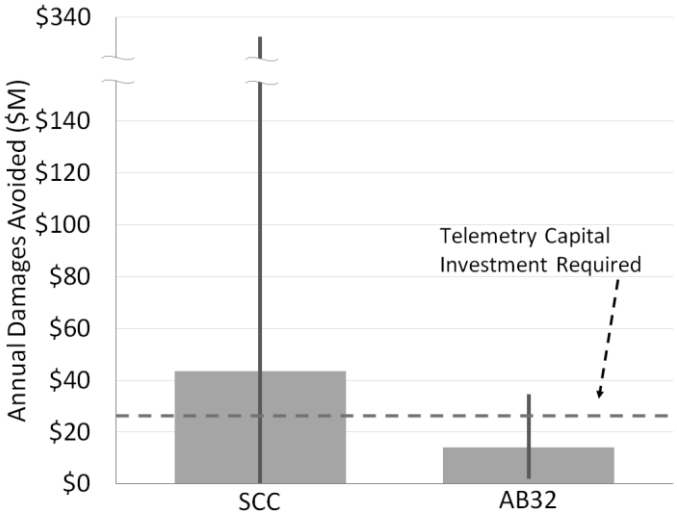

Figure 2-6: Damages avoided from carbon emission savings due to DR procurement in spinning reserve market. Uncertainty bars reflect 90% confidence interval for uncertainty in the value of damages per metric ton and the uncertainty in the estimated magnitude of carbon savings (low to high savings scenarios of Table 2-5). No correlation was assumed between the value of damages per metric ton and the savings scenario. Uncertainty in the value of damages per metric ton for SSC were derived from the distribution of carbon value per ton for the 3% discount rate for emission year 2010 [35]. Uncertainty in the value of damages per metric ton for AB32 were derived from the variance of carbon allowance futures prices during 2014. Capital investment for telemetry calculated at $50/kW.

Figure 2-6 demonstrates that meaningful incentives for DR might be justified by avoided damages from carbon emissions. The value of avoided damages under AB32 produce far less compelling results than under the SCC, but still reflect a payback of the up-front telemetry capital costs in approximately 2 years.

2.5 Discussion and Conclusion

To allow DR to participate in spinning reserve in California, WECC must modify the definitions that govern eligible resources by removing the requirement to be immediately and automatically responsive to system frequency; thereby bringing its policy into alignment with most other U.S. wholesale markets. Diversifying the resources providing ancillary services will allow the grid to be more resilient and less operationally expensive.

With an average revenue of ~$35/kW-year, steady end uses (e.g., lighting) have more than twice the revenue than seasonal end uses (e.g., cooling) because spinning reserve is needed year-round. Similarly, business segments with longer operating hours, such as groceries or lodging, have more revenue potential. We find that niche applications of DR could present an attractive business opportunity: certain business segments in southern California can achieve nearly $60/kW-year in revenue from interior lighting. However, this will depend on the total cost to attract spinning reserve resources. To achieve a simple payback of 5 years or less, the median DR resource in California would need to have a total enablement cost of $173/kW or less. Refrigeration resources with more constant profiles could be profitable with median enablement costs of $200/kW, while cooling loads would require costs below $90/kW to be profitable. This is plausible given data on equipment installation costs for automatic DR in California, but the large range of cost data suggests an aggregator would need to be careful in targeting participants.

Enablement costs for DR are likely to decrease in the future as technologies find a common standard and production volumes increase. NIST is working on smart grid interoperability standards [41] and California recently required new control systems for lighting, heating and air conditioning be able to receive automated DR signals [42]. Our analysis included a cost reduction for telemetry of a factor of 4 under current cost estimates. This will help make DR for

spinning reserve more economically attractive. At the same time, load patterns may change as end-use equipment evolves and the climate changes. This could affect our results by altering the coincidence of load and low/high market prices.

Avoided carbon emissions from using DR instead of fossil fuel generation for spinning reserve could justify the provision of incentives for the cost of installing telemetry (~$50/kW) for DR resources. If 500MW of DR replaced fossil generation in the spinning reserve market, we estimate an annual carbon savings of approximately one million metric tons. Avoided emissions may be larger in other regions with higher proportions of coal-fired resources.

2.6 References

[1] US DOE, 2006. Benefits of Demand Response in Electricity Markets and Recommendations for Achieving Them. A Report to Congress in fulfillment of Sec. 1252(e) of the Energy Policy Act of 2005.

[2] Kirby, B., 2003. Spinning Reserve From Responsive Loads. Oak Ridge National Laboratory. ORNL/TM-2003/19.

[3] Eto, J.H., Nelson-Hoffman, J., Parker, E., Bernier, C., Young, P., Sheehan, D., et al., 2007. Demand Response Spinning Reserve Demonstration. Lawrence Berkeley National Laboratory. LBNL-62761.

[4] Callaway, D.S., 2009. Tapping the energy storage potential in electric loads to deliver load following and regulation, with application to wind energy. *Energy Conversion and Management*, 50(5), pp.1389–1400.

[5] Cappers, P., MacDonald, J., Goldman, C., 2013. Market and Policy Barriers for Demand Response Providing Ancillary Services in U.S. Electricity Markets. Lawrence Berkeley National Laboratory. LBNL-6155E.

[6] NERC, 2011. Balancing and Frequency Control: A Technical Document Prepared by the NERC Resources Subcommittee. Available at: http://www.nerc.com/docs/oc/rs/NERC%20Balancing%20and%20Frequency%20Control%20040520111.pdf. Accessed April 2014.

[7] CAISO 2014. Business Practice Manual for Market Operations. Version 40, last revised 7/9/2014. Available at: http://www.caiso.com/rules/Pages/BusinessPracticeManuals/Default.aspx. Accessed October, 2014.

[8] Ellison, J.F., Tesfatsion, L.S., Loose, V.W., Byrne, R.H., 2012. Project Report: A Survey of Operating Reserve Markets in U.S. ISO/RTO-managed Electric Energy Regions. Sandia National Laboratories. SAND2012-1000.

[9] Callaway, D.S., Hiskens, I., 2011. Achieving Controllability of Electric Loads. *Proceedings of the IEEE*, 99(1), pp.184–199.

[10] Watson, D.S., Matson, N., Page, J., Kiliccote, S., Piette, M.A., Corfee, K., et al., 2012. Fast Automated Demand Response to Enable the Integration of Renewable Resources. Lawrence Berkeley National Laboratory. LBNL-5555E.

[11] Southern California Edison, 2014. Demand Response Event History. Available at: https://www.sce.openadr.com/dr.website/scepr-event-history.jsf. Accessed November 2014.

[12] 145 FERC ¶ 61,141 (2013). Regional Reliability Standard BAL-002-WECC-2 – Contingency Reserve, Order No. 789.

[13] Mathieu, J.L., Dyson, M., Callaway, D.S., 2012. Using Residential Electric Loads for Fast Demand Response: The Potential Resource and Revenues, the Costs, and Policy Recommendations. In ACEEE Summer Study on Energy Efficiency in Buildings. pp. 189–203.

[14] MacDonald, J., Cappers, P., Callaway, D., Kiliccote, S., 2012. Demand Response Providing Ancillary Services. Presented at Grid-Interop Forum 2012. Irving, TX. LBNL-5958E. Available at: http://drrc.lbl.gov/sites/all/files/LBNL-5958E.pdf. Accessed March 2014.

[15] MacDonald, J., Kiliccote, S., Berkeley, L., 2014. Commercial Building Loads Providing Ancillary Services in PJM. In 2014 ACEEE Summer Study on Energy Efficiency in Buildings. pp. 192–206.

[16] Ma, O., Alkadi, N., Cappers, P., Denholm, P., Dudley, J., Goli, S., et al., 2013. Demand Response for Ancillary Services. *IEEE Transactions on Smart Grid*, 4(4), pp.1988–1995.

[17] Hummon, M., Palchak, D., Denholm, P., Jorgenson, J., Olsen, D., Kiliccote, S., et al., 2013. Grid Integration of Aggregated Demand Response, Part 2: Modeling Demand Response in a Production Cost Model. National Renewable Energy Laboratory. NREL/TP-6A20-58492.

[18] PG&E, 2009. 2009 Pacific Gas and Electric Company Participating Load Pilot Evaluation. Available at: http://www.pge.com/includes/docs/pdfs/mybusiness/energysavingsrebates/demandresponse/cs/2009_pacific_gas_and_electric_company_large_commercial_industrial_participating_load_pilot.pdf. Accessed September 2014.

[19] U.S. Energy Information Administration (EIA), 2014. Electric Power Annual.

[20] Ghatikar, G., Riess, D., Piette, M.A., 2014. Analysis of Open Automated Demand Response Deployments in California and Guidelines to Transition to Industry Standards. Lawrence Berkeley National Laboratory. LBNL-6560E.

[21] Siano, P., 2014. Demand response and smart grids—A survey. Renewable and Sustainable Energy Reviews, 30, pp.461–478.

[22] Itron, 2014a. California Commercial Saturation Survey. Prepared for the California Energy Commission. Available at: http://calmac.org/publications/California_Commercial_Saturation_Study_Report_Finalv2.pdf. Accessed October 2014.

[23] Itron, 2006. California Commercial End Use Survey. Prepared for the California Energy Commission. CEC-400-2006-005.

[24] US DOE, 2011. Load Participation in Ancillary Services: Workshop Report. Available at: https://www1.eere.energy.gov/analysis/pdfs/load_participation_in_ancillary_services_workshop_report.pdf. Accessed February 2014.

[25] Kiliccote, S., Lanzisera, S., Liao, A., Schetrit, O., Piette, M.A., 2014. Fast DR: Controlling Small Loads over the Internet. In 2014 ACEEE Summer Study on Energy Efficiency in Buildings. pp. 196–208.

[26] Prindle, W., de Fontaine, A., 2009. A Survey of Corporate Energy Efficiency Strategies. In ACEEE Summer Study on Energy Efficiency in Buildings. pp. 77–89.

[27] California Public Utilities Commission, 2010. Demand Response Cost Effectiveness Protocols. R.07-01-041.

[28] Fripp, M., 2011. Greenhouse gas emissions from operating reserves used to backup large-scale wind power. *Env. Sci. & Tech.*, 45(21), pp.9405–12.

[29] Koritarov, V., Veselka, T., Gasper, J., Bethke, B., Botterud, A., Wang, J., et al., 2014. Modeling and Analysis of Value of Advanced Pumped Storage Hydropower in the United States. Argonne National Laboratory. ANL/DIS-14/7.

[30] CAISO, 2013. 2013 Annual Report on Market Issues & Performance. Department of Market Monitoring. Available at: http://www.caiso.com/Documents/2013AnnualReport-MarketIssue-Performance.pdf. Accessed September 2014.

[31] Phinney, S., McCann, R., 2005. Potential Changes in Hydropower Production From Global Climate Change in California and the Western United States. Prepared for the California Energy Commission. CEC-700-2005-010.

[32] U.S. Energy Information Administration (EIA), 2014. California drought leads to less hydropower, increased natural gas generation. Available at: http://www.eia.gov/todayinenergy/detail.cfm?id=18271#tabs_SpotPriceSlider-1. Accessed November, 2014.

[33] Katzenstein, W., Apt, J., 2009. Response to Comment on "Air Emissions Due to Wind and Solar Power." *Env. Sci. & Tech.*, 43(15), pp.6108–6109.

[34] Katzenstein, W., 2010. Wind Power Variability, Its Cost, and Effect on Power Plant Emissions. Dissertation submitted for Doctor of Philosophy. July 2010. Carnegie Mellon University.

[35] Interagency Working Group on Social Cost of Carbon, 2013 Technical Support Document: Technical Update of the Social Cost of Carbon for Regulatory Impact Analysis Under Executive Order 12866 (US Government, Washington, DC). Revised November 2013.

[36] U.S. Energy Information Administration (EIA), 2014. Assumptions to the Annual Energy Outlook 2014. U.S. Department of Energy: Washington, DC, June 2014.

[37] National Research Council, 2010. *Hidden Costs of Energy: Unpriced Consequences of Energy Production and Use*. (National Academy, Washington, DC).

[38] Black & Veatch, 2012. Cost Report: Cost and Performance Data for Power Generation Technologies. Available at: http://bv.com/docs/reports-studies/nrel-cost-report.pdf%E2%80%8E. Accessed November 2014.

[39] Climate Policy Initiative, 2014. California Carbon Dashboard. Available at: http://calcarbondash.org/. Accessed November 24, 2014.

[40] US DOE, 2011. Recovery Act Selections for Smart Grid Investment Grant Awards – By Category. Available at: http://www.energy.gov/sites/prod/files/SGIG%20Awards%20by%20Category%202011%2011%2015.pdf. Accessed September 15, 2014.

[41] National Institute of Standards and Technology, 2014. NIST Framework and Roadmap for Smart Grid Interoperability Standards, Release 3.0. Special Publication 1108r3. http://dx.doi.org/10.6028/NIST.SP.1108r3

[42] California Energy Commission, 2013. 2013 Building Energy Efficiency Standards: Title 24. CEC-400-2012-004-CMF-REV2. Available at: http://www.energy.ca.gov/2012publications/CEC-400-2012-004/CEC-400-2012-004-CMF-REV2.pdf. Accessed November 2015.

Appendix A: Additional Modelling Details

DR availability proportional to load

Figure A-1 displays DR clearing MW in each hour of the day across 4 seasons for spinning reserve. The Pearson correlation coefficient between the median DR MW cleared in a given hour across all days of 2012-2013 and the median load for that hour of the day was 0.92. DR clearing amounts in the summer appears quite low – this may be due to other more lucrative DR opportunities (such as capacity) during those times.

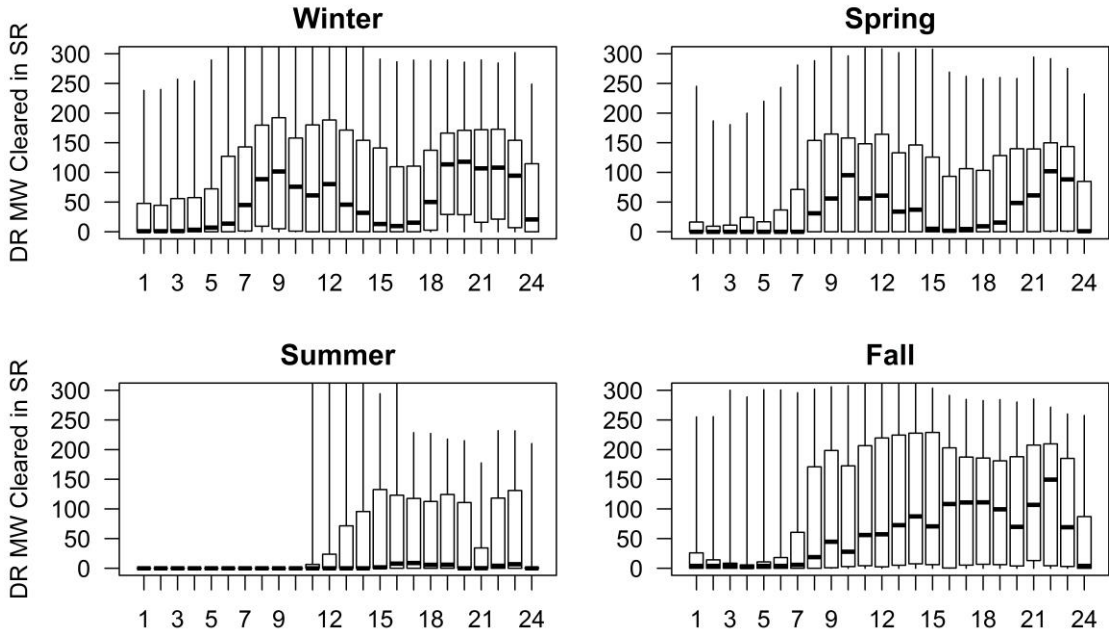

Figure A-1: Demand response MW cleared in spinning reserve market for each hour of the day in PJM during the period 2012-2013. The pattern of cleared demand response mimics the typical overall load pattern seen in each season. The heavy horizontal line in the middle of each box marks the median. The range of the box represents the interquartile range. The whiskers extend to the extremes of the distribution.

Reasoning for removal of projects from cost information in SCE

Figure A-2 displays the incentive information from PG&E and SCE.

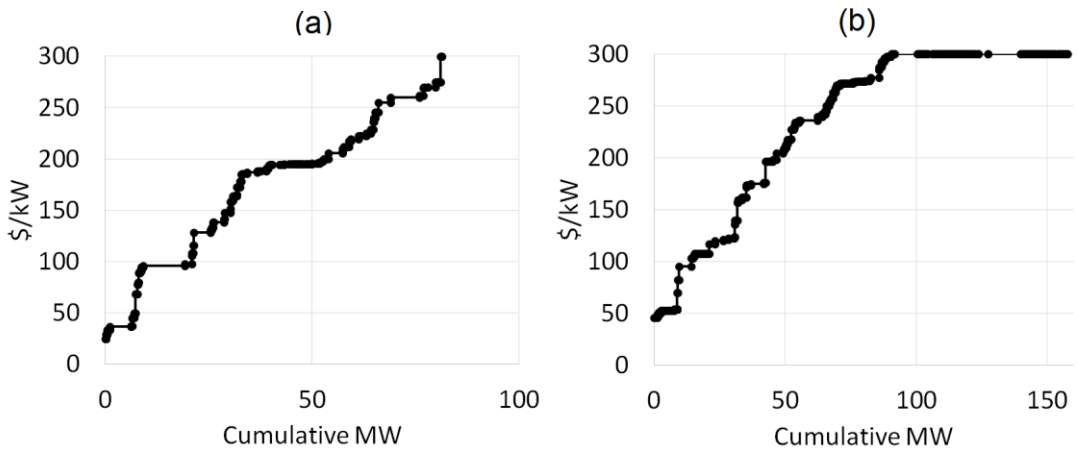

Figure A-2: (a) Incentives Provided by PG&E for AutoDR. (b) Incentives Provided by SCE for AutoDR.

We conducted an investigation into the AutoDR program costs and found that nearly all of the projects which had incentives of $300/kW in the SCE territory were likely from one contractor that received money from the American Recovery and Reinvestment Act (ARRA) grant funds. We surmise that the use of ARRA funds may have led to different recruitment practices and cost reporting. Thus, we do not believe that the incentive information reported for these projects is representative of the rest of the project population. The list below provides details on why we believe that these projects were from one contractor.

- An AutoDR program report stated that "the U.S Department of Energy's $11.4 million American Recovery and Reinvestment Act grant influenced a larger load shed and enablement cost in the SCE territory." [19]
- ARRA records show a total AutoDR project cost of $22.8M in SCE [40] attributable to one company. The 50% cost sharing required by ARRA leads to a grant of $11.4 million.
- There are 348 facilities in the project incentive database from SCE that had project incentives of $300/kW. These projects have a total load response of 67MW. The total

rebate amount given to these participants was just over $20M, which closely matches the ARRA project cost report.

We believe that most, if not all of the projects with incentive values at $300/kW were not representative of the true costs to install, program, and commission this equipment. This is especially apparent when you compare the incentive distribution from SCE with that of PG&E. There may be other projects in the database with incentive costs of less than $300/kW that were implemented by this DR contractor. However, we have no way of differentiating those projects.

Chapter 3: The Emissions and Economics of Behind-the-Meter Electricity Storage

Abstract

Annual installations of behind-the-meter (BTM) electric storage capacity are forecast to eclipse grid-side electrochemical storage by the end of the decade. Here we characterize the economic payoff and regional emission consequences of BTM storage without co-located generation under different tariff conditions, battery characteristics, and ownership scenarios using metered load for several hundred commercial and industrial customers. Net emissions are calculated as increased system emissions from charging minus avoided emissions from discharging. Net CO2 emissions range from 75 to 270 kg/MWh of delivered energy depending on location and ownership perspective, though in New York these emissions can be reduced with careful tariff design. Net NOx emissions range from -0.13 to 0.24 kg/MWh and net SO2 emissions range from -0.01 to 0.58 kg/MWh. Emission rates are driven primarily by energy losses, not by the difference between marginal emission rates during battery charging and discharging. Economics are favorable for many buildings in regions with high demand charges like California and New York, even without subsidies. Future penetration into regions with average charges like Pennsylvania will depend greatly on installation cost reductions and wholesale prices for ancillary services.

This paper was published as Fisher, M. J.; Apt, J. Emissions and Economics of Behind-the-Meter Electricity Storage. *Environ. Sci. Technol*. 2017, 51 (3), 1094–1101. DOI: 10.1021/acs.est.6b03536.

3.1 Introduction

Stationary electrochemical (battery) storage has seen significant improvements in cost in the last decade and is a promising way to perform many electric grid functions [1,2]. Battery storage is being installed both on the utility side of the customer meter at the transmission/distribution level ("grid-scale"), and "behind-the-meter" (BTM) for individual facilities. Grid-scale storage can be used to delay infrastructure upgrades, perform wholesale market transactions including energy price arbitrage and frequency regulation, and absorb over-generation by distributed generation resources, among other services. BTM batteries can reduce retail electricity costs by shifting the timing of utility purchases while also performing grid-scale services via aggregation or proper tariff structures. BTM storage is being adopted in areas that have high retail electricity prices and generous battery subsidies. BTM storage capacity is expected to double each year through 2019 in the U.S., when it will represent almost half (~400MW) of annual storage installations by capacity [3].

Policy makers are now implementing rules and subsidies that encourage large scale deployments of electric storage. California has set a storage procurement target of 1.3GW by 2020 [4] and provided an incentive of $1,300/kW [5]. New York City has an incentive of $2,100/kW [6]. At the federal level, FERC Order 755 [7] instructed grid operators to compensate fast-responding resources like storage for their speed and accuracy in frequency regulation markets.

The emissions consequences of deploying a storage technology depends in part on how it is operated; in turn the operating policies depend on who owns the storage. Previous research has focused on grid-scale storage. Investor-owned grid-scale batteries will be operated to maximize profit from wholesale market transactions, resulting in homogenous battery behavior across a

grid region. A number of studies have shown that grid-scale storage will increase total power system emissions under the grid's current fuel mix when operated for energy arbitrage [8–12], even in Texas which contains a relatively high penetration of natural gas and renewables [13]. Energy arbitrage shifts power from high cost periods (evening) to low cost periods (overnight). In most regions of the U.S., this use pattern will result in shifting generation from natural gas to coal [8] and in all regions more power is used, since storage has a round-trip efficiency that is less than 100%.

The operation of BTM batteries is more heterogeneous because profit maximizing behavior will depend on the interaction between the load profile of the building, rate structures (these vary widely among utility service territories), and possible wholesale market transactions. There has been little investigation of the average behavior and grid-level consequences of a large deployment of BTM batteries. A number of studies explore optimal behavior in storage systems, but test their efficacy on a limited dataset containing few buildings and/or less than a year of data, and few discuss emissions [14–16]. Neubauer and Simpson [17] used the National Renewable Energy Laboratory's (NREL) BLAST [18] model to study the behavior of a fleet of BTM batteries, but the work used load data from only 98 commercial buildings, used only one utility tariff scenario, did not consider ancillary services, and did not calculate emissions effects.

Our analysis focuses on the operation of commercial and industrial (C&I) BTM storage under several market and tariff conditions and across ownership perspectives in order to characterize economics and net emissions. C&I is important because recent data show the storage capacity installed in this segment has outstripped residential installations by an order of magnitude [3]. The goal of our work is to understand the economic conditions under which BTM

storage will experience rapid adoption, the effects on system emissions, and alternative incentive structures that might mitigate those environmental effects.

3.2 Methods

3.2.1 Battery Optimization Model

In this section we describe the model in general terms. The mathematical formulation and a detailed discussion of each equation can be found in Appendix B. Each building in our dataset is given a simulated battery. We assume a lithium-ion phosphate chemistry currently used by SonnenBatterie [19]. We formulate a linear program to minimize energy costs and maximize revenue to the battery owner for 1 year. Depending on the ownership perspective, the battery is able to perform energy arbitrage, reduce demand charges, and/or provide frequency regulation and spinning reserve. The optimization is conducted at 15-minute intervals to reflect the typical structure of demand charges and the sampling rate of many meters. We assume that the storage system is too small to affect market prices or marginal system emissions, though we assess the sensitivity of our results to ancillary service market prices. The battery charges from the grid only, not from co-located generation.

Battery characteristics, such as capacity (kW), duration of discharge (hours), cost ($/kWh and $/kW), and round-trip efficiency (%) were fixed at the following values for the base case results. A full sensitivity analysis is given in Appendix B. Battery power was sized to 20% of the building's peak load (sensitivity: 15%-25%) in increments of 18kW, the smallest SonnenBatterie unit [20]. Assumed capital costs of $600/kWh + $400/kW are taken from a 2011 Sandia National Laboratory report [21] (sensitivity: 33%-100% of base case). While these values are based on dated information, they provide a consistent way to scale costs across battery power and

duration, and match well to more recent values from Lazard [22] ($444 - $1,321/kWh; 4-hr duration) and Tesla [23] ($750/kWh; 2-hr duration). A 1 hour duration at rated power was chosen for energy capacity in our base case results, though we also show results for 0.5 – 4 hour durations. Round-trip efficiency was assumed to be 83% [24] (sensitivity: 83%-91%).

The economic incentives facing the battery owner will affect battery operations. In addition to a wholesale-only market participant and individual customer facing retail rates, an "aggregator" can pool retail resources for participation in wholesale markets. We examine all three ownership perspectives (customer, aggregator and wholesale-only) by varying the components of the objective function (Table 3-1) and constraints. BTM batteries would not be used solely for wholesale services, but the perspective is useful in benchmarking the performance of aggregator-owned batteries. All perspectives consider the economic tradeoff between battery use and degradation by multiplying the fraction of total lifetime energy used against the estimated replacement cost of the battery. This degradation model is accurate for the lithium-ion phosphate [25] chemistry we have assumed; degradation models for other lithium chemistries are more complex [26]. Analysis has demonstrated that our results are insensitive to assumptions around degradation. We do not account for the physical effects of degradation on charge capacity, which the California Public Utilities Commission estimates at 1% per year [27].

Table 3-1: Components of Total Energy Cost Minimization

Perspective	Customer Energy Cost	Customer Demand Charge	Wholesale Energy Cost	Frequency Regulation Revenue	Spinning Reserve Revenue	Battery Degradation
Customer	✓	✓				✓
Aggregator	✓	✓	✓	✓	✓	✓
Wholesale			✓	✓	✓	✓

We also vary the amount of information available to the battery owner. Accurate forecasting of future building load and market clearing prices is central to the battery's ability to minimize energy costs. Battery optimization software is proprietary, so we bound this real world scenario by assuming two different forecasts: a perfect forecast and a persistence forecast that makes a rolling-horizon prediction using the average of historical data. In practice, forecasting algorithms are likely to perform better than the persistence forecast, but not as well as the perfect forecast.

The simulated battery faces three main types of physical and market constraints.

1. Battery state of charge (SOC) – Expressed as a fraction of total energy capacity, SOC is restricted to 20% - 100%, with a penalty function above 90%, to prevent increased degradation from high/low voltages. These restrictions are also found on electric vehicle batteries [28].
2. Total capacity – The capacity used to charge/discharge the battery and held for ancillary services cannot be greater than the capacity of the battery.
3. Frequency regulation capacity – We assume that the frequency regulation signal is energy neutral (no net charging or discharging), similar to the dynamic regulation signal implemented in the PJM Interconnection (PJM) [29]. But during any given time period, the battery will gain and lose charge as it follows the regulation signal. Therefore, we place a constraint on capacity used for frequency regulation to ensure SOC limits are not violated. One year of regulation signal from PJM [30] was used to estimate the amount of charging/discharging possible during a single period.

For spinning reserve, we make a simplification to reduce model complexity without affecting the results. We assume the battery gains revenue from offering spinning reserve

capacity, but is never called to provide the service. In practice, spinning reserve is called infrequently and for relatively short periods of time. Modelling reserve deterministically with the events called by PJM in 2013 yielded a decrease of only 0.01% in total revenue under base case assumptions.

3.2.2 Data

3.2.2.1 Load Data

A utility in the Carolinas provided energy usage (kWh) data from 994 individual C&I meters at a 15-minute sample rate for 1 calendar year (2013). According to the utility, no customer had behind-the-meter generation. Data filters, including low power, missing data, and manual identification of meters attached solely to equipment were applied to screen unsuitable meters from our analysis, leaving us with 665 meters. Unfortunately, the data do not represent a true random sample. Our dataset was readily available to the utility because these customers had a long history of interval meter data. More details on the characteristics of the dataset and filters can be found in Appendix B.

A number of threats to internal and external validity are raised when using one dataset across geographic regions and tariff scenarios. Average customer type (e.g., manufacturing vs. service) and weather (see Figure B-5) may cause differences in load profiles that are masked by using data from a single region. While the Carolina customers in our dataset do not face time-of-use tariffs, such tariffs in other regions may shift when companies choose to consume energy, even without batteries, as commercial customers are somewhat price elastic [31]. We cannot comment on the size and direction of bias introduced by these threats. In figures B-12 – B-14 and B-24, we compare the results from our Carolina dataset to the results from a geographically

diverse set of 100 buildings made public by EnerNOC [32]. While this dataset introduces identical biases, we are encouraged by the similarity of results.

3.2.2.2 Emissions Data

Marginal emissions factors (MEFs) from Siler-Evans, et al [33,34] are used to calculate the net effects of battery behavior on system CO2, SO2, and NOx emissions (see Figure B-8). MEFs attempt to capture the emissions rate (kg/MWh) of the marginal generator in a grid region that would be used to respond to changes in load from battery use. Siler-Evans, et al. used hourly emissions and operation data from 1,400 power plants in the U.S. to calculate factors by hour-of-day and season. Estimates of MEF by North American Electric Reliability Corporation (NERC) region are used for each utility tariff in our analysis (California – Western Electricity Coordinating Council (WECC); New York – Northeast Power Coordinating Council (NPCC); Pennsylvania – ReliabilityFirst Corporation (RFC)). Our results use MEFs generated from 2014 emissions data. Appendix B contains an analysis using MEFs generated from average 2006-2014 emissions data which shows slightly higher net emissions. This reflects the ongoing shift from coal to natural gas in the U.S. power mix. We believe this shift will be long-lasting, and therefore chose to use emissions data from 2014.

The database used in Siler-Evans, et al. has an important limitation – it includes only fossil fuel generators larger than 25MW. MEFs do not account for renewables or small fossil generators on the margin. PJM is the grid operator for Pennsylvania and is the only operator to publish hourly marginal fuel data [35]. Using this database, we found that non-fossil generation was on the margin 5% of the hours in 2014 and those hours were distributed throughout the day (Figure B-11). This distribution will effect charging and discharging emissions on a similar scale; consequently, the bias in net emissions introduced by this limitation is small for PJM. This

may be different for California which has a larger percentage of non-fossil generation. MEFs also do not account for heat-rate improvements on partially-loaded thermal generators as ancillary services are shifted to batteries.

3.2.2.3 Tariff and Market Data

C&I customers face two separate charges: one for energy and one for peak demand. Peak demand is typically defined as the highest 15-minutes of power consumption in the billing time period. We use tariffs from 4 different utilities; Duquesne Light in Pennsylvania, Consolidated Edison (ConEd) in New York, and two California utilities – Pacific Gas & Electric (PG&E) and Southern California Edison (SCE). The highest demand charge in each tariff is as follows: Duquesne - $7/kW; ConEd - $32/kW; PG&E - $34; SCE - $39. Some of these charges vary by time-of-day and season – see Appendix B for a full description of each tariff.

While ConEd, PG&E and SCE were chosen because customers can receive incentives for installing batteries, they have very high electricity costs relative to the rest of the country. Duquesne Light in western Pennsylvania was chosen as a more nationally representative tariff; demand charges are 90% of a rough estimate of the national average and energy charges are 86% of the average. National averages were calculated from the OpenEI Utility Rate Database [36].

Hourly clearing prices for real-time energy and ancillary services markets were downloaded from grid operators corresponding to the utility tariff being used (California – CAISO; New York – NYISO; Pennsylvania - PJM). Calendar year 2013 data are used to match the timing of load data.

3.2.3 Revenue and Emissions Calculations

The charging and discharging time series are averaged over each hour of the year and matched against the hourly/seasonal MEFs described previously. Battery charging requires increased output, and therefore increased emissions, from the marginal generator, while discharging decreases output from the marginal generator. Net emissions are calculated as the sum of the increased and decreased emissions over the entire year and across all buildings in the dataset. Emissions are normalized to the delivered energy from the battery (e.g., kgCO2/MWh) for ease of comparison to values from other generation sources and studies.

Total annual revenue from retail and wholesale services is assumed to be constant over the lifetime of the battery (10 years [37,38]). The present value of the revenue stream from each building is calculated with a discount rate of 15%, and divided by the capital cost to determine the net present value ratio. A ratio equal to or greater than one indicates a building with favorable economics. We do not include regional subsidies for any scenario. We ignore operational costs in maintaining a battery, assuming that each component (battery cells, inverter, etc.) lasts for the given lifetime. Appendix B includes a discussion of the chosen discount rate and lifetime, including sensitivity analysis (Figure B-20).

3.3 Results

3.3.1 Storage Economics

Figure 3-1 shows averaged hourly battery charging/discharging behavior for each utility region under perfect forecasts. Capacity utilization is low because the load peaks that drive battery use are infrequent; the batteries are often idle for days. For the customer-owned and aggregator scenarios, discharging tends to coincide with peak building load because batteries

mitigate demand charges. However, charging occurs at different times. Aggregators are exposed to wholesale energy prices, waiting until they reach a minimum overnight before charging the battery. Customer owners face only retail pricing. Under flat-rate energy prices, as with Duquesne Light, customers will recharge as soon as their load profiles decrease in case an unexpected load spike occurs. This coincides with the late afternoon system peak in many U.S. locations. Wholesale-only participation leads to a charging profile similar to the aggregator scenario, but shifts the discharge profile later in the evening when energy prices peak. Tariff design under TOU rates must consider the distribution level impacts of many batteries suddenly charging at the same time when the lowest price block is reached; a similar concept to "smart-charging" schemes proposed for electric vehicle charging [39].

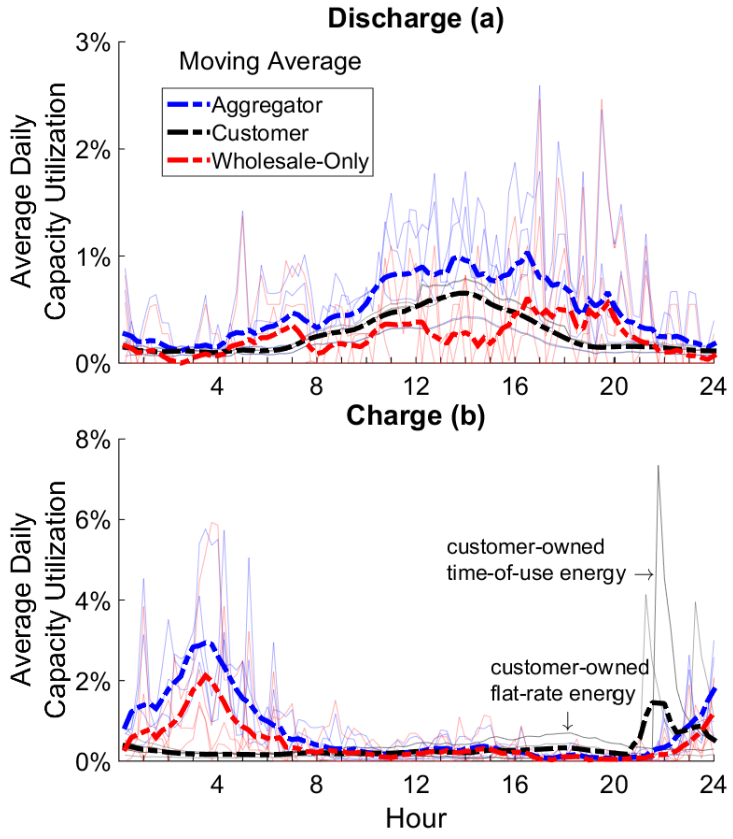

Figure 3-1: Average daily discharging (a) and charging (b) profile of battery fleet under perfect forecasts (note: different scales). Light solid lines are individual profiles for each

ownership perspective and utility region. Heavy dotted lines represent an hourly moving average of all utility regions for a particular ownership perspective. Average capacity utilization is low because the load peaks that drive battery use are infrequent. Customer and aggregator-owned batteries discharge during early afternoon hours when C&I building load peaks, in order to reduce demand charges. Wholesale-only batteries discharge later in the evening when wholesale energy prices peak. Aggregator and wholesale-only batteries charge in the early morning hours when wholesale energy prices are lowest. The charging profile of customer-owned batteries depends on the type of tariff; flat-rate tariffs provide no economic incentive to shift energy, and thus batteries charge as soon as building load begins to decrease in the afternoon while time-of-use tariffs encourage charging as soon as the lowest price block is reached.

Persistence forecasts do a poor job of predicting volatile market prices and building load, and the batteries fail to meaningfully mitigate demand charges. In reality, forecasting models are more sophisticated but computationally expensive and will fall in between the perfect and persistence results. All buildings are uneconomic for persistence forecasts under base case assumptions, and we therefore choose to discuss only the perfect information cases below, though we present persistence sensitivity results in Appendix B. The gap between perfect and persistence results emphasizes the importance of accuracy in forecasting algorithms, which is an ongoing area of research [40]. We note that the emissions results from the persistence and perfect forecast cases are very similar.

In the perfect information scenario, a significant number of buildings have favorable economics under ConEd, SCE, and PG&E tariffs without subsidies. This is driven by high demand charges. The economics for Duquesne Light's tariff are mixed. Demand charges are low which makes peak shaving less profitable, but ancillary service market prices are high in PJM, helping aggregator-owned batteries. For the 60-minute duration battery, average annual revenue ranged from \$25-\$112/kWh (installed energy capacity) for customer-owners and \$108-\$181/kWh for aggregators across utility tariffs, though amortized installation costs were

$200/kWh. The majority of aggregator revenue was generated from demand charge mitigation in all regions except Duquesne Light, where frequency regulation dominated.

Aggregators were able to successfully mitigate demand charges for the customer while simultaneously extracting high value from ancillary service markets. Across all tariffs, demand charge reduction under aggregators was nearly identical to the reduction under customer-owners for the same size battery, while ancillary service market revenue for aggregators was 89-99% of the revenue in the wholesale-only scenario.

Figure 3-2 shows battery economics are more favorable at lower durations. While total revenue is higher at longer durations, lower energy capacity utilization means there are decreasing marginal returns to installing more energy capacity. Moving from a 30-minute to 240-minute duration battery increases capital costs by 300% but revenue by only 57-100% and 64-84% for customer-owners and aggregators, respectively. Demand charge management is typically the largest proportion of revenue, though the revenue share by service can be significantly different across tariffs (Figure B-18).

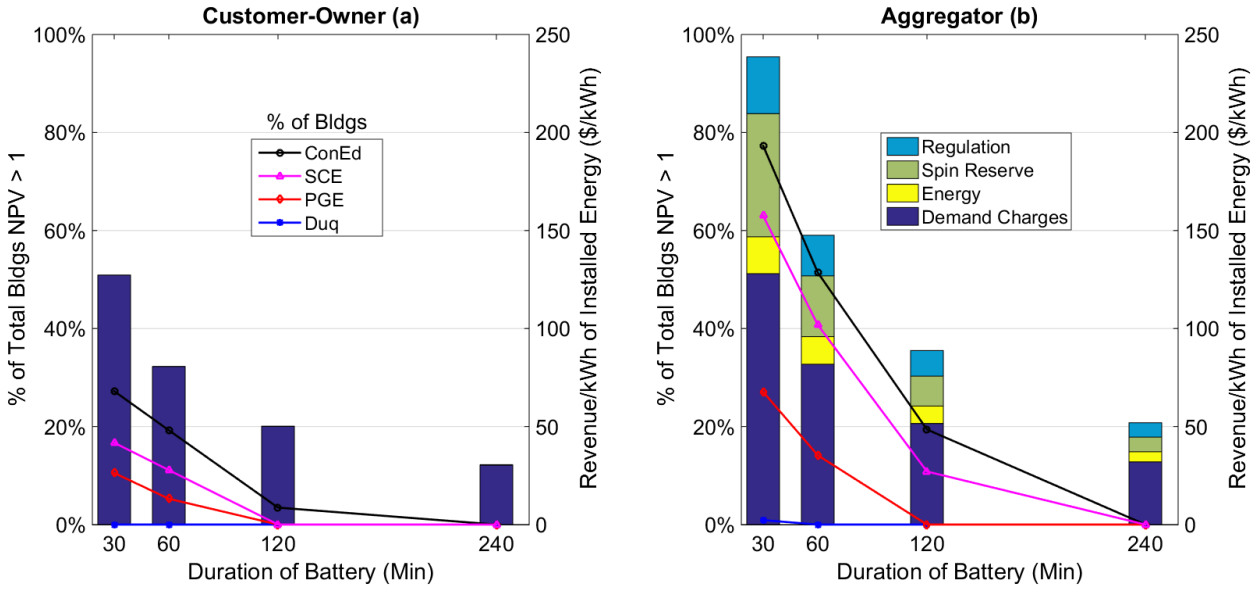

Figure 3-2: Project economics vs battery duration for customer owners (a) and aggregators (b). Solid lines represent the percent of total buildings that have a net present value greater than 1 in each utility territory. A discount rate of 15% and unsubsidized costs are used in net present value calculations. Bars show the average revenue by service across all tariffs normalized to the installed energy capacity of the battery. Installation costs amortized over the lifetime of the battery were $280, $200, $160, and $140/kWh for 30, 60, 120, and 240-minute durations, respectively. Revenue is largely driven by demand charge mitigation where longer duration batteries allow for deeper absolute reductions. However, there are greatly diminishing returns to increases in duration because the extra energy capacity faces a much lower utilization rate. Normalized revenue decreases by nearly 5x as you move from a 30-minute to 240-minute battery. Absolute revenue increases by approximately 75% across the same scale, but cost increases by 300%.

Revenue for batteries in Duquesne Light's territory was driven largely by high prices for ancillary services in PJM, although this could not offset low demand charges in creating positive project economics. This region is highly sensitive to installation costs and ancillary service market prices. If system installation costs decrease by 30%, the percent of buildings with positive project economics increases from 0% to 86% for aggregators. However, if ancillary service market prices concurrently decrease by 50%, we again find that no projects have favorable economics (Figure B-21). The sensitivity to ancillary service prices in all regions is noteworthy

(Figure B-19) given the small size of most markets (hundreds of megawatts). They may be quickly saturated with a wide deployment of batteries.

Roughly double the number of buildings have favorable battery economics as installation costs are decreased by one-third (~$1,000/kWh to ~$667/kWh), which is a conservative estimate of future costs given the 47% reduction in 5 years estimated by Lazard [22]. As battery capacity decreases from 20% to 15% of peak load, an additional 10% of the buildings in the sample become economic. Round-trip efficiency has a negligible effect on battery economics for most buildings (Figure S.19). Battery economics are sensitive to assumptions of lifetime and discount rate, with an additional 20% of the buildings becoming economic as you increase lifetime from 10 to 15 years or decrease discount rate from 15% to 10% (Figure B-20).

3.3.2 Net Emissions

Figure 3-3 shows average net emission rates across all storage devices for CO2, NOx, and SO2 for each utility region. Net rates are calculated as increased emissions from charging minus avoided emissions from discharging. If the set of buildings is restricted to only those that have favorable economics, the emissions results do not change significantly.

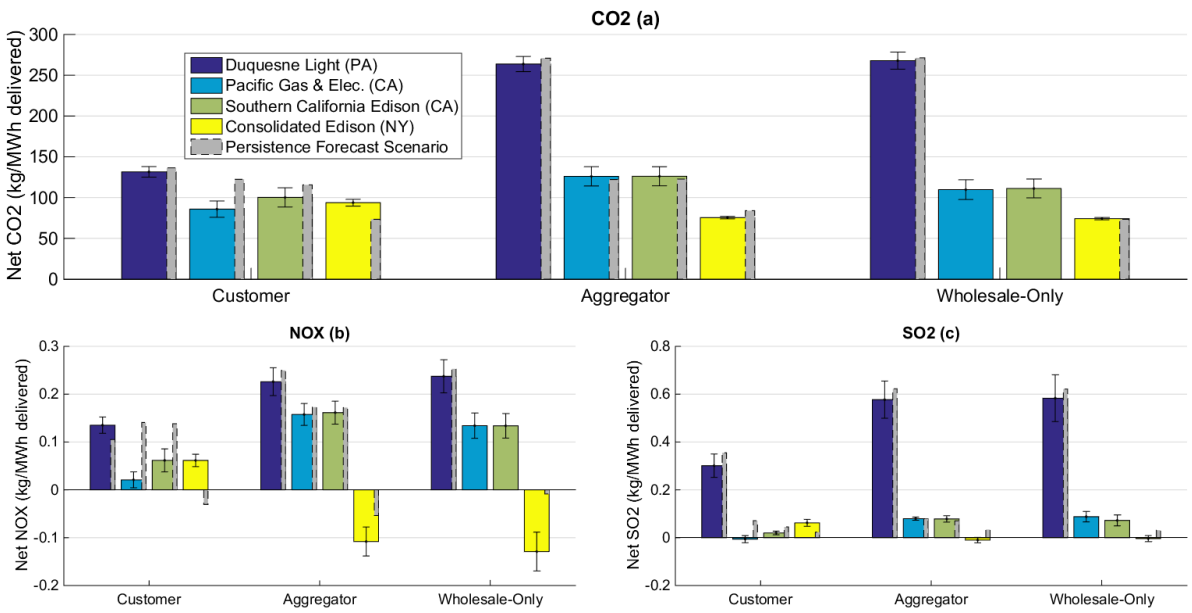

Figure 3-3: Net CO2 (a), NOx (b) and SO2 (c) emission rates from battery operation across utility tariffs and ownership perspectives. Net rates are calculated as increased emissions from charging minus avoided emissions from discharging. Emission rates are primarily driven by energy losses from inefficiency. Duquesne Light has the highest rates because MEFs are high in RFC and energy losses from frequency regulation are significant. Persistence forecast results are extremely similar to that of perfect forecasts despite their poor accuracy. Persistence forecast emission rates are not shown for the wholesale-only perspective in PG&E and SCE because the values are biased by capacity factors that were essentially zero. In other words, the battery was almost never used and provided very little delivered energy. Net CO2 emissions were -370 and -145 kg/MWh in those cases, respectively. Uncertainty bars represent uncertainty in the regression parameter estimates used to calculate marginal emissions factors.

Net CO2 emission rates with perfect forecasts range from 85 – 130 kg/MWh, 75 – 260 kg/MWh, and 75 – 270 kg/MWh for the customer, aggregator, and wholesale-only perspectives, respectively. Persistence forecast emissions rates are very similar despite low forecast accuracy (gray bars in Figure 3-3). Net NOx emissions with perfect forecasts range from 0.02 – 0.14 kg/MWh, -0.11 – 0.23 kg/MWh, and -0.13 – 0.24 kg/MWh for the customer, aggregator, and wholesale-only perspectives, respectively. Net SO2 emissions range from -0.01 – 0.30 kg/MWh, -0.01 – 0.58 kg/MWh, and 0.00 – 0.58 kg/MWh for the customer, aggregator, and wholesale-only perspectives, respectively. Emissions rates are higher for Duquesne Light for two reasons;

first, MEFs are higher in RFC and second, battery capacity factors are higher from performing significant amounts of frequency regulation. Higher capacity factors lead to higher inefficiency losses. While Duquesne Light, PG&E, and SCE have higher emission rates in the aggregator and wholesale-only perspectives than the customer perspective, ConEd's emission rates are lower. This is a result of differing marginal emission rates in each region during typical battery charging periods. MEFs in NPCC are lower in the early morning hours when aggregators and other wholesale market participants will charge than in evening hours when customer-owners will charge. RFC and WECC have higher MEFs during early morning hours. This hints at the benefits of a time-of-use (TOU) rate in ConEd that we discuss later.

Positive net emission rates can be attributed to two factors; (1) net positive energy consumption by the battery due to inefficiency losses, and (2) differences in MEFs between charging and discharging periods. We can isolate the effect of differences in MEFs by calculating the average MEF during battery charging minus the average during discharging, weighted by energy. The balance of the total emission rate can be attributed to internal energy losses from inefficiency. Across all tariffs, the difference in the average charging-discharging CO2 MEF is -22, 71, and 25 kg/MWh for customer-owners, aggregators, and wholesale participants, respectively. This represents only -5%, 12%, and 4% of total net emissions rates, respectively. Similar patterns were identified for SO2 and NOx. This means that most of the positive net emissions from battery operation can be attributed to inefficiency losses. Figure S.15 confirms that increases in round-trip efficiency dramatically reduce CO2 net emission rates (~50% reduction by improving from 83% to 91% efficiency). Emission rates are insensitive to other battery characteristics because the energy losses that drive total emissions (numerator) scale closely with the total energy delivered (denominator).

Tariff design can reduce the environmental impact of BTM batteries, but only with a close examination of a region's generation fuel mix. MEFs reach high and low points at different times during the day depending on your location. MEFs in western states peak in the early morning, while at the same time in the northeast they reach a minimum. The average daily MEF profile (Figure S.8) shows that TOU rates in California that end in the early evening, and flat rates in Pennsylvania that encourage charging in the late afternoon are optimal for minimizing emissions for customer-owners. ConEd, however, has a flat-rate tariff which encourages charging during late afternoon hours, while MEFs in NPCC reach a minimum in the early morning hours. We designed a revenue-neutral TOU rate to investigate the impact of tariff design on net emissions in New York. From 8am to midnight, we increase energy rates to 4.27 cents/kWh and decrease rates to 2 cents/kWh from midnight to 8am when MEFs are lowest. Relative to the flat-rate tariff, this lowered net CO2 emissions by 18% (to 77 kg/MWh), SO2 by 65% (to 0.02 kg/MWh), and switched batteries from net positive NOx emissions to net negative (-0.07 kg/MWh). The cost of wholesale energy to serve this load was essentially unchanged under the TOU tariff. We note that such tariffs must be periodically reexamined as the generation mix and MEFs in a region change.

3.4 Discussion

As previous studies have found for grid-scale batteries, BTM batteries increase system emissions in most cases by consuming more energy than they deliver and shifting load between generators. An important finding from our model is that most of the positive net emissions can be attributed to internal energy losses, not to the timing of charging/discharging. Net emission rates from BTM batteries are somewhat lower than rates from natural gas combined-cycle generators, but have the same order of magnitude. The net emission rates found here are similar

in magnitude to those from Hittinger and Azevedo [8], who calculated net emission rates across NERC regions from grid-scale batteries performing energy arbitrage only.

Tariff design can reduce the environmental effect of BTM batteries in certain regions, as we have shown with a TOU rate in New York. As the fuel composition of the generation fleet changes in response to regulatory or market forces, policy makers should periodically reassess tariffs for battery owners to encourage charging from low-emission sources. Encouraging wholesale market participants to shift energy purchases, however, is not an easy task since battery charging follows wholesale market prices. State regulators cannot change wholesale pricing with the stroke of a pen. Instead, this would require broad policy instruments like carbon prices.

The emissions consequences of adding BTM batteries is of significant concern to policy makers in New York [41] and California, and they should take care to differentiate between grid-scale and BTM batteries in their analyses. For example, California's Self-Generation Incentive Program (SGIP) mandates that incentivized technologies must have a net emission rate lower than that of the grid as a whole. For battery storage, they assume a natural gas combustion turbine is displaced by discharging during peak hours and a combined-cycle gas turbine is used to charge during off-peak hours, arriving at a rate of 350 kgCO2/MWh – 3 times higher than the rates found here. Future work to determine a more accurate emissions rate for SGIP may include production cost modelling [27]. These methods apply only to a grid-connected battery by failing to account for retail tariffs and the individual building load profiles which drive BTM battery behavior.

These policy makers are also incentivizing relatively long-duration storage (2-hours for SGIP). Our economic results suggest that greater market penetration may be achieved by

allowing shorter duration batteries, which have higher capacity utilization rates. Regulators can then create a distributed long-duration resource by sequentially calling short-duration assets.

Battery economics improve significantly for all regions as installation costs decrease by 30% (~$1,000/kWh to ~$667/kWh). Tesla forecasts at least a 30% reduction in battery pack cost by the end of the decade [42], which is in-line with academic reviews [43] and industry surveys [22]; if the market were to see a corresponding improvement in inverter and soft costs this could significantly increase BTM installations. The degree to which BTM batteries will penetrate locations with average demand charges in this scenario will depend significantly on the price of ancillary services and other location-dependent revenue sources (e.g., demand response programs and/or capacity payments).

Battery owners exposed only to retail tariffs may contribute to, rather than reduce system peak load. The C&I load in our sample peaks earlier than the typical daily system peak, which is consistent with data from national building modeling efforts [44]. Under flat-rate retail tariffs, these batteries begin to charge in the early evening as building load drops off. Unfortunately, this increased load coincides with the average system peak and could exacerbate problems experienced during high load, such as losses and capacity shortfalls.

In some areas of the country, a battery can gain additional revenue from participation in utility demand response (DR) programs or capacity markets. We chose not to include utility DR or capacity market events in our model due to the diversity of program rules in different jurisdictions that would make it difficult to compare our model's results across regions. However, DR revenue could materially improve the economics of BTM batteries. To investigate if DR revenue would be roughly additive to the revenue in our model, we examined the coincidence of DR events with the provision of other services from the battery. We found that in

the case of SCE in summer 2013, the average capacity utilization of the batteries in our model was 4% during DR hours (204 hours). This suggests that the batteries are mostly idle during these hours, so DR revenue should be roughly additive after subtracting increased energy costs from inefficiency losses.

The rationale for installing BTM energy storage is driven by demand charges, but demand charge design is often not reflective of intraday and seasonal variation in capacity supply costs. Increases in BTM storage will therefore magnify the misalignment between utility revenue and cost-to-serve by incentivizing demand reductions at times when those reductions do not reduce costs.

Our results are based on a load dataset from one geographic region under one tariff – generalizing to other regions and tariffs masks differences in customer type, weather, and price differences that could affect the underlying load profiles. Future work using load data from multiple regions would be more accurate, however, there are well-known challenges associated with accessing individual customer utility data.

The findings related to net emission increases hold for the present-day fuel composition of the generation fleet. Should the grid become significantly cleaner when batteries are charging, the addition of energy storage may decrease overall emissions through load shifting. Lin et al. showed how emissions changes can be related to fuel mix on a small test system [12]. However, the long lifetime of physical assets for power systems combined with regulatory uncertainty regarding emission reductions from existing generation sources leads us to conclude that significant de-carbonization is many years away, while BTM battery systems are being installed today. Policy makers should be aware of how battery characteristics and tariff design can alter use patterns, and that, short of emissions prices, an adaptive process of tariff redesign may be

necessary to link use patterns with emission goals. A regulatory framework that allows for frequent alterations to rates or incentives based on external variables like grid emission rates is a subject ripe for research. The implementation of such a framework would represent a significant departure from the status quo, and would benefit from further research to examine the market and policy barriers it would face.

3.5 References

[1] J. Eyer, G. Corey, Energy Storage for the Electricity Grid: Benefits and Market Potential Assessment Guide, Sandia National Laboratories, Albuquerque, NM, 2010. http://www.sandia.gov/ess/publications/SAND2010-0815.pdf.

[2] Grid Energy Storage, US Department of Energy, Washington, D.C., 2013. http://energy.gov/sites/prod/files/2014/09/f18/Grid Energy Storage December 2013.pdf.

[3] U.S. Energy Storage Monitor, GTM Research & Energy Storage Association, Boston, MA, 2014.

[4] Application of San Diego Gas & Electric Company (U902M) for Approval of its Energy Storage Procurement Framework and Program As Required by Decision 13-10-040, California Public Utilities Commission, 2014. http://docs.cpuc.ca.gov/PublishedDocs/Published/G000/M127/K426/127426247.PDF.

[5] PG&E Self-Generation Incentive Program, (2016). http://www.pge.com/en/mybusiness/save/solar/sgip.page (accessed February 10, 2016).

[6] Consolidated Edison Demand Management Incentives, (2016). http://www.coned.com/energyefficiency/demand_management_incentives.asp (accessed February 10, 2016).

[7] Frequency Regulation Compensation in the Organized Wholesale Power Markets, 2011. https://www.ferc.gov/whats-new/comm-meet/2011/102011/E-28.pdf.

[8] E.S. Hittinger, I.M.L. Azevedo, Bulk energy storage increases United States electricity system emissions., Environ. Sci. Technol. 49 (2015) 3203–10. doi:10.1021/es505027p.

[9] E. Hittinger, J.F. Whitacre, J. Apt, Compensating for wind variability using co-located natural gas generation and energy storage, Energy Syst. 1 (2010) 417–439. doi:10.1007/s12667-010-0017-2.

[10] P. Denholm, G.L. Kulcinski, Life cycle energy requirements and greenhouse gas emissions from large scale energy storage systems, Energy Convers. Manag. 45 (2004) 2153–2172. doi:10.1016/j.enconman.2003.10.014.

[11] R. Lueken, J. Apt, The effects of bulk electricity storage on the PJM market, Energy Syst. 5 (2014) 677–704. doi:10.1007/s12667-014-0123-7.

[12] Y. Lin, J.X. Johnson, J.L. Mathieu, Emissions impacts of using energy storage for power system reserves, Appl. Energy. 168 (2016) 444–456. doi:10.1016/j.apenergy.2016.01.061.

[13] R.T. Carson, K. Novan, The private and social economics of bulk electricity storage, J. Environ. Econ. Manage. 66 (2013) 404–423. doi:10.1016/j.jeem.2013.06.002.

[14] K. Zheng, Z. Zheng, H. Jiang, J. Ren, Economic analysis of applying the used EV battery to commercial electricity customer, in: 2015 5th Int. Conf. Electr. Util. Deregul. Restruct. Power Technol., IEEE, 2015: pp. 2100–2103. doi:10.1109/DRPT.2015.7432593.

[15] Y. He, Z. Wang, Two-stage optimal demand response with battery energy storage systems, IET Gener. Transm. Distrib. 10 (2016) 1286–1293. doi:10.1049/iet-gtd.2015.0401.

[16] R.T. de Salis, A. Clarke, Z. Wang, J. Moyne, D.M. Tilbury, Energy storage control for peak shaving in a single building, in: 2014 IEEE PES Gen. Meet. | Conf. Expo., IEEE, 2014: pp. 1–5. doi:10.1109/PESGM.2014.6938948.

[17] J. Neubauer, M. Simpson, Deployment of Behind-The-Meter Energy Storage for Demand Charge Reduction, National Renewable Energy Laboratory, Golden, CO, 2015. http://www.nrel.gov/docs/fy15osti/63162.pdf.

[18] Battery Lifetime Analysis and Simulation Tool (BLAST) Documentation, National Renewable Energy Laboratory, Golden, CO, 2014. http://www.nrel.gov/docs/fy15osti/63246.pdf.

[19] SonnenBatterie Pro, SonnenBatterie. (2016). https://sonnen-batterie.com/en-us/sonnenbatterie?_ga=1.42115749.10813948.1465480047#sonnenbatterie-pro (accessed September 6, 2016).

[20] T. Woody, The $100,000 Battery That Could Help Hotels Save Bundles of Money, Atl. (2013). http://www.theatlantic.com/technology/archive/2013/11/the-100-000-battery-that-could-help-hotels-save-bundles-of-money/281194/ (accessed June 5, 2016).

[21] S. Schoenung, Energy Storage Systems Cost Update, Sandia National Laboratories, Albuquerque, NM, 2011. http://prod.sandia.gov/techlib/access-control.cgi/2011/112730.pdf.

[22] Lazard's Levelized Cost of Storage Analysis - Version 1.0, Lazard, 2015. https://www.lazard.com/media/2391/lazards-levelized-cost-of-storage-analysis-10.pdf.

[23] Tesla Energy: Design Your Powerpack System, Tesla Mot. (2016). https://www.teslamotors.com/powerpack/design#/ (accessed February 6, 2016).

[24] Tesla Motors, Tesla Power System Specifications, (2016). https://www.teslamotors.com/powerpack (accessed June 5, 2016).

[25] S.B. Peterson, J. Apt, J.F. Whitacre, Lithium-ion battery cell degradation resulting from realistic vehicle and vehicle-to-grid utilization, J. Power Sources. 195 (2010) 2385–2392. doi:10.1016/j.jpowsour.2009.10.010.

[26] B.Y. Liaw, R.G. Jungst, G. Nagasubramanian, H.L. Case, D.H. Doughty, Modeling capacity fade in lithium-ion cells, J. Power Sources. 140 (2005) 157–161. doi:10.1016/j.jpowsour.2004.08.017.

[27] Order Instituting Rulemaking Regarding Policies, Procedures and Rules for the California Solar Initiative, the Self-Generation Incentive Program and Other Distributed Generation Issues, California Public Utilities Commission, 2015. http://docs.cpuc.ca.gov/PublishedDocs/Published/G000/M156/K044/156044151.PDF.

[28] M. Eberhard, A Bit About Batteries, Tesla Mot. Blog. (2006). https://www.teslamotors.com/blog/bit-about-batteries (accessed January 1, 2016).

[29] Order on Compliance Filing, Washington, D.C., 2012. https://www.ferc.gov/whats-new/comm-meet/2012/051712/E-4.pdf.

[30] PJM RTO Regulation Signal Data, PJM Ancillary Serv. (2015). http://www.pjm.com/markets-and-operations/ancillary-services.aspx (accessed January 10, 2015).

[31] M. Bernstein, J. Griffin, Regional Differences in the Price-Elasticity of Demand for Energy, RAND Corporation, Santa Monica, CA, 2005. http://www.rand.org/pubs/technical_reports/TR292.html.

[32] EnerNOC Open Data, (2013). https://open-enernoc-data.s3.amazonaws.com/anon/index.html (accessed January 1, 2016).

[33] K. Siler-Evans, I.L. Azevedo, M.G. Morgan, Marginal Emissions Factors for the U.S. Electricity System, Environ. Sci. Technol. 46 (2012) 4742–4748. doi:10.1021/es300145v.

[34] K. Siler-Evans, I.L. Azevedo, M.G. Morgan, J. Apt, Regional variations in the health, environmental, and climate benefits of wind and solar generation, Proc. Natl. Acad. Sci. 110 (2013) 11768–11773. doi:10.1073/pnas.1221978110.

[35] Monitoring Analytics, Marginal Fuel Posting, (n.d.). http://www.monitoringanalytics.com/data/marginal_fuel.shtml (accessed January 1, 2016).

[36] OpenEI Utility Rate Database, (2016). http://en.openei.org/wiki/Utility_Rate_Database# (accessed September 6, 2016).

[37] B. Kaun, S. Chen, Cost-Effectiveness of Energy Storage in California: Application of the EPRI Energy Storage Valuation Tool to Inform the California Public Utility Commission Proceeding R. 10-12-007, Palo Alto, CA, 2013. http://www.epri.com/abstracts/Pages/ProductAbstract.aspx?ProductId=000000003002001162.

[38] 2016 Self-Generation Incentive Program Handbook, 2016. http://www.cpuc.ca.gov/General.aspx?id=5935.

[39] J.A.P. Lopes, F.J. Soares, P.M.R. Almeida, Integration of Electric Vehicles in the Electric Power System, Proc. IEEE. 99 (2011) 168–183. doi:10.1109/JPROC.2010.2066250.

[40] H. Zhao, F. Magoulès, A review on the prediction of building energy consumption, Renew. Sustain. Energy Rev. 16 (2012) 3586–3592. doi:10.1016/j.rser.2012.02.049.

[41] New York Battery and Energy Storage Technology (NY-BEST) Consortium, (n.d.). https://www.nyserda.ny.gov/Researchers-and-Policymakers/Energy-Storage/NY-BEST (accessed January 11, 2016).

[42] T. Motors, Tesla Gigafactory Presentation, Palo Alto, CA, 2015. https://www.teslamotors.com/sites/default/files/blog_attachments/gigafactory.pdf (accessed January 1, 2016).

[43] B. Nykvist, M. Nilsson, Rapidly falling costs of battery packs for electric vehicles, Nat. Clim. Chang. 5 (2015) 329–332. doi:10.1038/nclimate2564.

[44] DOE Office of Energy Efficiency & Renewable Energy, Commercial and Residential Hourly Load Profiles for all TMY3 Locations in the United States, (2016). http://en.openei.org/doe-opendata/dataset/commercial-and-residential-hourly-load-profiles-for-all-tmy3-locations-in-the-united-states (accessed January 1, 2016).

Appendix B: Additional Modelling Details and Results

Data Cleaning and Validation

The utility provided data from a subset of their entire commercial and industrial population. The subset were those customers who had interval meters and a sufficiently long history for this study. This may introduce selection bias. The subset of customers with interval meters would suggest a skew toward higher usage customers relative to the general commercial/industrial population. Our results could also be biased because the data come from one geographic area of the country. Commercial/industrial customers in other parts of the country could have different load shapes that would affect battery behavior.

Meters covering loads unsuitable for this study were removed according to usage characteristics. This included any meters with maximum power draw less than 25kW, average power draw less than 13kW, or any meter missing a total of more than 2 days of data within 2013. Data gaps for meters with less than 2 days of missing data were filled with an average profile from two surrounding days of the same type (weekday/weekend). 270 meters were removed during this step. A subsequent visual inspection of each meter's load profile identified meters that were attached to specific pieces of equipment (e.g., switching between 2 discrete load values throughout the year). 59 meters were removed during this step.

It is very difficult to validate the results of our model by comparing to real-world battery behavior. BTM batteries are currently installed at a small fraction of customer sites even in California. Metered output data from these batteries is confidential to the customer, and proprietary to the third-party aggregators who may have installed the battery. There is some capacity factor data from PG&E impact evaluation reports for the Self-Generation Incentive

Program (SGIP) [1], though it is quite course and calculated from only 4 projects. The impact report states 80% of monthly capacity factors for installed batteries were below 10%, with nearly 60% below 2.5%. For the batteries modeled in this study under a PG&E tariff, 100% of monthly capacity factors were below 10%, and 95% below 2.5%. For SCE's tariff, 100% of monthly capacity factors were below 10%, and 76% below 2.5%. The lower capacity factors found in this study could be the result of our decision not to model demand response (DR) events or behind-the-meter (BTM) solar photovoltaic generation. DR event participation is a requirement of receiving an incentive under SGIP.

Load and Market Data

Our dataset included energy usage (kWh) data from 994 individual commercial and industrial meters at a 15-minute sample rate for 1 calendar year (2013). According to the utility, none of the customers had behind-the-meter generation. As described in the previous section, data filters were applied to screen unsuitable meters from our analysis, leaving us with 665 meters.

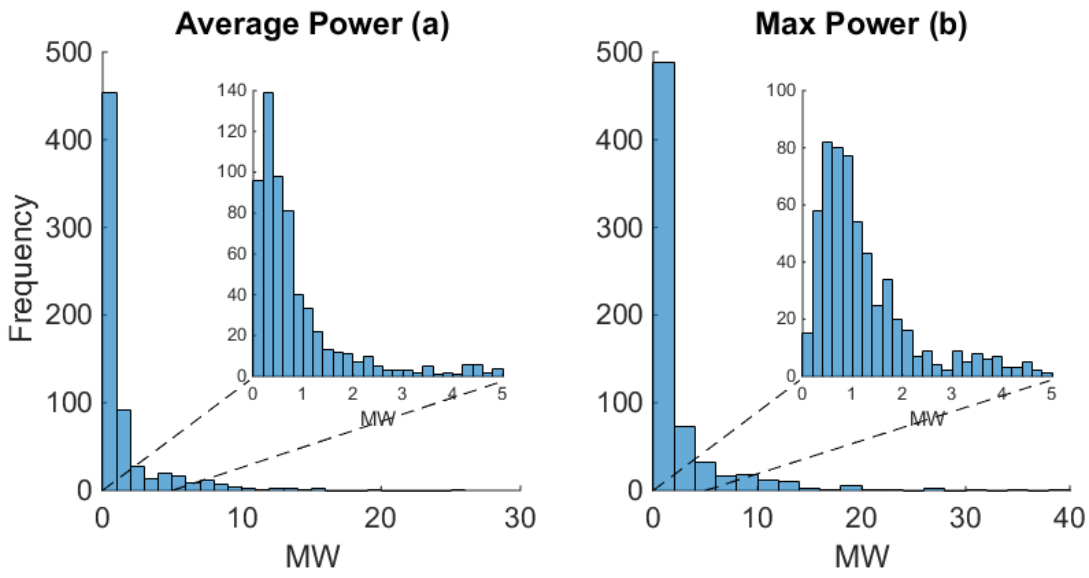

Figure B-1: Distribution of annual average (a) and maximum (b) power consumption across 665 buildings in dataset.

Figure B-1 shows the distribution of annual average and maximum power consumption for the 665 buildings in the sample. The median annual average power consumption is 600 kW, and the median peak power consumption is 1,094 kW. These distributions expose a long tail in power consumption. Removing all buildings with maximum annual power consumption greater than 10 MW (37 buildings) changes the emission rates for all pollutants by less than 2% when compared with the results of the full sample.

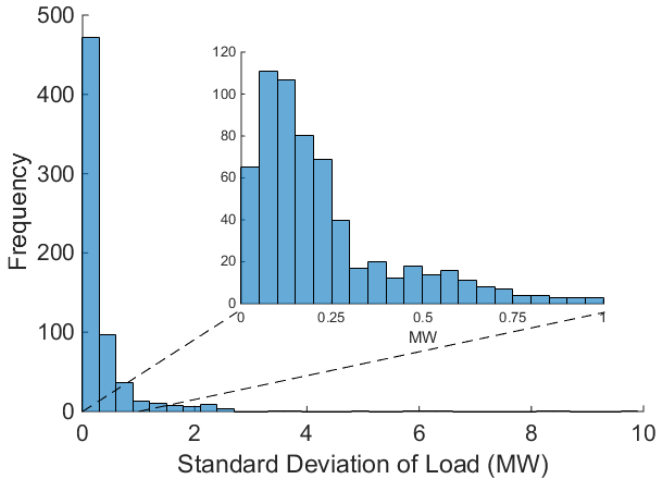

Figure B-2: Distribution of standard deviation of load across buildings in our sample.

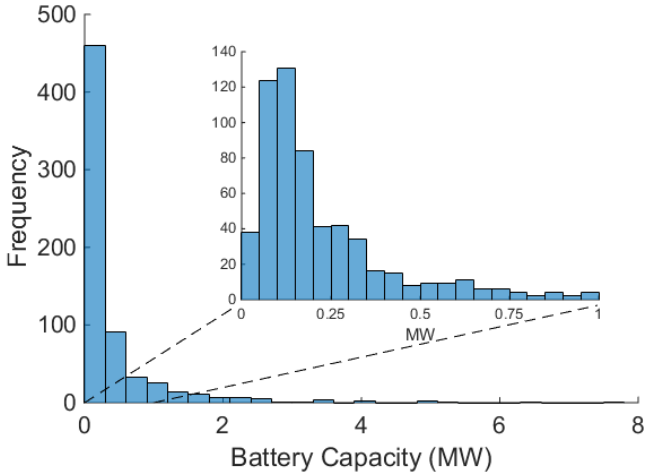

Figure B-3: Resulting distribution of battery capacity when sized to 20% of peak load.

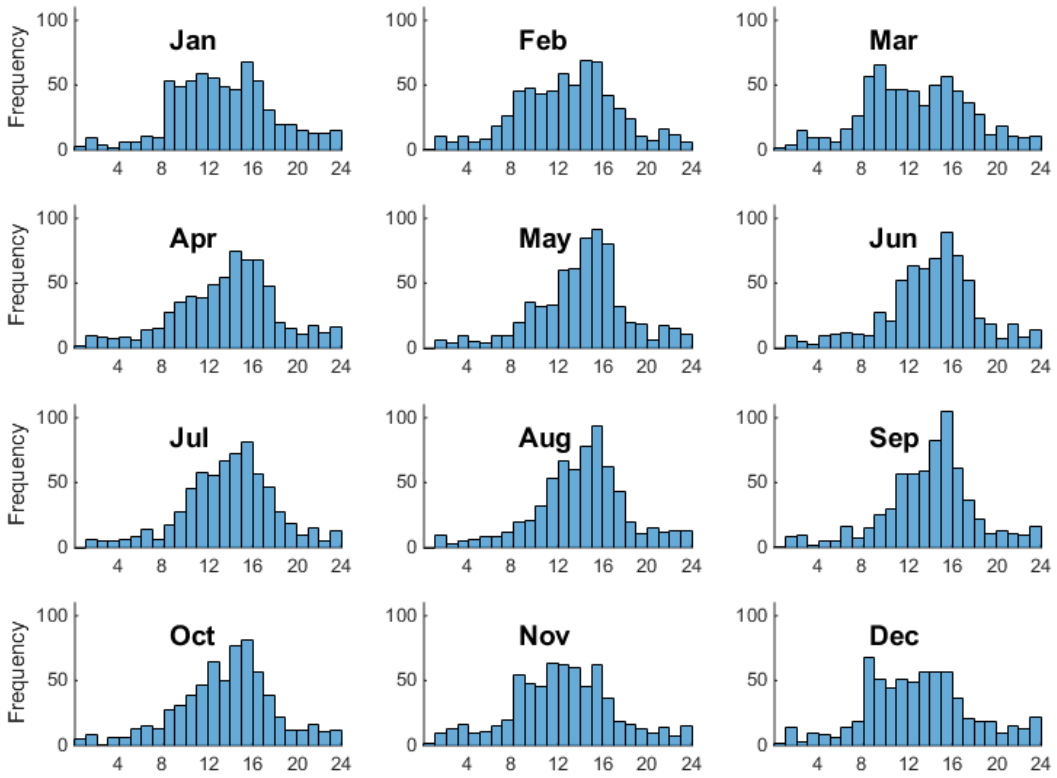

Figure B-4: The hour-of-day when the monthly peak building load occurs, given as a distribution across all buildings. Monthly peaks tend to concentrate in the early afternoon hours during the summer, while in the winter they spread out over a wider portion of the day. This is likely due to the effect of air conditioning load driven by the southern climate where the data originate.

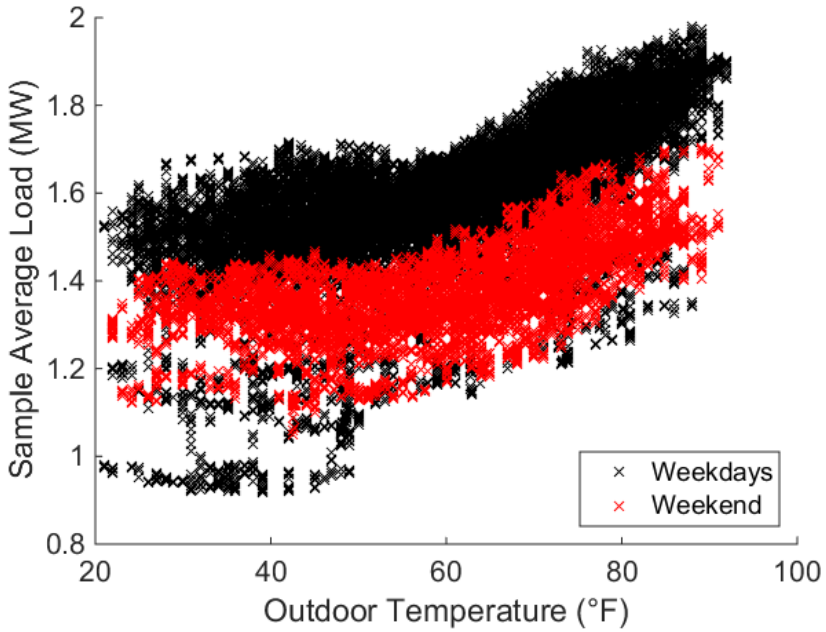

Figure B-5: Hourly average load across all buildings in the sample vs. outdoor temperature. Air conditioning load is likely responsible for the temperature dependence of load above approximately 60 degrees Fahrenheit.

Calendar year 2013 hourly clearing prices for real-time energy and ancillary services markets were downloaded from grid operators in the United States corresponding to the utility tariff being used (California – CAISO; New York – NYISO; Pennsylvania - PJM). Table B-1 shows the grid node location where data were selected. Some California ancillary services only have a day-ahead market.

Table B-1: Grid Node Locations for Market Data

Grid Region	Node ID
PJM (Duquesne Light)	Western Hub (51288)
NYISO (ConEd)	N.Y.C. (61761)
CAISO (PGE)	TH_NP15_GEN_APND
CAISO (SCE)	TH_SP15_GEN_APND

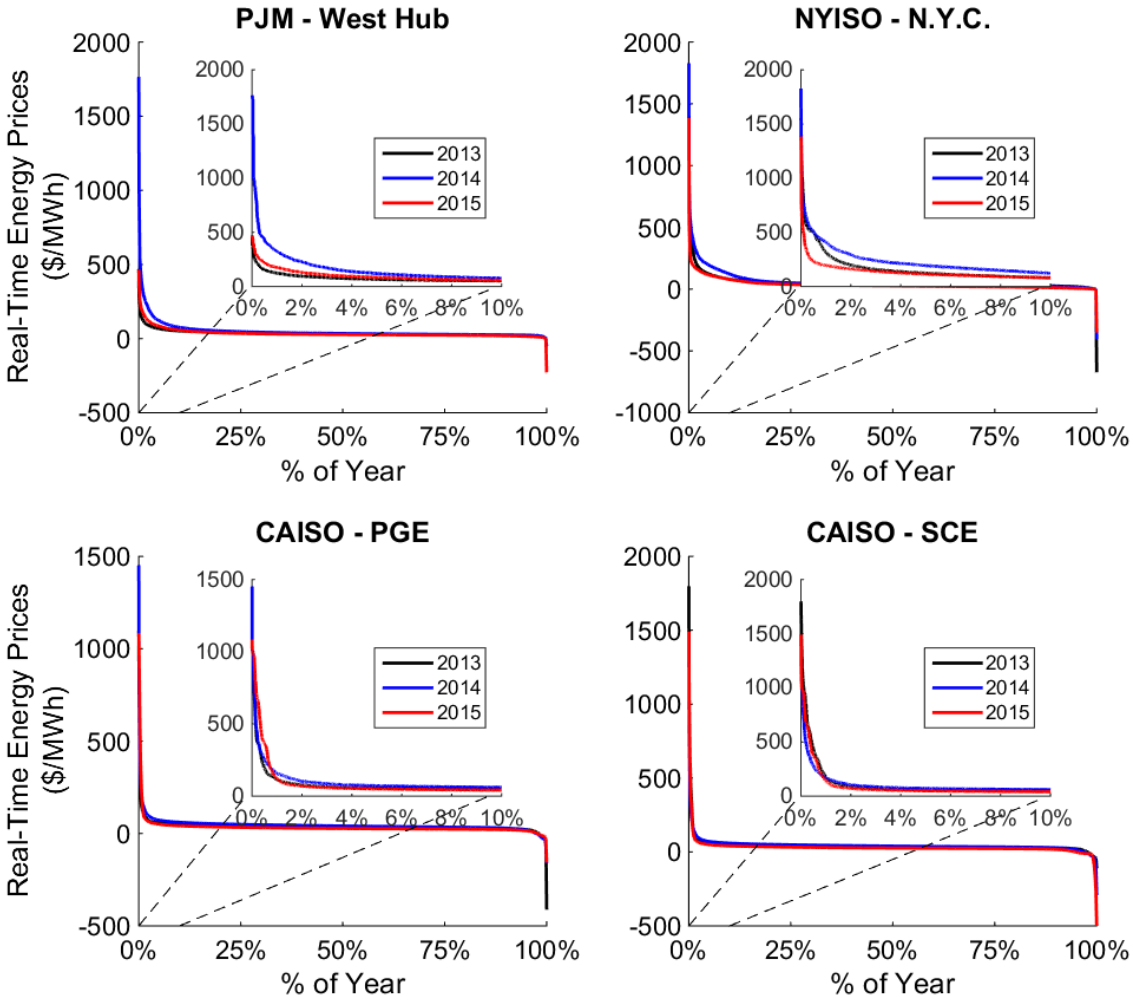

Figure B-6: Price-duration curves for real-time energy prices from 2013-2015. Ancillary service prices show similar trends because the largest component of ancillary service prices is typically the lost opportunity cost of producing energy (valued at the real-time price).

Figure B-6 shows that 2013 market prices are not significantly different from 2015 prices, with 2014 prices in NYISO and PJM affected by extreme cold temperatures ("polar vortex" event). It would be inappropriate to compare 2013 data to earlier periods due to changes in market structure, such as the implementation of FERC Order 755[2].

Table B-2: Utility Tariffs. Demand and energy charges include the published rate plus all applicable adjustments. Data from OpenEI Utility Rate Database [3].

Utility	Demand Charges ($/kW) Summer / Winter	Energy Charges ($/kWh) Summer / Winter
ConEd – NY SC-9 – General Large Low Tension Service (NYC)	$31.66 / 27.06	$0.035385 / 0.035385
Pacific Gas & Electric (PG&E) – CA E-19 – Medium General Demand TOU (Secondary)	$15.07 – all periods + $19.04 / 0.24 – peak + $4.42 / 0 – mid-peak	$0.16233 / 0.10185 – peak $0.10893 / 0.10185 – mid-peak $0.07397 / 0.07797 – off-peak
Southern California Edison (SCE) – CA General Service – Large; TOU-8, Option B (under 2kV)	$15.57 – all periods + $22.95 / 0 – peak + $6.49 / 0 – mid-peak	$0.14202 / 0.08899 – peak $0.08749 / 0.08899 – mid-peak $0.06288 / 0.0681 – off-peak
Duquesne Light – PA General Service Medium	$7.09 / 7.09	$0.090308 / 0.090308

Optimization Formulation and Computational Methods

Problem Formulation

Constants

$\overline{SoC}$ Max state of charge of battery (kWh)

SoC(0) Initial state of charge of battery (kWh)

$\bar{P}$ Rated power of battery (kW)

η round-trip efficiency of battery (%)

BL(t) building load at time t (kW)

EC(t) Energy cost at time t ($/kWh)

DC_k	Demand charge for demand period k ($/kW)
BRC	Battery Replacement Cost ($)
LMP(t)	Wholesale energy cost at time t ($/kWh)
REGP(t)	Wholesale regulation market price at time t ($/kWh)
SPINP(t)	Wholesale spinning reserve market price at time t ($/kWh)
RDNE	Regulation Down Net Energy (kWh/kW) – maximum amount of net energy charge during a typical hour of frequency regulation. Expressed as a fraction of the regulation capacity offered.
RUNE	Regulation Up Net Energy (kWh/kW) – maximum amount of net energy discharge during a typical hour of frequency regulation. Expressed as a fraction of the regulation capacity offered.
ABSE	Absolute Energy (kWh/kW) – total energy processed by a battery during frequency regulation. Expressed as a fraction of the regulation capacity offered.

Variables

c(t)	battery charging at time t (kW)
d(t)	battery discharge at time t (kW)
reg(t)	frequency regulation capacity participation at time t (kW)
spin(t)	spinning reserve participation at time t (kW)
pd_k	peak demand during demand period k (kW)
soc(t)	state of charge of battery at time t (kWh)

nl(t) net load at time t (kW)

deg(t) battery degradation cost at time t ($)

pen(t) penalty function to prefer 90% idle state of charge ($)

Sets

T Set of 15-minute time periods

K Set of demand periods (e.g. peak, mid-peak and off-peak - depends on tariff), each of which is a subset of T

Objective Functions

$$\min \sum_{t \in T} [EC(t) * nl(t) + deg(t) + pen(t)]/4 + \sum_{k \in K} DC_k * pd_k \quad (1)$$

$$\min \sum_{t \in T} [(LMP(t) + EC(t)) * nl(t) - REGP(t) * reg(t) - SPINP(t) * spin(t)]/4 + deg(t) + pen(t) + \sum_{k \in K} DC_k * pd_k \quad (2)$$

$$\min \sum_{t \in T} [LMP(t) * nl(t) - REGP(t) * reg(t) - SPINP(t) * spin(t)]/4 + deg(t) + pen(t) \quad (3)$$

Equation 1 is the objective function for the customer ownership perspective. Equation 2 is for aggregators and equation 3 is for the wholesale-only perspective. We divide the energy cost and ancillary service revenue by 4 to convert kW to kWh for a 15-minute time-step to match the units of market clearing prices ($/kWh). This initial portion of the objective function represents real costs/revenues to the battery owner. Degradation is an amortization of the assumed replacement cost into the use phase of the battery; it prevents the use of the battery to perform

services when market prices are low. The penalty function is used to restrict battery SOC as discussed below.

The last term in the customer and aggregator objective functions sums demand charges over each demand period k; the form of this portion of the equation will change depending on the structure of demand charges in each utility tariff. For example, Duquesne Light's demand charge is a flat-rate charge covering all hours of a month and does not depend on time-of-day or month – therefore there is only one demand period k. Southern California Edison (SCE), on the other hand, has a more nuanced demand charge that has a flat-rate charge for all hours of a month, as well as time-of-day adders that depend on the month. In this case, there are 4 different demand periods to track in any given month. The implementation of tracking peak demand in each demand period in the GAMS software, while maintaining a linear programming problem, warrants some discussion. The use of a maximum function (MAX) common to many software packages is not a linear function, and therefore would necessitate the use of a non-linear solver in the optimization calculations. This would drastically slow the solution time. Fortunately, there is an equivalent method to a MAX function that maintains a linear programming problem. We create a number of extra variables equal to the number of demand periods we need to track (for SCE, this was 4). The variables will track the peak demand in each of these periods. We then add an equivalent number of constraints at each time step to our problem (again, 4 for SCE at each time step) that force the variable to assume the maximum load experienced during that period. These take the form $nl(t) \leq pd_k \ \ \forall t \in k$ where $nl(t)$ is the net load at time t where t falls in demand period k and pd_k is the variable that holds the max load for demand period k. A similar method is used in the imperfect information scenarios to provide "memory" of the previous demand peak across each rolling-horizon optimization in a given month.

$$nl(t) = BL(t) + c(t) - d(t) \quad (4)$$

$$deg(t) = \frac{\sqrt{\eta} * c(t) + \frac{d(t)}{\sqrt{\eta}} + reg(t) * ABSE}{4 * \overline{SoC} * 4598} * BRC \quad (5)$$

Equation 4 calculates the net load of the building at time t (the load seen by the meter) from the underlying building load and the charging or discharging of the battery.

Equation 5 calculates degradation cost at time t as the product of the replacement capital cost and the fraction of total lifetime energy processed by the battery at time t. As determined by experimental results in Peterson, et al. [4], we account only for amp-hours processed by the battery, not depth of discharge, when calculating battery degradation for lithium-ion phosphate batteries. Based on data in Peterson, et al., we assume that the energy consumed to reach the end of battery lifetime (80% of initial battery capacity) is 4,598 times the maximum SOC. We derive this number from an average of the model coefficients reported in the paper. To express the energy processed by the battery at time t in fractions of lifetime energy, we divide the energy processed (sum of charging, discharging, and regulation energy) by the lifetime energy capacity of the battery (4,598 times maximum SOC). We divide by 4 to convert charge and discharge kW to kWh. Dividing regulation energy by 4 converts the hourly Absolute Energy (ABSE) metric into a 15 minute metric (see paragraph below for more on ABSE). Battery replacement cost is assumed to be 70% of the current system cost. Battery behavior is relatively insensitive to the replacement cost assumption.

ABSE, used in equations 5 and 8, is the total amount of energy processed by the battery during 1 hour of frequency regulation, both by charging and discharging, expressed as a fraction of the regulation capacity offer (kWh/kW). In other words, it's the integral of the absolute value

of the regulation signal with respect to time. We derive a single value for ABSE (0.26 kWh/kW) from 1 year of PJM regulation D signal [5] (2 second sample rate). For each hour of the dataset, we calculate the integral as described above. A period of one hour was chosen to match the period over which PJM attempts to maintain energy neutrality in the regulation signal. The final parameter value is calculated as the mean of the distribution of hourly energy values.

Equation 5 does not have a term addressing the provision of spinning reserve. We assume that the battery clears its idle capacity in the wholesale market, and therefore receives payment for that capacity, but is never actually called to provide spinning reserve. We make this simplification because spinning reserve is called infrequently and for relatively short periods of time. Using PJM as an example, spinning reserve events were called 18 times in 2013, 37 times in 2014, and 21 times in 2015 where the average length of an event was 15 minutes [6]. Attempting to model spinning reserve in a probabilistic manner (reserve events typically occur as a result of the unforeseen loss of a power plant or transmission line) would increase computational complexity with little change in the overall results. As a test, we modelled spinning reserve events at the exact times they occurred during 2013 in PJM and found overall revenue decreased by 0.01% under the base case assumptions. The one constraint we do place on spinning reserve in our model is limiting the capacity offer by the capacity used for other services (equation 12).

$$pen(t) \geq \left(\overline{SoC} * 0.9 - soc(t)\right) * 10^{-7} \quad (6)$$

$$pen(t) \geq \left(soc(t) - \overline{SoC} * 0.9\right) * 10^{-1} \quad (7)$$

Equations 6 and 7 implement a penalty function for deviations from 90% state of charge. Equation 6, which creates a penalty for SOC lower than 90%, is only used in the customer

ownership scenario where taking advantage of negative wholesale energy prices is not possible. Equation 6 forces the battery to prefer a 90% SOC when idle, reflecting a desire for higher states of charge to be ready for unexpected spikes in energy use. Equation 7 is used to discourage operation above 90% SOC which may be harmful to the battery (due to high voltage) [7]. Different scaling factors are used to accomplish different objectives. A small scaling factor of 10E-7 is used in Equation 6 to reflect the preference for higher SOC, but not at the expense of revenue generating activities that require discharging. A larger scaling factor of 10E-1 is used for Equation 7, which creates a penalty for SOC higher than 90%, to reflect higher degradation rates at high voltages. The combination of these two formulas are mathematically equivalent to an absolute value calculation, but this formulation preserves the overall problem as a linear program and allows different penalties for SOC above and below 90%.

The problem is initialized with a 90% SOC at t = 0.

Constraints

$$soc(t+1) = soc(t) + \frac{\sqrt{\eta} * c(t) - \frac{d(t)}{\sqrt{\eta}} - reg(t) * ABSE * (1-\eta)}{4} \quad (8)$$

Equation 8 is an intertemporal constraint to track changes in SOC. Charging and discharging power is modified by internal energy loss, which is characterized by the round-trip efficiency (η). The frequency regulation service does not directly affect SOC changes because we assume the regulation signal is designed to be energy neutral, as with PJM's dynamic signal for fast-responding resources [8]. However, frequency regulation causes rapid charging/discharging and therefore internal energy losses. ABSE is used to calculate the amount of energy processed while providing frequency regulation and the round-trip efficiency is used to convert this value into

energy losses. Again, we assume that the battery is never called to provide spinning reserve, and thus does not suffer any energy losses for this service. We divide by 4 to convert charge and discharge kW to kWh. Dividing regulation energy by 4 converts the hourly ABSE metric into a 15 minute metric. We ignore standby losses as they are small (~1-2% per month) [9], which causes us to slightly underestimate emissions rates and slightly overestimate revenues to the owner.

$$0 \leq c(t) \leq \bar{P} \quad (9)$$

$$0 \leq d(t) \leq \bar{P} \quad (10)$$

Equations 9 and 10 restrict the charging and discharging power to the rated power of the battery.

$$0.2 \leq soc(t) \leq \overline{SoC} \quad (11)$$

The state of charge (SOC), expressed as a fraction of total charge carrying capacity, is restricted to values between 20% and 100% in Equation 11. The lower limit of 20% is imposed to prevent degradation at low voltages. Lithium-ion batteries in electric vehicles have similar constraints imposed by car manufacturers [10].

$$reg(t) \leq \bar{P} - c(t) - d(t) - spin(t) \quad (12)$$

Equation 12 limits the amount of regulation capacity the battery can offer to the rated power of the battery minus any net charging or discharging of the battery and the capacity held for spinning reserve. In the customer ownership case where participation in ancillary service markets is not allowed, this equation is still valid and simply limits the charging and discharging of the battery.

$$\overline{SoC} \geq soc(t) + RDNE * reg(t)/4 \quad (13)$$

$$\overline{SoC} \leq 5 * (soc(t) - RUNE * reg(t)/4) \quad (14)$$

Equations 13 and 14 constrain the amount of regulation capacity the battery can offer based on the state of the charge of the battery. Equation 13 prevents the SOC from exceeding the maximum SOC while Equation 14 ensures a minimum 20% SOC. The frequency regulation signal will cause the battery to temporarily charge and/or discharge. We do not want the battery to violate the state of charge constraints at any time during regulation participation so we must adjust the regulation capacity offer to account for the maximum amount of net energy charge/discharge typically experienced while providing frequency regulation. We derive the values for RDNE (0.1 kWh/kW) and RUNE (0.2 kWh/kW) from 1 year of PJM regulation D signal [5] and express the value as a fraction of the regulation capacity offer. These parameters are set at the 97.5% percentile of the distribution of net energy charge/discharge during each hour of regulation signal, as opposed to the 100% percentile, to not overly constrict frequency regulation participation due to a few hours of atypical regulation signal patterns. The resulting values for RDNE and RUNE are very similar to the values of corresponding parameters used in EPRI's battery storage modelling for California (0.13 and 0.11, respectively) [11]. We then divide by 4 to convert RDNE and RUNE from hourly metrics to 15-minute metrics.

An anonymous reviewer correctly identified that our model does not implement a constraint to restrict simultaneous charging and discharging, which is functionally impossible, but could be economic in certain circumstances. In practice, our results contain no instances of simultaneous charging and discharging, obviating the need for this constraint.

Computational Methods

We have six optimization runs to perform for every choice of tariff scheme or battery configuration – three ownership perspectives mixed with two forecasting scenarios. In the perfect information scenarios, we feed an entire calendar month of data to the optimization model to minimize energy costs for that billing period. Some information, such as the battery state of charge and building net load are stored to initialize the next month's optimization run. We conduct 12 separate monthly optimizations for each building, totaling approximately 8,000 optimizations across all buildings. With a 12-core Intel Xeon E5-2680 v3 CPU at 2.5GHz and 64GB of memory this took approximately 10 minutes.

In reality, battery operation software would need to make operational decisions about the current time period using imperfect forecasts and update those forecasts as time progressed. Our persistence forecast scenarios therefore require much more computational effort. We conduct a rolling horizon optimization for each 15-minute window in which we save only the operational decision about the current period. We then step forward 15 minutes, make a new forecast, and re-optimize over the selected time horizon. We selected a horizon of 14 hours based on a set of trials to determine the best performance across horizon lengths. In this way, we conduct approximately 35,000 optimizations (1 year of 15-minute periods) for each building, totaling 23 million separate optimizations across all buildings. These optimizations were performed on the Bridges Supercomputer at the Pittsburgh Supercomputing Center through an allocation by the National Science Foundation's Extreme Science and Engineering Discovery Environment (XSEDE) Program [12]. A single computing node with two 14-core Intel Xeon E5-2695 v3 CPU at 2.3GHz and 128GB of memory took approximately 3 hours to run all buildings for a single set of parameters. Sensitivity analysis was performed by feeding multiple parameter scenarios to different computing nodes at the same time.

The persistence forecasts were generated by averaging the changes in load between consecutive periods for the same 15 minute interval in the preceding 8 days of a similar day-type (weekday or weekend). For example, if we are generating the forecast for a Wednesday at 8:15am, we average the change in load for the previous 8 weekdays between 8:00am and 8:15am. We build the forecast by adding these changes in load to the current period's actual load. Taking the average of the change in load rather than the load itself allows us build load forecasts that make sense in the context of the last known load level. Simply using the average of the historical load would produce discontinuous jumps between the load in the current period and the first forecasted period.

Software Used

The battery configuration, data and optimization parameters are initially set in MATLAB. MATLAB selects the appropriate window of data for each building and performs the persistence forecasts. These data are written to a .GDX file that can be read by the optimization software. MATLAB creates a set of parallel workers on all but one available core (to allow for a "scheduling" core) and the parallel code is executed via a parallel loop. When the optimization software finishes its routine, the results are again written to a .GDX file which MATLAB can read and store. The battery optimization is performed in the General Algebraic Modeling System (GAMS) using the CPLEX solver.

Additional Model Details

Battery Sizing

As stated in the main article, battery power is sized to 20% of the building's peak load under base case assumptions. However, for some buildings the coefficient of variation of load was low

and sizing battery power as a percentage of peak load would drastically oversize the battery (see Figure B-7). Some of these batteries would have more capacity than would be required to completely flatten the building's load profile. In these circumstances, the batteries were sized to be no greater than 50% of the total annual range of load. This reduced the weighted average battery size across all buildings to 17% of peak load.

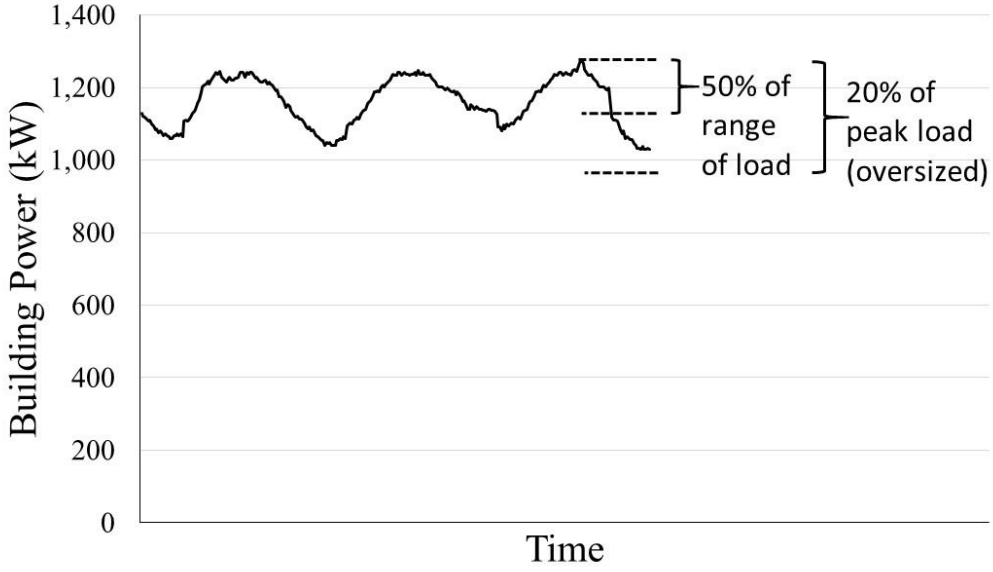

Figure B-7: Battery sizing for buildings with low coefficient of variation of load. Sizing to 20% of peak load would oversize the battery. In these cases, batteries were sized to 50% of annual range of load.

Discount Rate

Our base case results use a discount rate of 15%, which some may consider high for commercial and industrial firms. While rational commercial firms may evaluate investment decisions using a weighted average cost of capital around 7-10%, there is evidence that gaps in information [13], the "principal-agent" problem [14], and ingrained institutional behaviors raise the implicit discount rate to higher levels, even among commercial firms which are thought of as more energy-savvy. A survey by the Pew Center on Global Climate Change [15,16] of large

companies found that most use a simple payback metric to evaluate energy efficiency investments (which we believe they would extend to energy storage investments), and all of these companies used a threshold of 5 years or less. Based on this 5-year threshold, we chose a discount rate where the number of buildings with a simple payback less than 5 years closely matches the number of buildings with a net present value ratio greater than 1. With a 15% discount rate, the number of buildings that satisfy those criteria are often within 1-2% of each other. See figure B-20 for a sensitivity analysis of the results to discount rate.

Battery Lifetime

The economics of all battery storage systems are sensitive to the length of useful life of the equipment. In the main manuscript, we assume a value of 10 years, which is commonly used in many studies. Additionally, SonnenBatterie warrants their battery systems for 10 years or 10,000 cycles [17]. The average number of annual cycles for the batteries in our model was 84 – or only 840 cycles at 10 years. Batteries used mainly for peak shaving applications are only used on a few days of the month. The maximum for any battery was 385 annual cycles, or 3,850 cycles in 10 years. We believe that the 10 year lifetime assumption is well within the feasible range for these systems. Please see Figure B-20 for a sensitivity analysis of battery lifetime.

Calculating Delivered Energy While Performing Frequency Regulation

Emissions results presented in this paper are normalized to the amount of energy delivered by the battery for ease of comparison to emissions values from other generation sources and emissions studies. The amount of energy delivered while performing frequency regulation is not a straightforward calculation – it depends on what other services the battery is providing at the same time.

1. Frequency Regulation Only – if the battery is only performing frequency regulation, we estimate the delivered energy by multiplying the capacity offered for frequency regulation by half the value of the ABSE metric. Since we assume the frequency regulation signal is energy neutral over a given timeframe, the amount of energy delivered during that timeframe must be half the total energy processed.
2. Frequency Regulation while Charging – if the battery is charging and providing frequency regulation, we estimate that it will deliver zero energy if the charge energy is higher than half the ABSE times the regulation capacity offered. In other words, if the battery is charging at a sufficiently fast rate we assume that dips in the frequency regulation signal will not cause the battery to discharge at any point while providing this service. If the charge energy is lower than half the ABSE times the regulation capacity offered, we subtract the former from the latter to calculate the delivered energy.
3. Frequency Regulation while Discharging – similarly, if the battery is discharging and providing frequency regulation, we make no adjustments to the delivered energy from discharging as long as the discharge energy is more than half the ABSE times the regulation capacity offered. If not, we adjust the delivered energy from discharging by half the ABSE times the regulation capacity offered.

Summary of Model Parameter Assumptions

Table B-3: Summary of Model Parameter Assumptions

Parameter	**Description**	**Assumption (sensitivity)**
Battery Size (kW)	Chosen battery size as a percentage of building peak load	20% (15-25%)
Duration (hr)	Duration of battery	1 (0.5 – 4)

Parameter	Description	Assumption (sensitivity)
	discharge at full rated power	
System installation cost ($/kWh + $/kW)	Installed cost of battery system, broken into power and energy components	$600/kWh + $400/kW (33% - 100% of costs)
Round-trip efficiency (%)	Internal energy losses suffered in storing and then discharging power	83% (83 – 91%)
Battery Lifetime (years)	Years that all system components will last	10 (5-20)
Discount Rate	Discount rate used to value future cash flows	15% (5-20%)

Additional Results

Emissions – Perfect Forecast

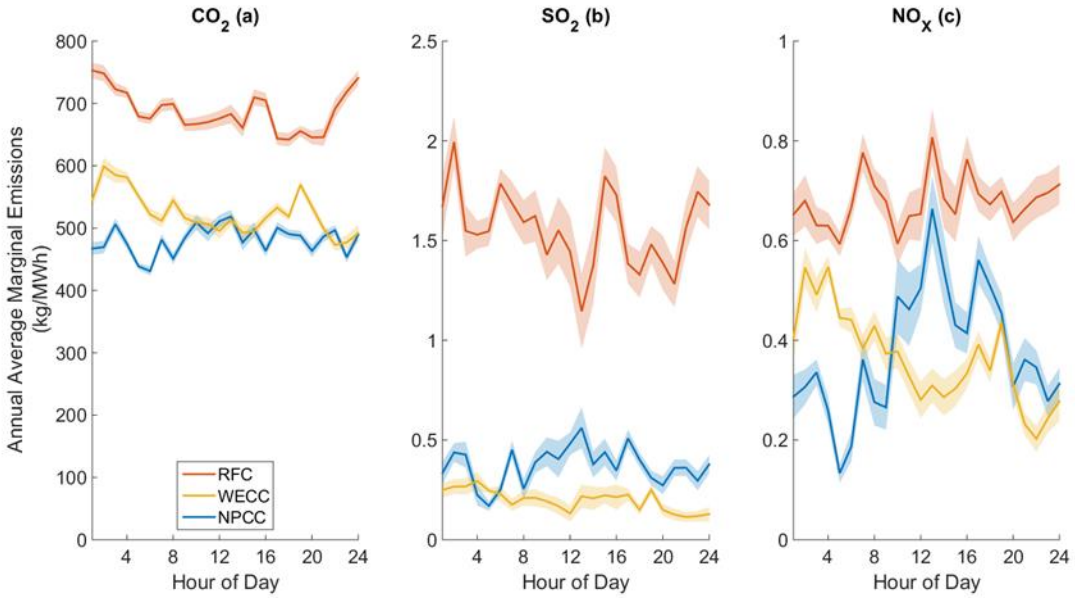

Figure B-8: 2014 annual average marginal CO2 (a), SO2 (b), and NOx (c) emission rates by time-of-day and NERC region. Data from Siler-Evans, et al [18,19]. Shaded areas represent one standard error in the regression coefficients used to estimate the emission rates.

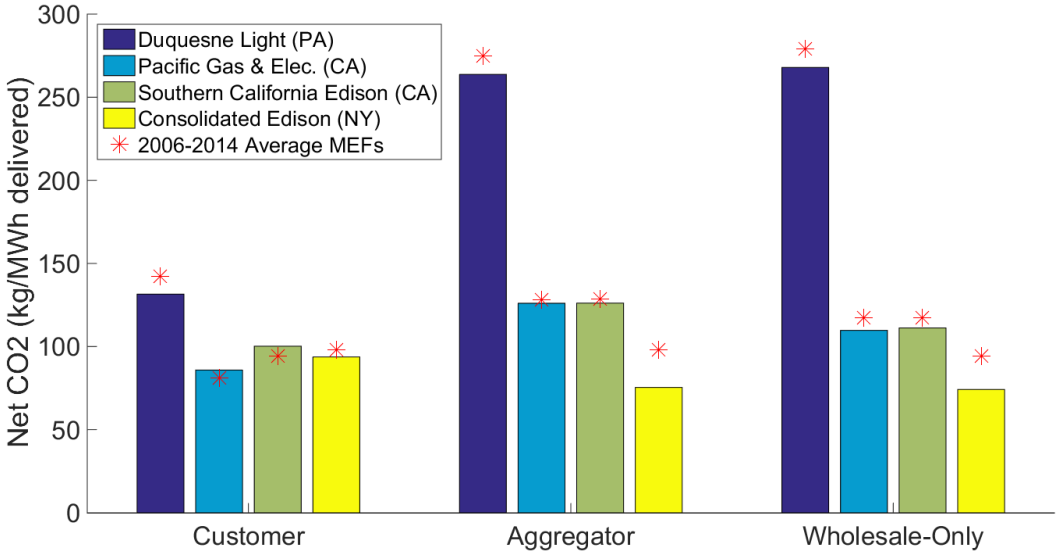

Figure B-9: Net CO2 emission rates using 2014 MEFs vs 2006-2014 average MEFs. Colored bars show results using 2014 MEFs, which were presented in the main article (Figure 3-3). Red asterisks show results using 2006-2014 average MEFs.

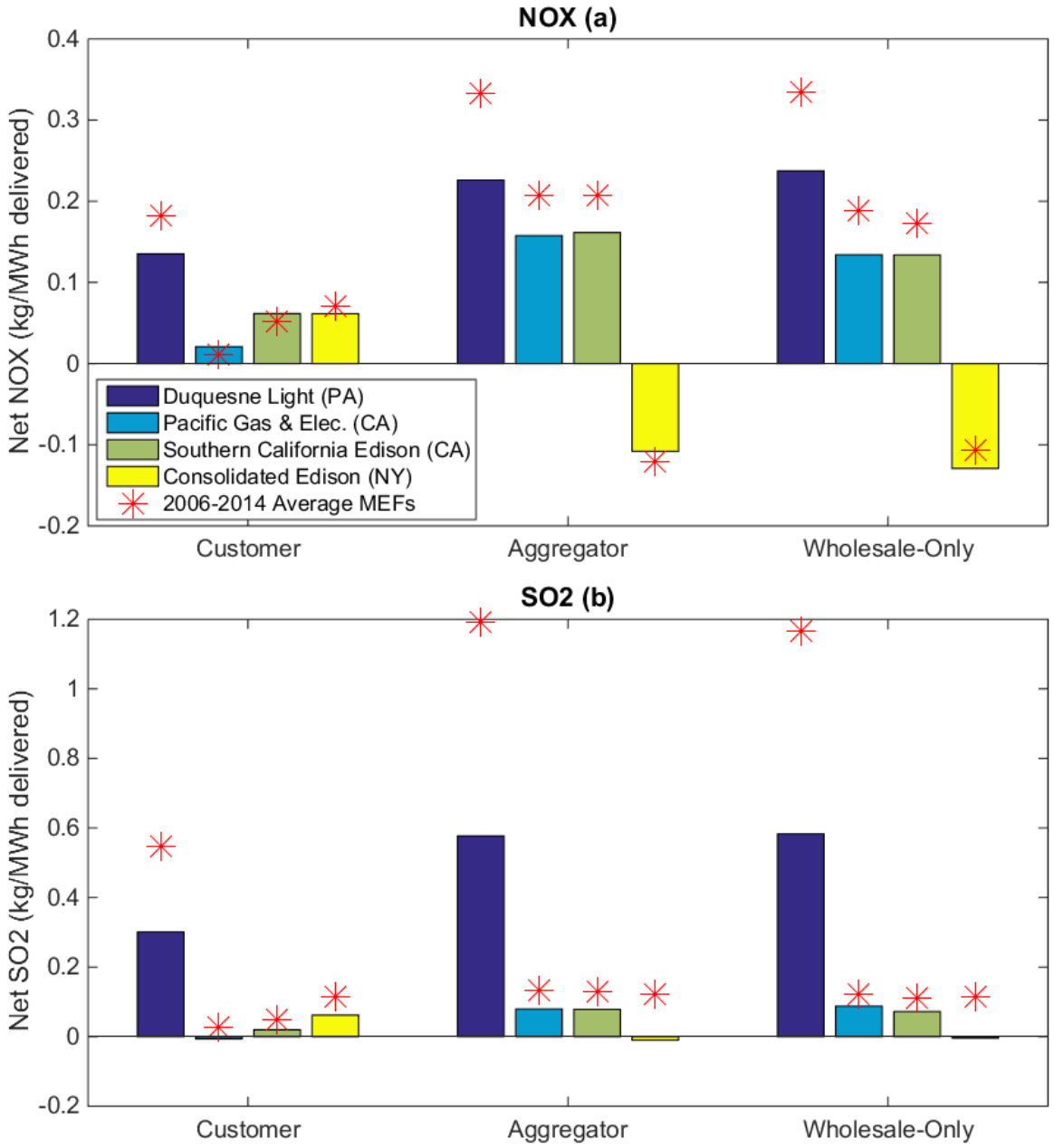

Figure B-10: Net NOx (a) and SO2 (b) emission rates using 2014 MEFs vs 2006-2014 average MEFs. Colored bars show results using 2014 MEFs, which were presented in the main article. Red asterisks show results using 2006-2014 average MEFs.

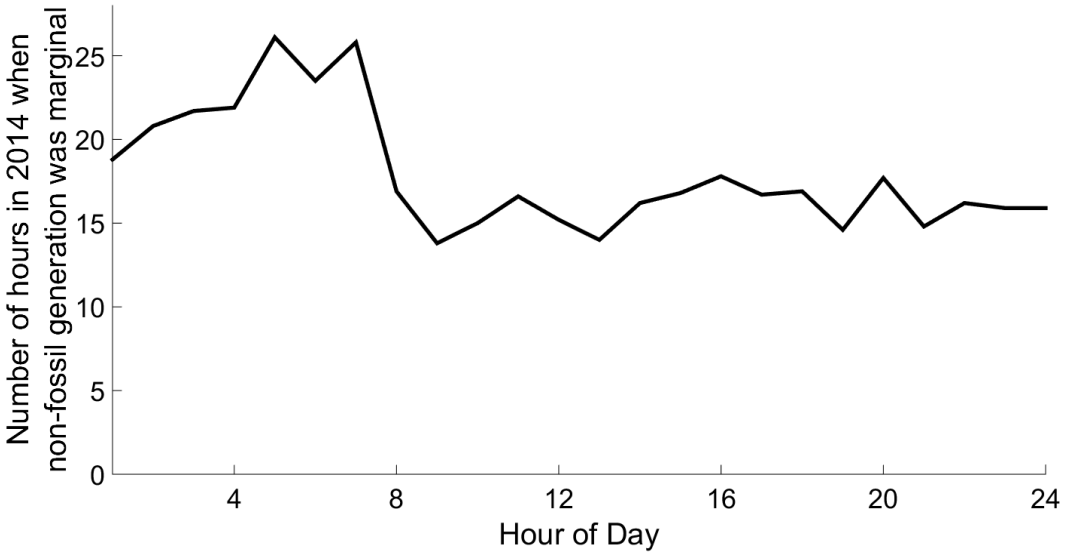

Figure B-11: Number of hours in 2014 when non-fossil generation was the marginal fuel in PJM. Non-fossil fuels include wind (400 hours), land fill gas (20), municipal waste (5), demand response (5), solar (~0), and biomass (~0).

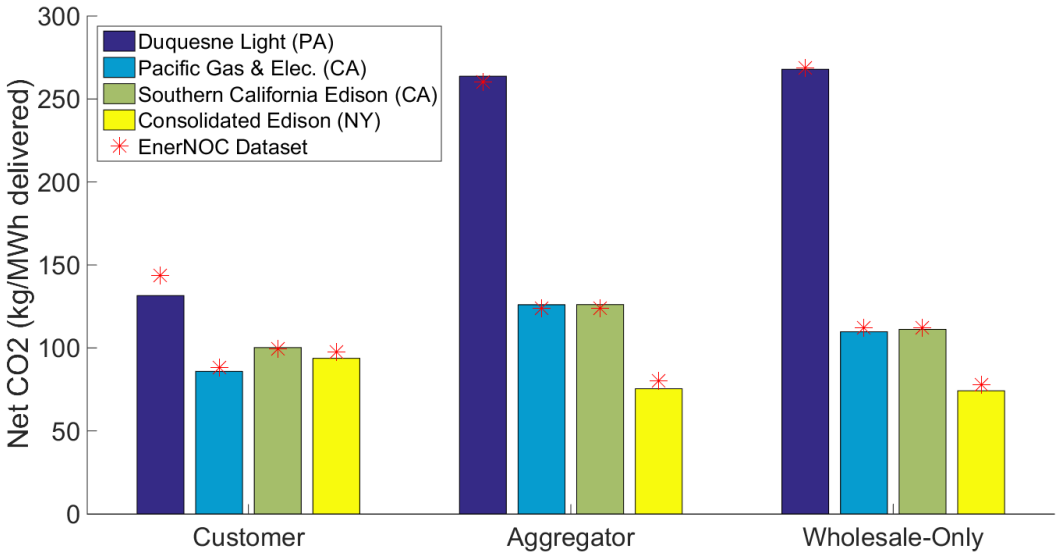

Figure B-12: Net CO2 emission rates using 2014 MEFs from Carolinas dataset vs EnerNOC dataset. Colored bars show results using Carolinas dataset, which were presented in the main article (Figure 3-3). Red asterisks show results using EnerNOC dataset of 100 buildings. See Figure B-14 for EnerNOC building locations.

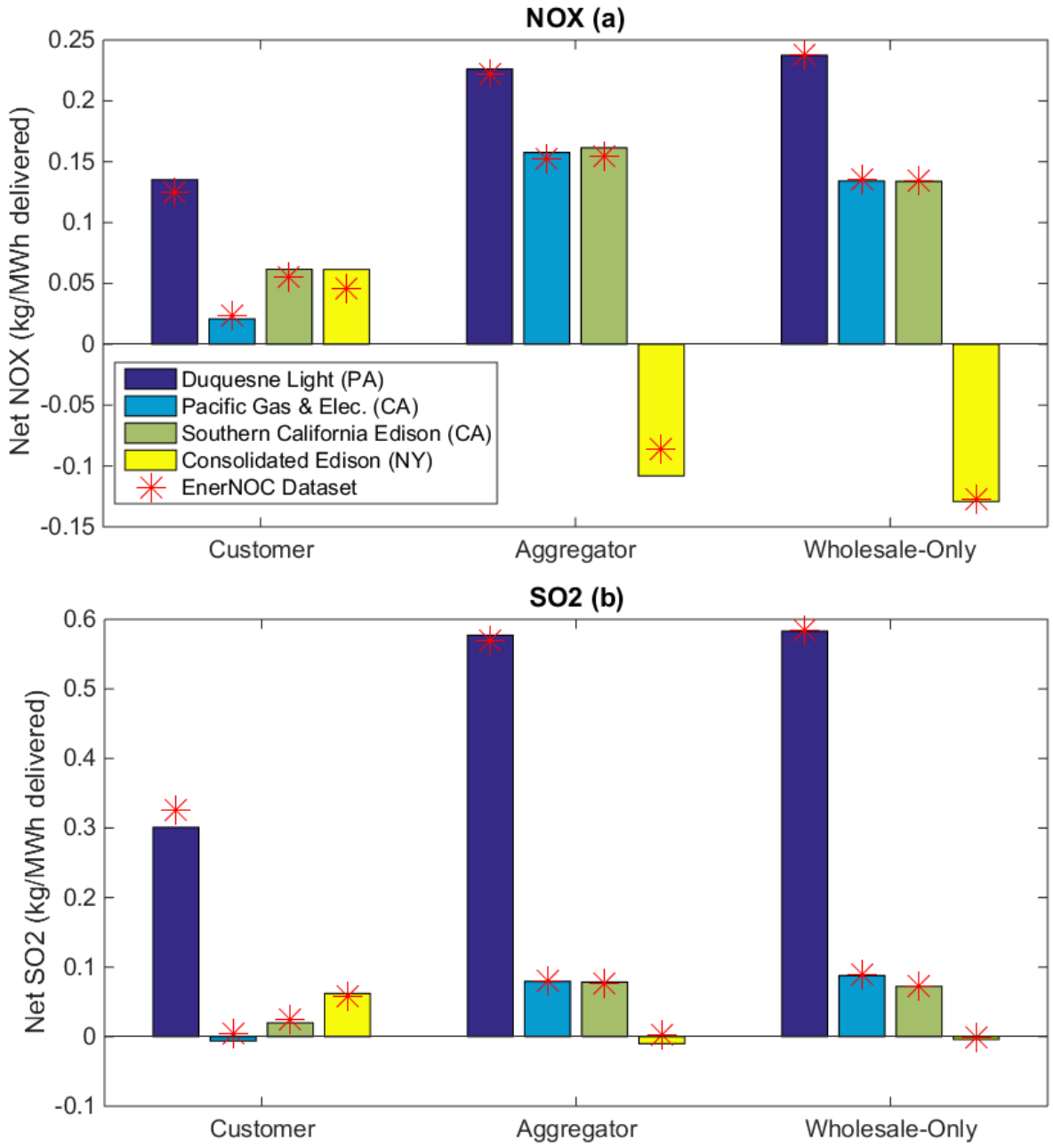

Figure B-13: Net NOx (a) and SO2 (b) emission rates using 2014 MEFs from Carolinas dataset vs EnerNOC dataset. Colored bars show results using Carolinas dataset, which were presented in the main article (Figure 3-3). Red asterisks show results using EnerNOC dataset of 100 buildings. See Figure B-14 for EnerNOC building locations.

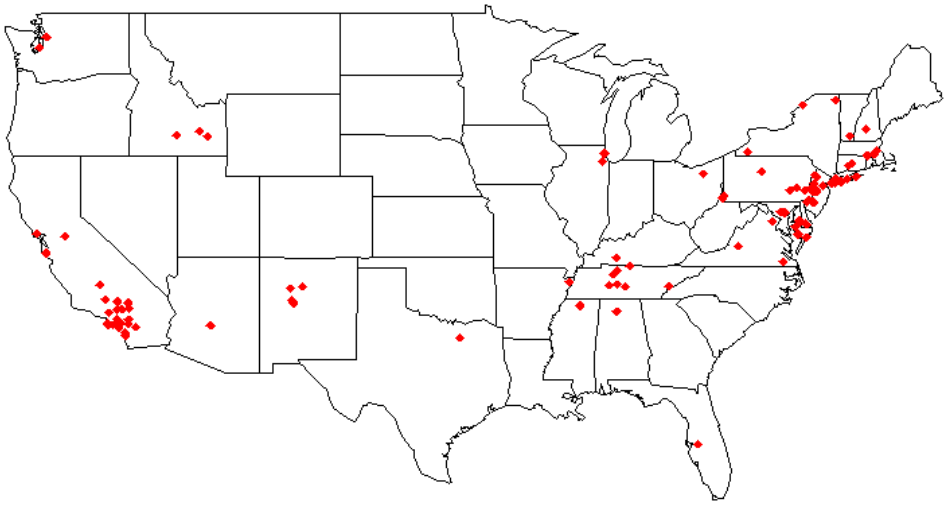

Figure B-14: Approximate location of 100 buildings in EnerNOC building dataset.

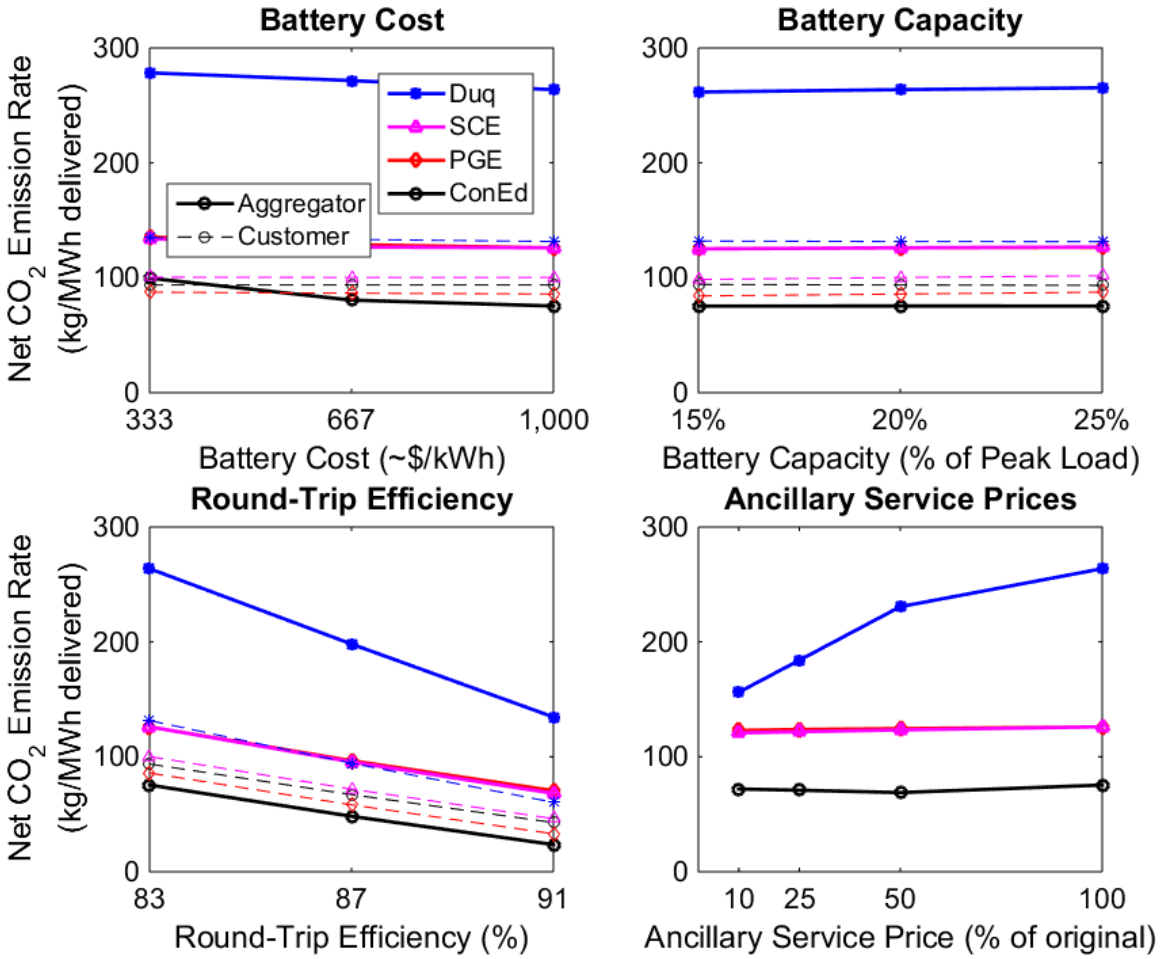

Figure B-15: Sensitivity of net CO2 emission rate to battery traits and market conditions. In our model, lower capital costs lead to higher capacity factors and thus larger emission rates. Lower battery cost can actually boost revenue by decreasing perceived degradation costs. A drop in degradation costs depresses the threshold for profitable participation in peak shaving or ancillary services, allowing the battery to generate more revenue through higher utilization.

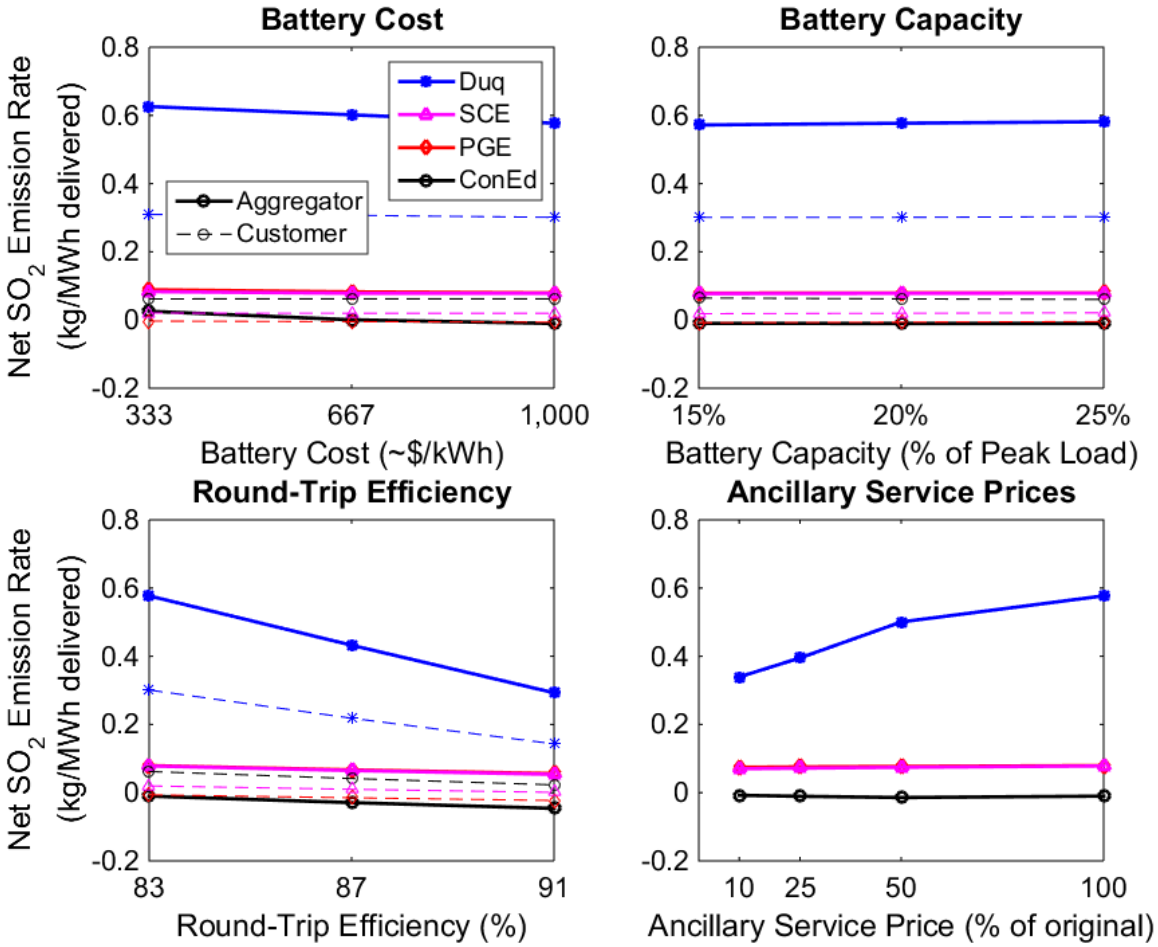

Figure B-16: Sensitivity of net SO2 emission rate to battery traits and market conditions.

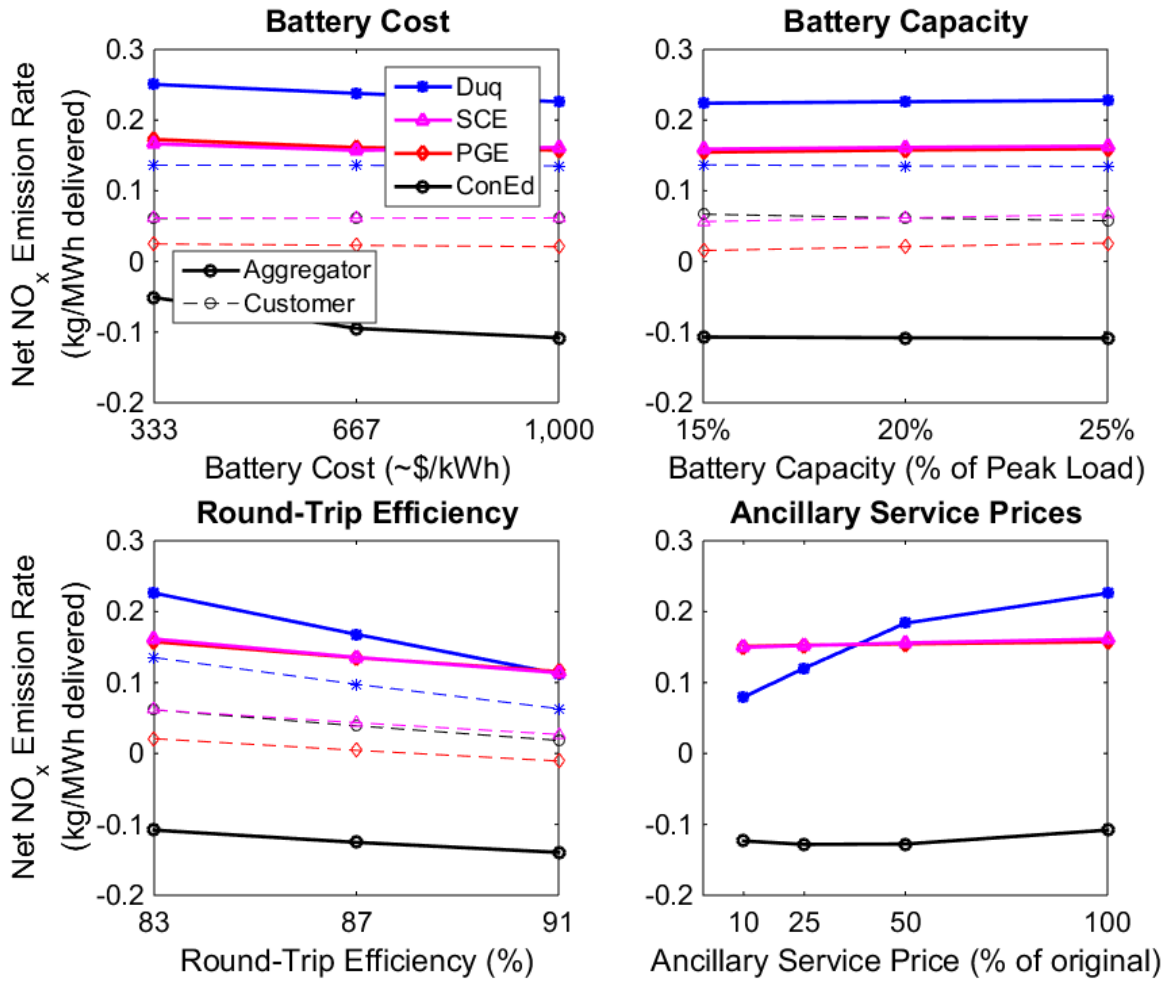

Figure B-17: Sensitivity of net NOx emission rate to battery traits and market conditions.

Economics – Perfect Forecast

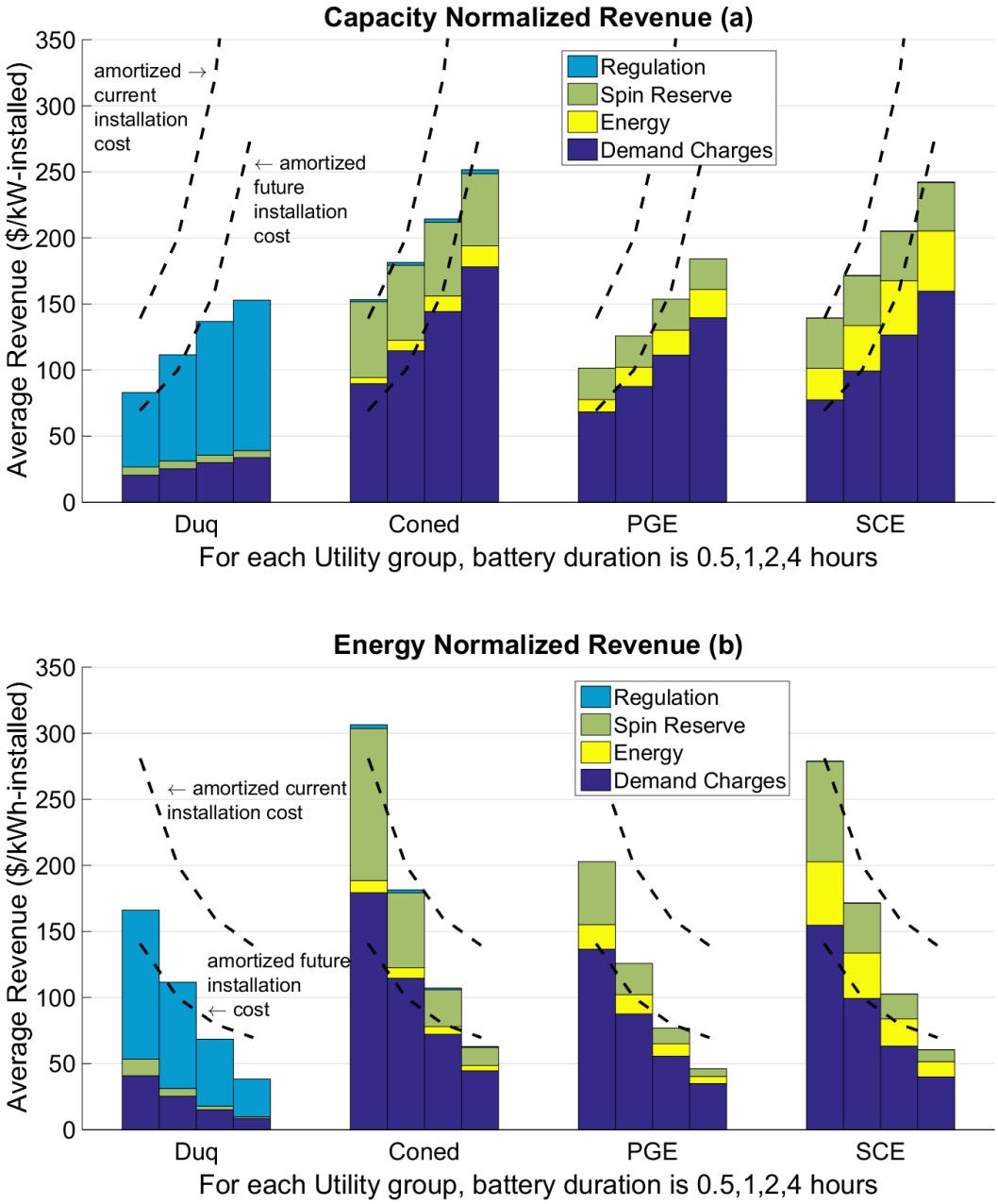

Figure B-18: Breakdown of capacity normalized (a) and energy normalized (b) average revenue by service for each utility across different battery durations. Current and future amortized installation costs are given by dashed lines for comparison. A Lazard survey [20] of industry participants estimates battery costs could fall by approximately 50% in the next 5 years.

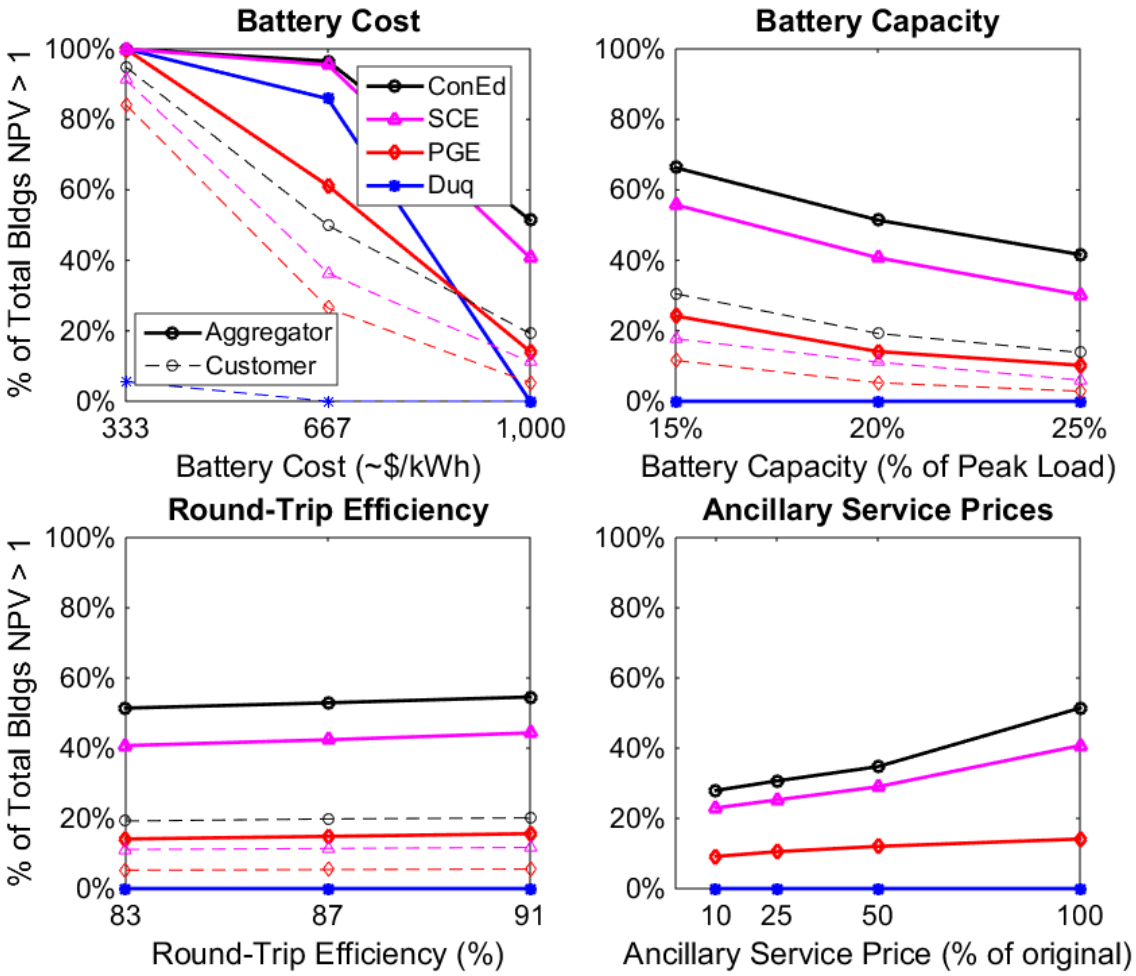

Figure B-19: Sensitivity of economic results to battery characteristics and market conditions.

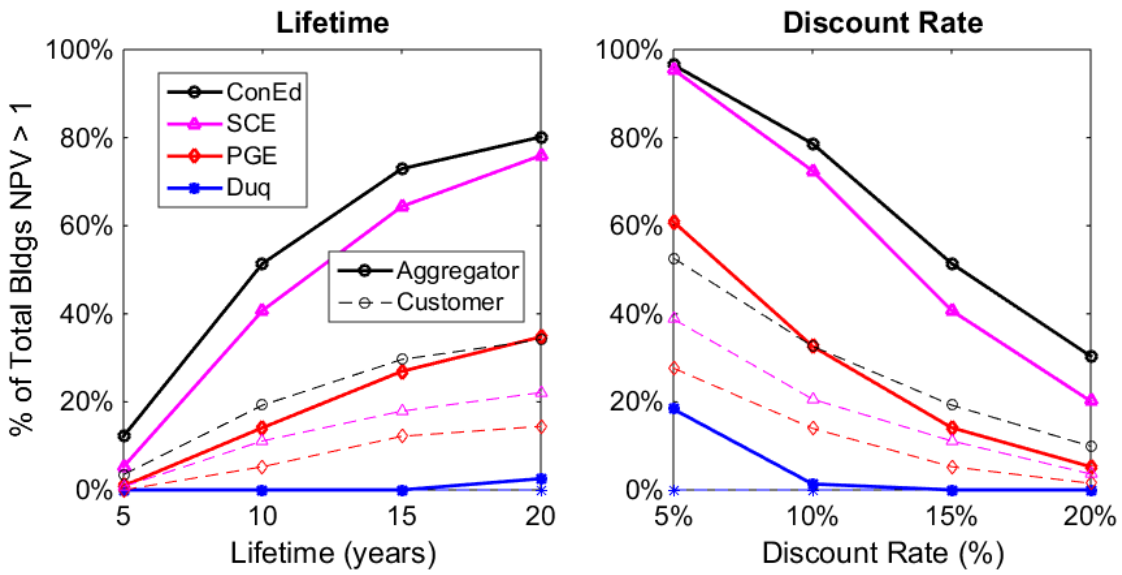

Figure B-20: Sensitivity of economic results to financial assumptions.

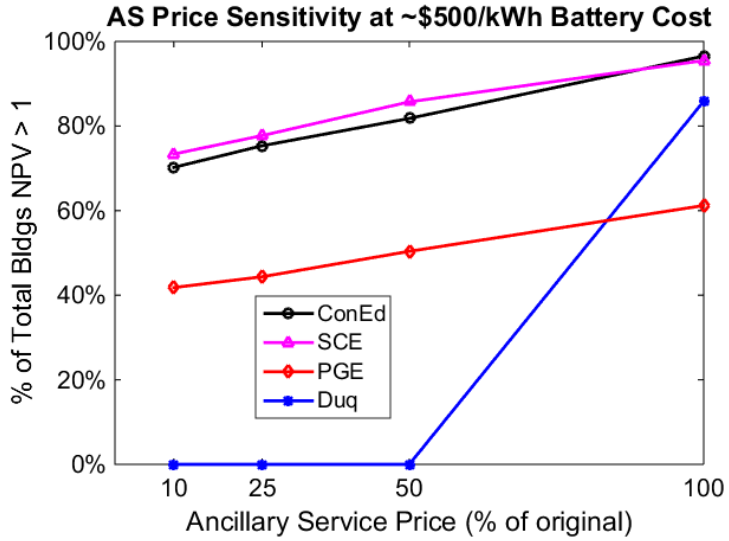

Figure B-21: Sensitivity of economic results to ancillary service prices when battery cost declines ~30% to $400/kWh + $267/kW. Duquesne Light is extremely sensitive to ancillary service prices because a large proportion of battery revenue is derived from frequency regulation.

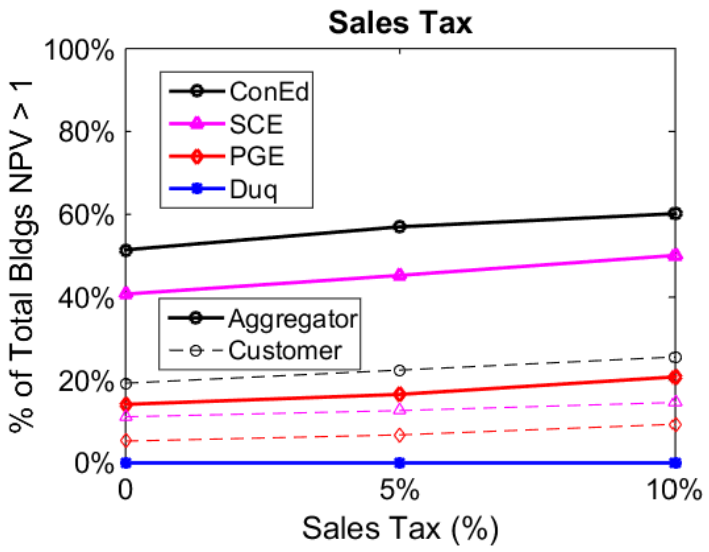

Figure B-22: Effect of sales tax on project economics. Sales taxes are assessed on customer energy bills. The consideration of sales tax improves project economics because batteries lower total energy bills, and therefore taxes. The main article does not consider sales taxes for ease of comparison across utility tariffs.

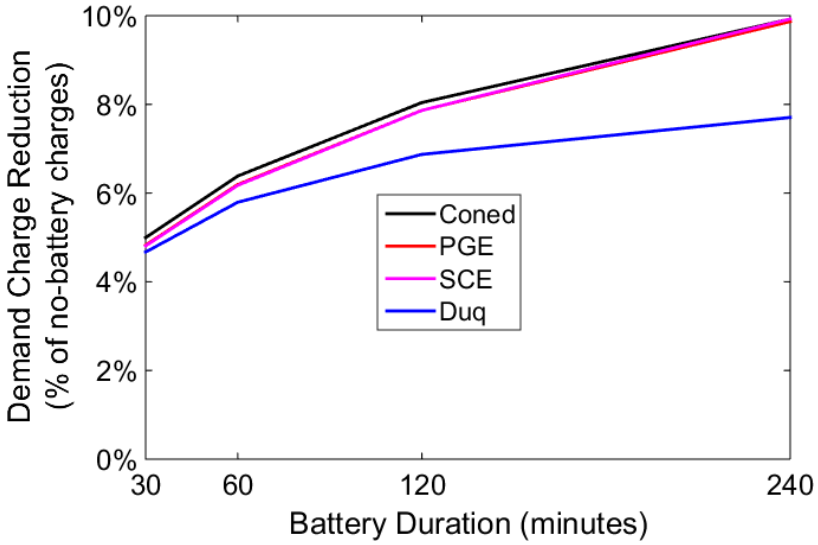

Figure B-23: Demand charge reduction under aggregator ownership across different battery durations. Aggregators are able to mitigate 6% of demand charges with a 60-minute battery sized to 20% of peak load while increasing customer energy costs by only 0.1%.

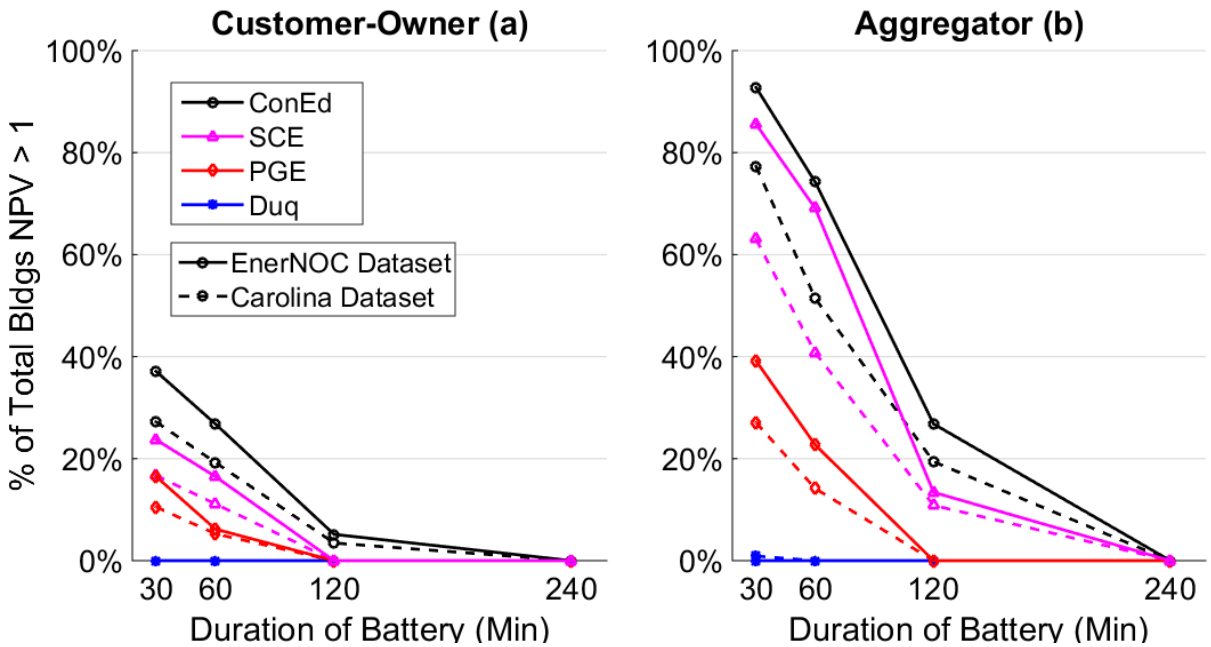

Figure B-24: Comparison of economic results between Carolinas dataset and EnerNOC dataset. Results are similar for customer owners (a) and aggregators (b) between datasets despite differences in location and building-type composition. The load factor (ratio of average load to peak load) of the EnerNOC dataset is lower, which may explain why a larger percentage of buildings have NPV>1 (batteries favor "peakier" buildings). See Figure B-14 for EnerNOC building locations.

Persistence Forecast Results

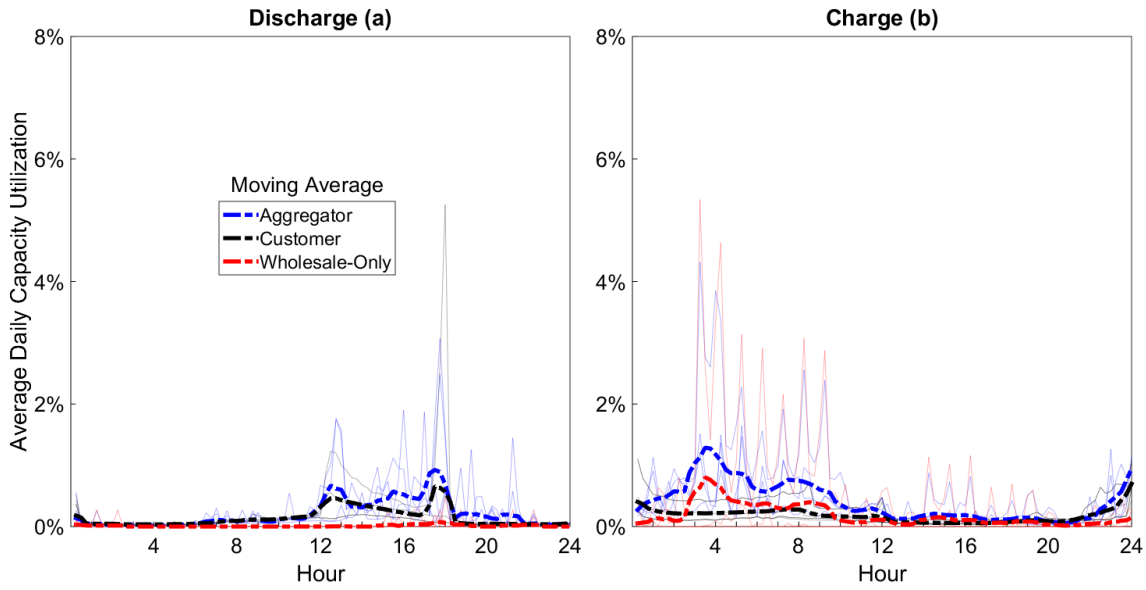

Figure B-25: Average daily discharging (a) and charging (b) profile of battery fleet under perfect forecasts. Light solid lines are individual profiles for each ownership perspective and utility region. Heavy dotted lines represent an hourly moving average of all utility regions for a particular ownership perspective. Average capacity utilization is lower than in perfect forecast scenarios because the persistence algorithm does not forecast peak loads accurately, leading to missed load shifting opportunities and thus fewer profitable opportunities to use the battery.

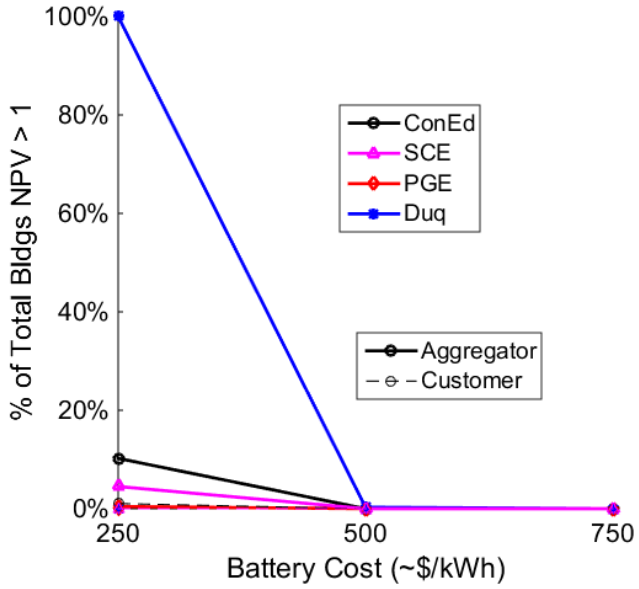

Figure 3-4: Sensitivity of economic results to system cost under persistence forecasts.

In all other parameter scenarios, there are no buildings that have NPV > 1.

References

[1] Itron, 2013 SGIP Impact Evaluation, Pacific Gas & Electric, 2015. http://www.cpuc.ca.gov/General.aspx?id=7890.

[2] Frequency Regulation Compensation in the Organized Wholesale Power Markets, 2011. https://www.ferc.gov/whats-new/comm-meet/2011/102011/E-28.pdf.

[3] OpenEI Utility Rate Database, (2016). http://en.openei.org/wiki/Utility_Rate_Database# (accessed September 6, 2016).

[4] S.B. Peterson, J. Apt, J.F. Whitacre, Lithium-ion battery cell degradation resulting from realistic vehicle and vehicle-to-grid utilization, J. Power Sources. 195 (2010) 2385–2392. doi:10.1016/j.jpowsour.2009.10.010.

[5] PJM RTO Regulation Signal Data, PJM Ancillary Serv. (2015). http://www.pjm.com/markets-and-operations/ancillary-services.aspx (accessed January 10, 2015).

[6] PJM Ancillary Services, (n.d.). http://www.pjm.com/markets-and-operations/ancillary-services.aspx (accessed January 1, 2016).

[7] S.S. Choi, H.S. Lim, Factors that affect cycle-life and possible degradation mechanisms of a Li-ion cell based on LiCoO2, J. Power Sources. 111 (2002) 130–136. doi:10.1016/S0378-7753(02)00305-1.

[8] Order on Compliance Filing, Washington, D.C., 2012. https://www.ferc.gov/whats-new/comm-meet/2012/051712/E-4.pdf.

[9] M. Broussely, S. Herreyre, P. Biensan, P. Kasztejna, K. Nechev, R.. Staniewicz, Aging mechanism in Li ion cells and calendar life predictions, J. Power Sources. 97–98 (2001) 13–21. doi:10.1016/S0378-7753(01)00722-4.

[10] M. Eberhard, A Bit About Batteries, Tesla Mot. Blog. (2006). https://www.teslamotors.com/blog/bit-about-batteries (accessed January 1, 2016).

[11] B. Kaun, S. Chen, Cost-Effectiveness of Energy Storage in California: Application of the EPRI Energy Storage Valuation Tool to Inform the California Public Utility Commission Proceeding R. 10-12-007, Palo Alto, CA, 2013. http://www.epri.com/abstracts/Pages/ProductAbstract.aspx?ProductId=000000003002001162.

[12] J. Towns, T. Cockerill, M. Dahan, I. Foster, K. Gaither, A. Grimshaw, V. Hazlewood, S. Lathrop, D. Lifka, G.D. Peterson, R. Roskies, J.R. Scott, N. Wilkens-Diehr, XSEDE: Accelerating Scientific Discovery, Comput. Sci. Eng. 16 (2014) 62–74. doi:10.1109/MCSE.2014.80.

[13] H. Allcott, M. Greenstone, Is There an Energy Efficiency Gap?, J. Econ. Perspect. 26 (2012) 3–28. doi:10.1257/jep.26.1.3.

[14] S.J. DeCanio, Barriers within firms to energy-efficient investments, Energy Policy. 21 (1993) 906–914. doi:10.1016/0301-4215(93)90178-I.

[15] W. Prindle, A. de Fontaine, A Survey of Corporate Energy Efficiency Strategies, in: ACEEE Summer Study Energy Effic. Build., 2009. http://www.c2es.org/docUploads/Final ACEEE survey paper.pdf.

[16] W. Prindle, From Shop Floor to Top Floor: Best Business Practices in Energy Efficiency, Pew Center on Global Climate Change, 2010. http://www.c2es.org/docUploads/PEW_EnergyEfficiency_FullReport.pdf (accessed January 1, 2016).

[17] SonnenBatterie Pro, SonnenBatterie. (2016). https://sonnen-batterie.com/en-us/sonnenbatterie?_ga=1.42115749.10813948.1465480047#sonnenbatterie-pro (accessed September 6, 2016).

[18] K. Siler-Evans, I.L. Azevedo, M.G. Morgan, Marginal Emissions Factors for the U.S. Electricity System, Environ. Sci. Technol. 46 (2012) 4742–4748. doi:10.1021/es300145v.

[19] K. Siler-Evans, I.L. Azevedo, M.G. Morgan, J. Apt, Regional variations in the health, environmental, and climate benefits of wind and solar generation, Proc. Natl. Acad. Sci. 110 (2013) 11768–11773. doi:10.1073/pnas.1221978110.

[20] Lazard's Levelized Cost of Storage Analysis - Version 1.0, Lazard, 2015. https://www.lazard.com/media/2391/lazards-levelized-cost-of-storage-analysis-10.pdf.

Chapter 4: A Simple Metric for Predicting Revenue from Electric Peak-Shaving and Optimal Battery Sizing

Abstract

Quantifying the value proposition of behind-the-meter (BTM) storage for individual customers currently requires an optimization model, the development of which can be costly in human and computing resources. We disclose here a simple econometric model to predict revenue from retail peak-shaving. Geared toward electric utilities, third-party storage providers and consumers, this model eliminates the need to formulate a model in specialized optimization software. The model is based on a novel predictive metric that is derived from the building's load profile. While our model is easier to implement, it is somewhat less accurate than an optimization model, and we quantify this added uncertainty. During model fitting, we discovered that the revenue estimates generated are independent of the power capacity of the battery if the maximum power-to-energy ratio of the storage is held constant. This effect can be used to calculate the profit-maximizing storage size, which we explore in a case study.

This paper was submitted to the Journal of Energy Technology in July 2017 with co-authors Jay Whitacre and Jay Apt.

4.1 Introduction

Commercial and industrial behind-the-meter (BTM) electricity storage is growing rapidly [1] as a way for customers to offset utility demand charges and for utilities to procure distributed capacity resources [2]. As storage costs fall and demand increases, utilities and other third-party storage providers marketing to retail customers face a familiar problem: which customers benefit most from BTM storage and how are these cases identified [3]? The optimization models required to answer these questions necessitate sophisticated software and in-house expertise which many organizations may not have. We present here a novel metric, called the "threshold ratio," which can be used in a univariate econometric model to predict peak-shaving revenue for individual customers and the corresponding profit-maximizing battery size. The metric is derived exclusively from the customer's load shape and no optimization model is required. The econometric model distills much of the complexity of an optimization model into a simple non-linear equation with one variable.

A wide body of work has investigated the use of storage to reduce energy costs in current markets or plausible future scenarios. For example, research has been done on wholesale market participation [4–6], storage paired with renewable generation [7–9], and electric cars [10,11]. Much of this work relies on mathematical programming models to calculate the change in energy costs when installing storage. In this study, we develop an alternative to mathematical programs that can be used by non-experts to calculate potential revenue from storage under one particular use-case (demand charge reduction).

The literature concerning predictive metrics for the economics of a BTM peak-shaving battery is generally focused on analyses of regional demand charges [12–16] rather than on the characteristics of load shape that drive economics. An assessment of demand charges can

indicate which regions may be appropriate for BTM storage, but cannot identify promising individual customers. There is a related literature on the optimal sizing of storage that explores mathematical programming methods by which one could size storage. Prior work has explored optimal sizing for grid load-leveling [4,17–20], hybrid renewable/storage installations [21–23], and BTM storage for peak shaving. Mathematical programming methods are useful and accurate, but can require significant expertise and computational time. For example, Oudalov, et al. [24] investigated optimal battery sizing for peak shaving, but their exhaustive search algorithm requires the computation of net battery profits using an optimization model at multiple discrete battery sizes in order to find the global optimum. Oh and Son [25] designed a gradient search algorithm for optimal sizing, but this still requires an optimization model to compute net battery profits at each iteration of battery size. Neither quantitatively characterize the tradeoff between battery size (cost) and potential profit. While understanding these methods is useful, this literature does not identify the underlying characteristics of building load shapes that drive battery economics, and it does not allow for non-expert stakeholders to calculate potential revenue or properly size storage resources.

Wu, et al. [26] formulated a novel analytical solution to the optimal sizing problem that does not rely on mathematical programming. However, they make use of a restrictive assumption that may not be satisfied in practice. Their solution assumes that the building load profile monotonically increases from valley to peak and back to valley again. Of the hundreds of metered building load profiles used in our work, none satisfy this condition. While we do not have an analytical solution, we have developed a more general approach that makes use of empirical data.

Our model constitutes a tool for practitioners and incorporates load shape and demand charges in predicting revenue for individual customers. In this paper, we explore the relationship between our new metric, the *threshold ratio*, and annual revenue from peak shaving, where peak shaving revenue is calculated using a battery optimization model designed to minimize total energy cost. We quantitatively determine this relationship for many battery duration / demand charge scenarios by fitting an exponential curve, which leads to an easy-to-use econometric model for storage providers. By calculating the threshold ratio for each customer and mapping it onto the appropriate curve, storage providers can quickly understand which customers have sufficient revenue potential over the accepted return on investment period to justify the installation cost of a battery system. Paired with knowledge of local installation costs, storage providers can also use this information to find the profit-maximizing battery size. To demonstrate this, we provide a case study showing the use of the threshold ratio in both revenue prediction and optimal sizing.

4.2 New Metric Development – the Threshold Ratio

The metric for storage revenue prediction we call the threshold ratio is based on two observations. First, the economics of customer-side storage are largely determined by avoiding charges for peak demand. Second, a battery's ability to reduce demand charges is a function of the total energy consumed during the largest load spike per billing period relative to the total energy capacity of the battery. While there are other factors (e.g., recharge period) that contribute to this effect, we ignore them in favor of a simpler model. The threshold ratio allows a storage provider to use a simple characteristic of the customer load shape to size the battery system.

In this section, for pedagogical reasons we first discuss an intermediate metric called the "spike-to-battery" ratio that relates the energies in the load spike and battery. This metric does not fully capture how load shape contributes to demand charge reduction potential, so a "threshold" ratio is derived from the spike-to-battery ratio to provide this information. The threshold ratio alone is ultimately used for revenue prediction.

We characterize a battery in terms of power (kW) and energy (kWh) capacity. The ratio of energy capacity to power capacity gives the battery's duration of discharge at full power. For example, a 20kWh / 10kW - rated battery would have a minimum discharge duration of 2 hours provided that the battery is able to deliver its full energy at the necessary current level.

4.2.1 An Intermediate metric: the Spike-to-Battery Ratio

We begin by finding the largest energy spike (in kWh) above a target load (equation 2). The target load (kW) is set equal to the maximum building load (kW) minus the battery power capacity (kW) in equation 1. We do this for each month and building in the dataset. Battery power capacity, and thus the target load, is treated parametrically in this analysis. Each time the building load exceeds the target, the total kWh consumed above the target load is calculated until the spike ends as the load drops below the target. We presume that the battery can be recharged as needed during times when the actual load is below the load target. Figure 4-1 provides a hypothetical example of this routine, where there are 4 load spikes above the target load (in solid black). We note the number of kWh in the largest spike for that billing period (in our case, one calendar month) for future calculations. No other information is retained.

$$Target = \max_{t \in T}(Load_t) - kW_{Bat} \quad (1)$$

$$MaxSpike = \max_{S}\left(\sum_{t \in S_i}[Load_t - Target]\,/4\right) \quad (2)$$

Where T is all time segments t in the billing period. kW_{Bat} is the rated power of the battery. S is the set of all spikes S_i. A spike is defined as a contiguous period where building load is greater than the target load ($Load_t \geq Target$). The *MaxSpike* formula is divided by 4 to convert power to energy for 15-minute intervals.

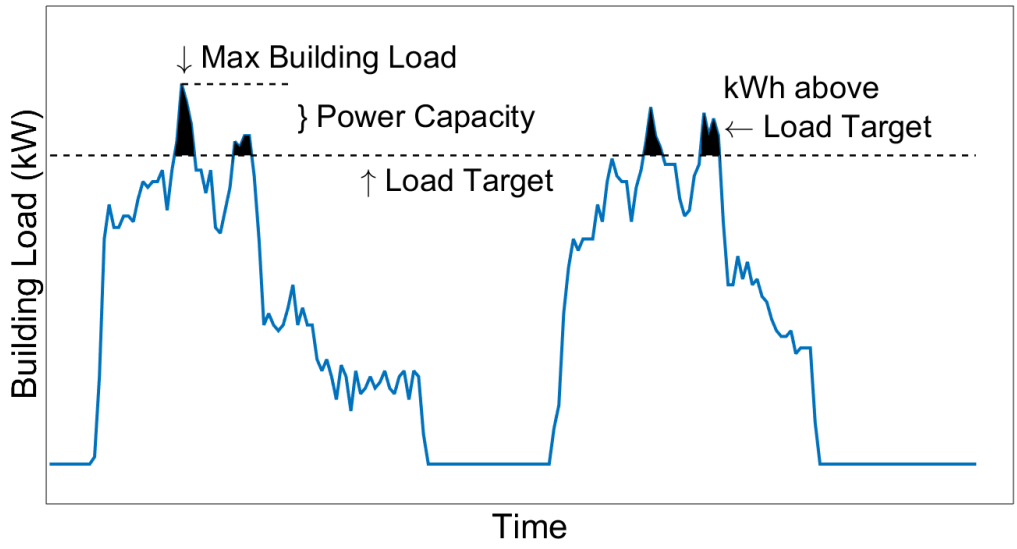

Figure 4-1: Example calculation of energy consumed above load target. There are 4 spikes above the load target. Only the number of kWh from the largest spike is recorded.

A single normalized ratio for each building is calculated by taking the median energy spike value of the 12 monthly values and dividing it by the battery energy capacity (equation 3). This provides a convenient unit-less ratio to describe the size of the maximum load spike (a ratio of 1 indicates that the typical maximum load spike in a billing period is the same size as the battery). Calculating the mean instead of the median does not significantly affect the resulting model fit.

$$Spike - to - Battery = \frac{\underset{m \in M}{\text{median}}(MaxSpike_m)}{kWh_{Bat}} \quad (3)$$

Where M is the set of all months m. kWh_{Bat} is the energy capacity of the battery.

4.2.2 Spike-to-Battery Ratio Behavior

We will now walk through a few examples to demonstrate how this spike-to-battery ratio behaves under different load shapes to provide context for the introduction of the threshold ratio. For this discussion, we display the time series load data (kW) as a step function to accurately display the area under the graph given the time resolution of the data. We use 15-minute energy consumption data to calculate average power in each 15-minute interval.

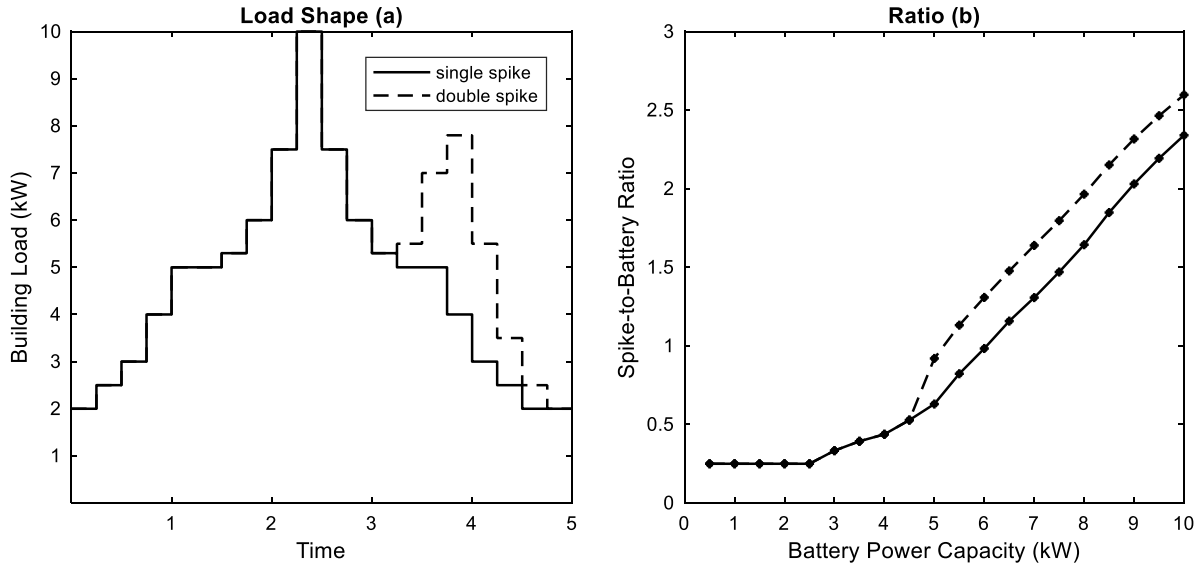

Figure 4-2: Behavior of Spike-to-Battery Ratio. Panel (a) shows the two example load shapes and (b) the resulting ratio at many levels of battery power capacity. The example assumes a 1hr storage discharge duration.

Figure 4-2 illustrates how the spike-to-battery ratio behaves under two different hypothetical load shapes (shown in panel (a)). Battery power capacity is treated parametrically from 0.5 to 10 kW in increments of 0.5 kW (horizontal axis of panel (b)). A 1hr battery duration is assumed throughout this example.

As the maximum battery power rating increases from 0.5 to 2.5 kW, the ratio remains constant. The vertical walls of the load spike in this initial load region mean that load energy and battery energy increase such that their ratio remains constant.[1]

From 2.5 to 4.5 kW of power capacity, the ratio increases as the base of our spike grows wider. The ratio remains the same for both the single and double spike examples because the second spike (t = 4hr) is not included in the ratio calculation. Only the largest spike above the target load is included, and the original spike (t = 2.5hr) remains the largest spike.

As the power capacity increases above 4.5 kW, we now see a difference in the spike-to-battery ratio. The target load is now below the base of the second spike, and it is therefore treated as part of the same spike as the original. This large difference in spike energy, while keeping battery energy capacity the same, is what accounts for the difference in spike-to-battery ratio between the two profiles.

As battery power capacity increases past 6kW, we see that both profiles have spike-to-battery ratios greater than 1. This means that the battery energy capacity is not large enough to eliminate the entire spike (in other words, the battery cannot reduce net building load to the target load). In the next section we will explore how differences in building load shape affect the depth of load reduction for spike-to-battery ratios greater than 1.

4.2.3 Threshold Ratio

For those spikes which are larger than the energy capacity of the battery (i.e. the spike-to-energy ratio is greater than 1), the time profile of the power spike will determine the magnitude

[1] This raises an important aside: the spike-to-battery ratio is always non-decreasing because load spikes cannot "invert," or get thinner on the bottom.

of demand charge reductions since the battery cannot provide the entire needed energy; this is why we introduce an additional metric to capture the relationship between load shape and peak demand reduction. For example, Figure 4-3 highlights how demand charge reduction is realized under hypothetical “thin” and “wide” spikes. Both spikes have the same total energy (17 kWh) and we assume the same size battery in both scenarios (10 kW max power; the duration is fixed at 0.5 hours at max power). We plot the resulting spike-to-battery ratio for many intermediate power levels below the maximum rated power in the final panel. These intermediate power levels are hypothetical – they have no relation to physical characteristics of the battery and act only as data points to aid in the calculation of the threshold ratio. As both spikes embody the same amount of total energy, and the battery is assumed to be the same size for both spikes, the spike-to-battery ratio at the maximum power (10 kW) will be the same for both spikes. However, demand charge reduction will be different for each spike. A thin spike has less energy in the top of the spike than a wide spike, and therefore peak demand reduction is more effective in this scenario. In our example, a 5 kWh battery will reduce peak demand by 7.5 kW and 5.8 kW for the thin and wide spikes, respectively. The spike-to-battery ratio is unable to capture this behavior, and we therefore need an additional metric.

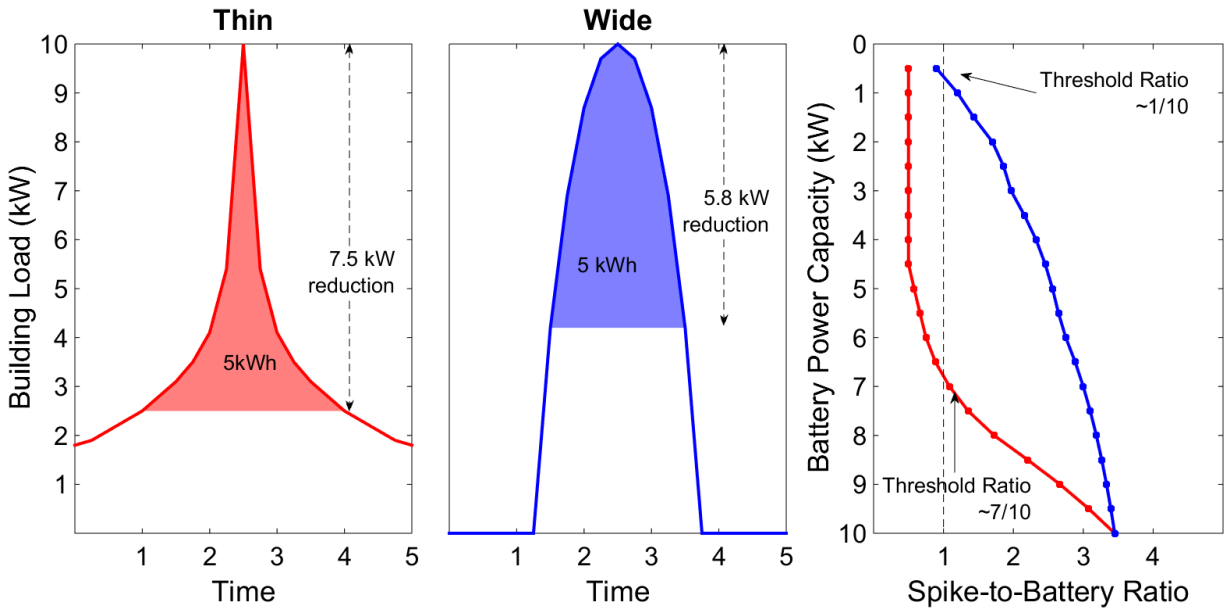

Figure 4-3: Illustration of threshold ratio for thin and wide load spikes. Read horizontally across from building load to the final panel to find ratio values at a particular target load. Note the reverse vertical scale in the last panel; it allows for ease of comparison to (a) because the target load is the maximum load minus the power capacity.

We define the threshold ratio as a unit-less ratio of power capacity levels. The numerator is the intermediate power level at which the spike-to-battery ratio crosses the threshold of 1 (i.e. when the battery is no longer large enough to service the entire load spike). The denominator is the maximum rated battery power. Again, a single annual metric for each building is calculated as the median of the 12 monthly values. This calculation is summarized in Table 4-1. In our example of a 10 kW maximum rated battery power, the thin spike has a threshold ratio of approximately 0.7, while the wide spike has a threshold ratio of approximately 0.1. Hence, the threshold ratio captures the intended relationship between load shape and demand reduction potential for a given battery energy capacity. The higher the threshold ratio, the greater the economic benefit to be realized per unit energy stored in the battery. For those buildings that have spike-to-battery ratios less than 1 at the maximum rated power, we set the threshold ratio at 1.0.

Table 4-1: Summary of Threshold Ratio Calculation

Step	Calculation
Numerator	
1	For each month, calculate the Spike-to-Battery Ratio at many intermediate power capacities up to the full power capacity of the battery
2	Find the lowest intermediate power capacity for which the Spike-to-Battery Ratio is greater than or equal to 1
Denominator	
1	Max rated power output of the battery
Final Ratio	
1	Divide numerator by denominator for each month. The final threshold ratio is the median of the monthly values.

In addition to the shape of the largest spike, another factor that could affect demand reduction capability is the shape of the recovery period between two load spikes; if the load "valley" between two spikes is not sufficient in depth or length, the battery may not be able to shave the second peak because a complete recharge would not have occurred. We found that including a measure for the shape of this valley in our model can reduce the unexplained variance, but the predictive accuracy gains are not sufficient to warrant the extra complexity.

4.3 Data and Optimization Model

A storage provider will likely have an estimate of the electric load profile of target customers. In order to develop our model, we use metered energy consumption data from 665 commercial and industrial buildings in the Carolinas to populate an optimization model from which we develop the predictive metric. The data have a 15-minute sample rate for 1 calendar year, 2013. In Appendix C, we compare the results from this Carolina dataset to those from 100

geographically diverse buildings provided by EnerNOC, finding good agreement. The optimization model is a linear program to minimize retail energy costs to the battery owner, and also considers battery degradation in making decisions. We assume perfect foresight of building load, which will somewhat overestimate revenue to the battery. In reality, building load forecasts would be used in the battery optimization. Short-term building load forecasting algorithms are an active area of research, and average forecast errors of 5-10% are routinely feasible [27,28]. Hence, we do not believe the perfect foresight assumption distorts our conclusions. Detailed information about the optimization model can be found in the SI. The battery can perform peak-shifting (reduce demand charges) or energy arbitrage, though we found that retail energy arbitrage is largely uneconomic even with time-of-use rates. Our metric thus emphasizes predicting demand charge reduction.

We assume a lithium-ion phosphate chemistry in our model with an 83% round-trip efficiency [29]. The battery can charge and discharge at the maximum rated power for the entire rated duration; both power and duration are treated parametrically in our analysis. The average monthly depth of discharge for any of the scenarios we ran does not exceed 50%. The treatment of capacity degradation from battery use is discussed in Appendix C.

In this work, we investigate only tariffs with demand charges that do not change intraday (no peak or off-peak periods) or seasonally (summer/winter). We also assume a constant energy charge. Our findings are still valid for locations that have seasonal demand charges (though the model parameters must be scaled) because inter-seasonal load shifting cannot be done at scale. Buildings can, however, shift load intraday even in the absence of storage, and therefore our findings may not apply to regions with variable intraday demand charges.

4.3.1 Data Cleaning

A utility in the Carolinas initially energy consumption data from approximately 1,000 commercial and industrial meters. The utility provided data from a subset of their entire commercial and industrial population. The subset were those customers who had interval meters and a sufficiently long history for this study.

Meters covering loads unsuitable for this study were removed according to usage characteristics. This included any meters with maximum power draw less than 25kW, average power draw less than 13kW, or any meter missing a total of more than 2 days of data within 2013. Data gaps for meters with less than 2 days of missing data were filled with an average profile from two surrounding days of the same type (weekday/weekend). 270 meters were removed during this step. A subsequent visual inspection of each meter's load profile identified meters that were attached to specific pieces of equipment (e.g., switching between 2 discrete load values throughout the year). 59 meters were removed during this step. This left the 665 buildings used for our analysis.

4.4 Revenue Prediction

After investigating a number of model forms, we found that the threshold ratio alone is sufficient to predict peak shaving revenue with relatively low error. A non-linear model was fit using equation 4.[2]

[2] Any building with a spike-to-battery ratio of 1 or lower (corresponding to a threshold ratio of 1) was removed for model fitting purposes (see Appendix C). Located far from the mean threshold ratio, these buildings held very high influence in parameter estimates, and increased modelling error for the rest of the dataset. In practice, it should be sufficient to know that if a building has a threshold ratio of 1, its normalized revenue is likely above the model prediction.

$$Rev = a * e^{b*Thresh} + c \quad (4)$$

Equation 4 parameters *a*, *b*, and *c* are fit by non-linear least squares, *Rev* is the annual revenue per kWh of installed energy capacity, and *Thresh* is the threshold ratio. Parameters *a* and *c* can be thought of as scaling factors that adjust the vertical position of the fit, while *b* adjusts the concavity of the fit. Figure 4-4 shows the model fit across battery power capacity scenarios with associated confidence and prediction intervals. The results shown here assume a $20/kW demand charge and 1hr duration, though the results are similar for other input assumptions. Duration is held constant across scenarios, so as power capacity increases, total energy capacity increases as well.

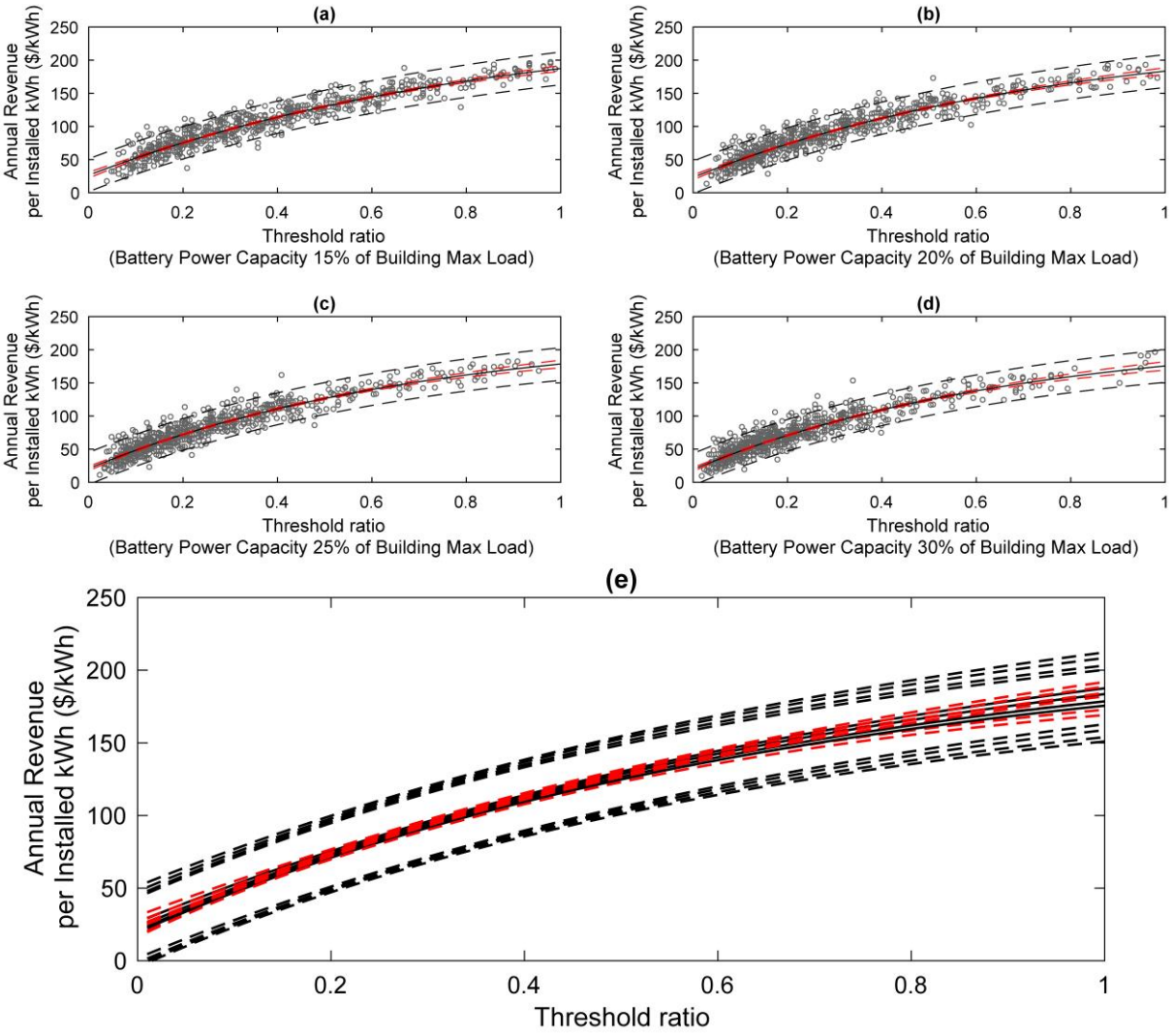

Figure 4-4: Plot of annual revenue per unit of installed energy capacity as a function of the threshold ratio across a number of battery power capacities. Each point represents a building. Subplots (a) through (d) represent 15% to 30% battery capacity as a percentage of the building's maximum load. Red dashed lines show the 95% confidence interval for the fit; black dashed lines show the 95% prediction interval for the data. Subplot (e) shows all fits on the same plot. Assumed $20/kW demand charge, 1hr duration, and 83% round-trip efficiency. Duration is held constant across scenarios, so as power capacity increases, total energy capacity increases as well.

The relationship between the threshold ratio and normalized revenue does not change significantly across battery power capacities (Figure 4-4 panel (e)); the prediction and confidence intervals are quite similar. To be clear, total revenue will increase as power and energy capacity

increases, but revenue per unit of installed energy capacity remains the same across threshold ratios. Our model's coefficient estimates are also similar across power capacities. Figures C-2 to C-6 show coefficient estimates and confidence intervals across battery capacities, including a combined scenario where data are aggregated across the 4 battery power capacities before model fitting. The coefficient estimates are statistically indistinguishable between power capacity scenarios. We extended our analysis to include power capacities from 10% to 35% of maximum building load and found that this relationship held. Therefore, we will assume that normalized revenue as a function of threshold ratio is independent of power capacity for a given discharge duration at maximum power; in other words, the same fundamental link between normalized revenue and load shape governs across power capacity scenarios. This is a powerful insight that allows the selection of optimal battery size by finding the profit maximizing threshold ratio (an example is provided in section 4.5). The coefficient and error estimates provided in Appendix C are the combined estimates derived from aggregating data across the 4 battery power capacity scenarios. This information can be used to recreate the prediction curves for any duration or tariff scenario.

The resulting curve and prediction intervals can be compared to estimates of battery installation cost to find breakeven and maximum profit levels as a function of threshold ratio, and therefore as a function of battery power capacity.

One way of validating the model is to determine if the results of the more accurate optimization model follow the shape of the model's prediction curve. That is, do reductions in battery power capacity (increases in threshold ratio) lead to gains in normalized revenue as predicted by our model? In Figure 4-5, we use the results from our optimization model to plot the path of two individual buildings as they reduce maximum battery power capacity (from 30% to

15% of maximum building load), finding that the results from the optimization model confirm the shape of the prediction curve. While this is true for many of the buildings, some buildings exhibited their own trend relative to the predicted trend. This example also assumed a $20/kW demand charge and 1hr battery duration, though the results were the same for other input assumptions.

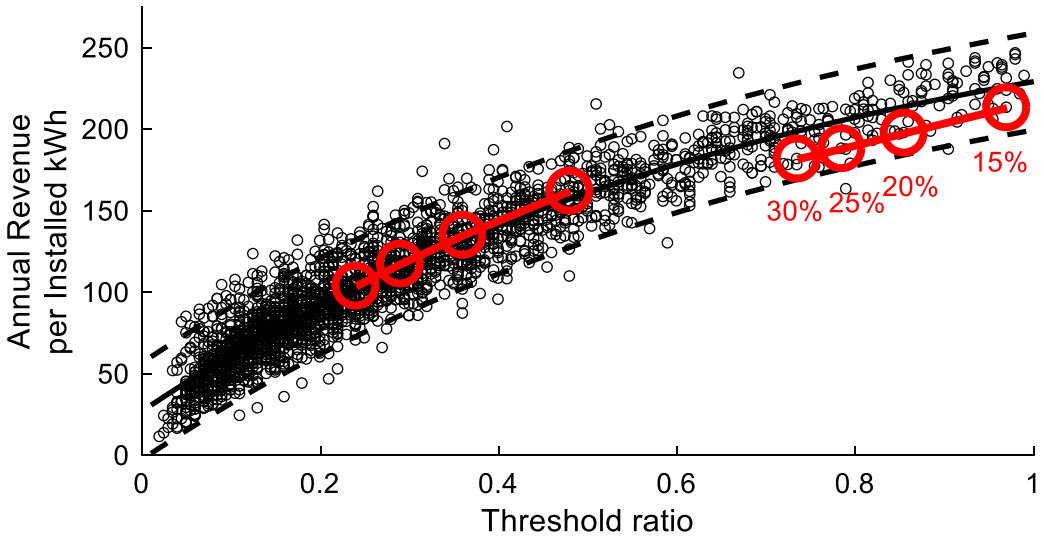

Figure 4-5: Plot of annual normalized revenue versus threshold ratio for all buildings and battery power capacity scenarios. Two buildings are highlighted in red, showing the path taken as maximum battery power capacity is reduced from 30% to 15% of building maximum load (while holding duration constant). Each circle represents the results from a battery optimization model. The solid black line represents our econometric model, with associated 95% prediction intervals shown in dotted black lines.

4.4.1 Sensitivity to Battery and Economic Parameters

Figure 4-6 shows that our model's parameters change in a predictable way as demand charges and duration change. In panel (a) model curvature, captured by parameter b, does not change as demand charges increase, but scaling parameters a and c change at a linear rate to reflect a steepening of the curve. In panel (b), all parameters except for the curvature parameter (b) follow exponential decay as battery duration increases. Figure C-2 shows that changes in

round-trip efficiency do not significantly affect the coefficient estimates. The lack of change in the curvature of our predictions across demand charges, duration, and efficiency lends support to our choice of mathematical model.

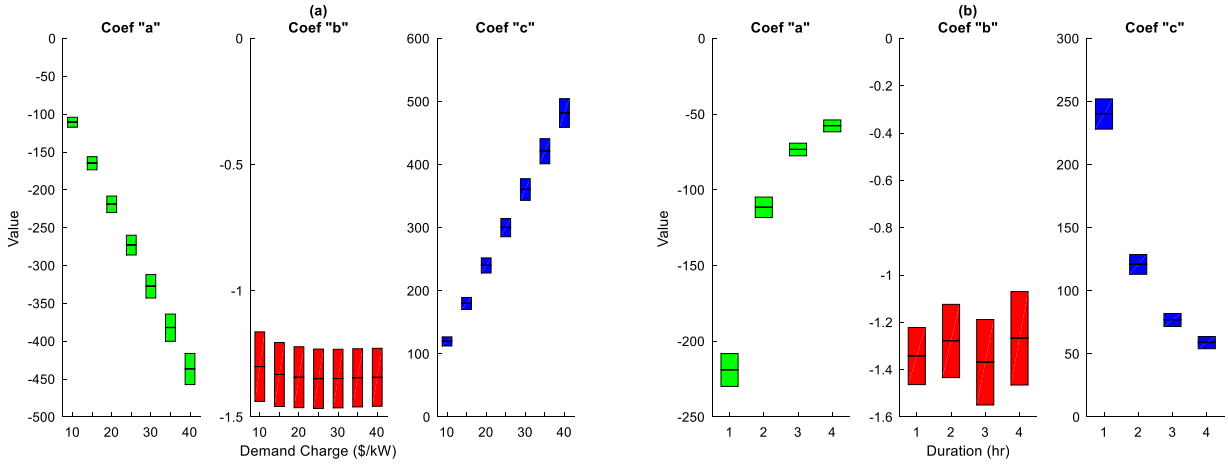

Figure 4-6: Comparison of parameters across demand charges (a) and duration (b). The shape parameter (coefficient *b*) does not change across demand charge levels or duration. Scaling parameters *a* and *c* change linearly in demand charges to reflect a steepening of the curve. Scaling parameters *a* and *c* change exponentially in duration to reflect a flattening of the curve.

4.5 Example

We will now step through an example of how this information can be used to predict revenue across many battery sizes and find the profit-maximizing size for an individual building. The first step is to calculate the spike-to-battery ratio for many different battery power capacities. If the desired duration is also unknown, then this step will be repeated for different durations. We can then calculate the threshold ratio at each of these power capacities, as shown in Figure 4-7.

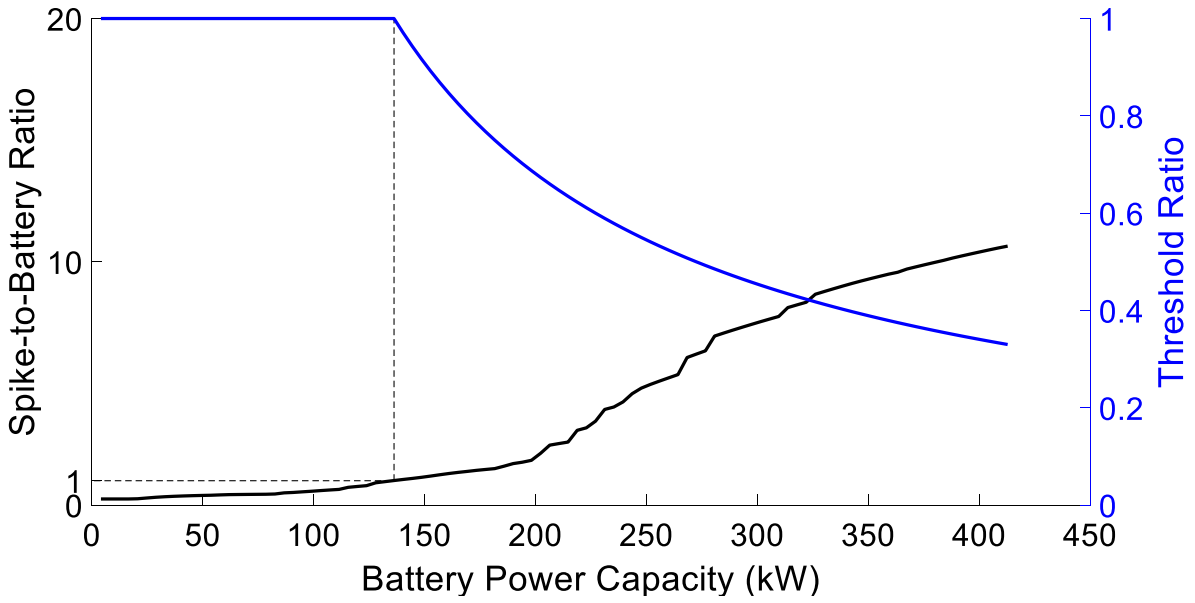

Figure 4-7: Example plot of spike-to-battery and threshold ratios as a function of battery power capacity. The threshold ratio is a simple ratio of battery power capacities – the power capacity currently being investigated divided by the power capacity at which the spike-to-battery ratio equals 1. The spike-to-battery ratio (black curve) is not smooth because it reflects the variability of the building's load shape.

We now have the relationship between the threshold ratio and battery power capacity for this building. In Figure 4-8, we switch the axes to plot power capacity as a function of threshold ratio in panel (a). Then, we overlay the predicted revenue as a function of the threshold ratio. All coefficient and error information necessary to recreate the revenue prediction curve is supplied in Appendix C. Section 4.4 details how we derived the revenue prediction curves.

We can convert power capacity to energy capacity by multiplying by our chosen duration. Multiplying energy capacity and normalized revenue gives total revenue versus threshold ratio in panel (b). Total cost is also plotted in this panel, assuming an installation capital cost of $750/kWh amortized over 10 years at a 10% discount rate, though in practice this assumption should be replaced with costs based on local conditions (installation costs are expected to be significantly lower in coming years[30]). The total profit curve as a function of threshold ratio is

then calculated as the difference between total revenue and cost in panel (b). Finally, we find the profit maximizing battery power capacity for the selected duration by plotting the profit against the power capacity in panel (c).

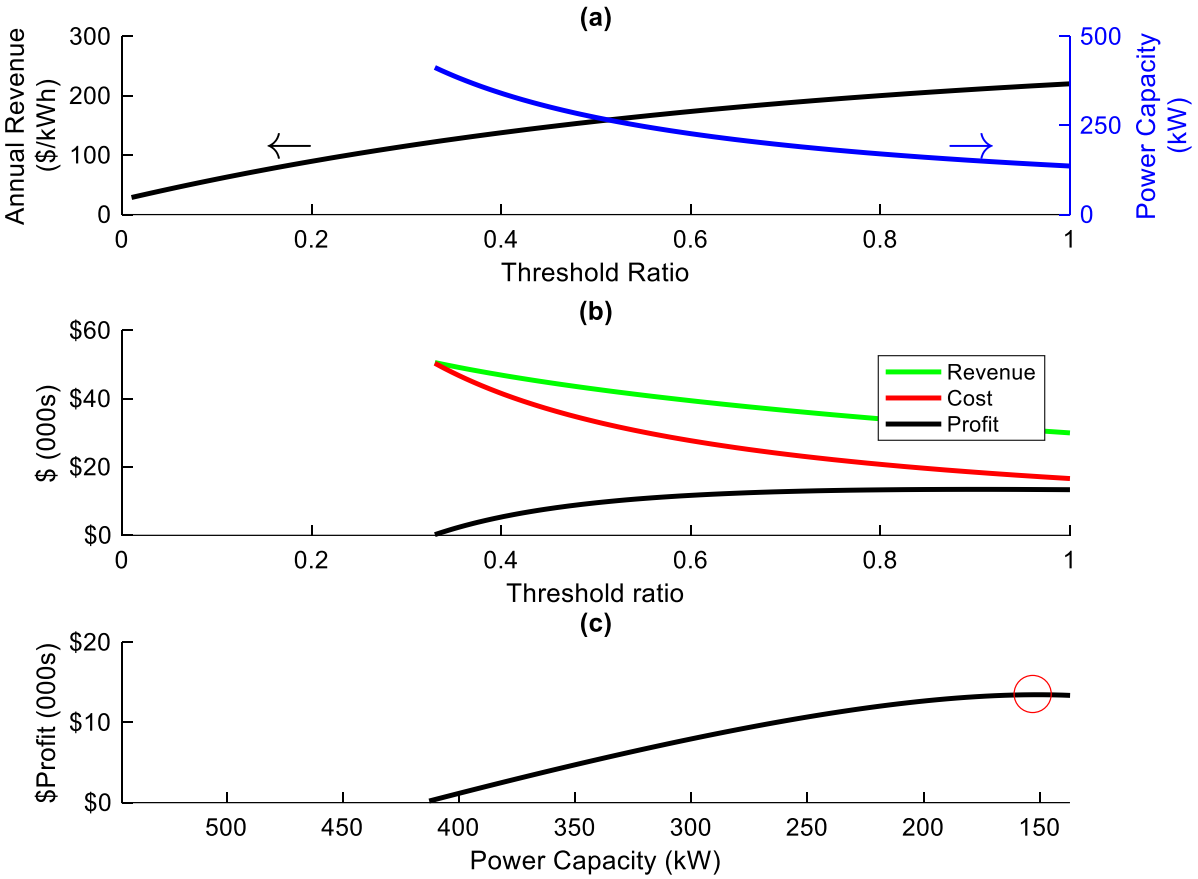

Figure 4-8: Example plot of normalized annual revenue and battery power capacity as a function of threshold ratio (a). Arrows point to corresponding y-axis for each line. The combination of normalized revenue and battery power capacity can be used to calculate total revenue, cost, and profit for a particular building (b) after multiplying by the duration. Finally, plotting profit against power capacity (c) allows for optimal sizing. The point of maximum profit is shown as a red circle.

The profit maximizing power capacity is highly sensitive to the shape of the assumed cost function. The accuracy of this step relies upon a good understanding of local installation costs. In reality, the cost as a function of battery power capacity is not linear. Inverter sizes are not continuous – as battery capacity is increased, larger inverters, or a greater number of inverters,

will need to be installed, which will increase costs in a non-linear manner. However, given an accurate cost function, the methods in the above example still lead to the profit maximizing power capacity.

4.6 Conclusions

We have shown that the threshold ratio, a new metric derived directly from a building's load profile that generally characterizes the power spikes encountered in aggregate over a year at that site, can be used to analytically predict revenue from retail peak-shifting across different battery and tariff scenarios. Commonly available spreadsheet software can be used to perform the calculations. This method trades accuracy for a vast reduction in the human and computing resources required for model development. Our key findings include:

- The threshold ratio incorporates load shape and magnitude information to predict peak-shaving revenue for individual customers.
- Our model provides an easily reproducible revenue prediction curve based on 3 parameters (provided in Appendix C).
- The regression based model allows for explicit calculations of uncertainty.
- Model parameters are independent of battery power capacity given a fixed discharge duration (power capacities of 10-35% of building maximum load examined in this work). This provides a closed-form solution to optimal sizing.

Future work could investigate if this analysis applies to tariffs that have intraday changes in demand charges (e.g., many utilities in California and Consolidated Edison in New York). Our algorithm could be changed to find only those spikes in load above the target during the hours of

highest demand charges. However, this still may not adequately capture the battery's load shifting decision between demand charge periods. Such research may be necessary if BTM batteries become more prevalent, and more utilities shift away from flat-rate demand charges to reflect the time-varying nature of capacity supply costs.

4.7 References

[1] U.S. Energy Storage Monitor, GTM Research & Energy Storage Association, Boston, MA, 2014.

[2] J. Eyer, G. Corey, Energy Storage for the Electricity Grid: Benefits and Market Potential Assessment Guide, Sandia National Laboratories, Albuquerque, NM, 2010. http://www.sandia.gov/ess/publications/SAND2010-0815.pdf.

[3] M.J. Shaw, C. Subramaniam, G.W. Tan, M.E. Welge, Knowledge management and data mining for marketing, Decis. Support Syst. 31 (2001) 127–137. doi:10.1016/S0167-9236(00)00123-8.

[4] C.H. Lo, M.D. Anderson, Economic dispatch and optimal sizing of battery energy storage systems in utility load-leveling operations, IEEE Trans. Energy Convers. 14 (1999) 824–829. doi:10.1109/60.790960.

[5] R. Walawalkar, J. Apt, R. Mancini, Economics of electric energy storage for energy arbitrage and regulation in New York, Energy Policy. 35 (2007) 2558–2568. doi:10.1016/j.enpol.2006.09.005.

[6] E.S. Hittinger, I.M.L. Azevedo, Bulk energy storage increases United States electricity system emissions., Environ. Sci. Technol. 49 (2015) 3203–10. doi:10.1021/es505027p.

[7] G.N. Bathurst, G. Strbac, Value of combining energy storage and wind in short-term energy and balancing markets, Electr. Power Syst. Res. 67 (2003) 1–8. doi:10.1016/S0378-7796(03)00050-6.

[8] P. Denholm, R. Sioshansi, The value of compressed air energy storage with wind in transmission-constrained electric power systems, Energy Policy. 37 (2009) 3149–3158. doi:10.1016/j.enpol.2009.04.002.

[9] C.A. Hill, M.C. Such, D. Chen, J. Gonzalez, W.M. Grady, Battery Energy Storage for Enabling Integration of Distributed Solar Power Generation, IEEE Trans. Smart Grid. 3 (2012) 850–857. doi:10.1109/TSG.2012.2190113.

[10] W. Kempton, J. Tomić, Vehicle-to-grid power fundamentals: Calculating capacity and net revenue, J. Power Sources. 144 (2005) 268–279. doi:10.1016/j.jpowsour.2004.12.025.

[11] S.B. Peterson, J.F. Whitacre, J. Apt, The economics of using plug-in hybrid electric vehicle battery packs for grid storage, J. Power Sources. 195 (2010) 2377–2384. doi:10.1016/j.jpowsour.2009.09.070.

[12] A. Oudalov, D. Chartouni, C. Ohler, G. Linhofer, Value Analysis of Battery Energy Storage Applications in Power Systems, in: 2006 IEEE PES Power Syst. Conf. Expo., IEEE, 2006: pp. 2206–2211. doi:10.1109/PSCE.2006.296284.

[13] V. Koritarov, T. Veselka, J. Gasper, B. Bethke, Modeling and Analysis of Value of Advanced Pumped Storage Hydropower in the United States, 2014.

[14] G. Fitzgerald, J. Mandel, J. Morris, H. Touati, The Economics of Battery Energy Storage, Rocky Mountain Institute, Boulder, CO, 2015. http://www.rmi.org/Content/Files/RMI-TheEconomicsOfBatteryEnergyStorage-FullReport-FINAL.pdf.

[15] R. Manghani, The Economics of Commercial Energy Storage in the U.S.: The Outlook for Demand Charge Management, GTM Research, 2016. https://www.greentechmedia.com/research/report/the-economics-of-commercial-energy-storage-in-the-us.

[16] J. Neubauer, M. Simpson, Deployment of Behind-The-Meter Energy Storage for Demand Charge Reduction, National Renewable Energy Laboratory, Golden, CO, 2015. http://www.nrel.gov/docs/fy15osti/63162.pdf.

[17] J.T. Alt, M.D. Andersen, R.G. Jungst, Assessment of utility side cost savings from battery energy storage, IEEE Trans. Power Syst. 12 (1997) 1112–1120. doi:10.1109/59.630450.

[18] D.K. Maly, K.S. Kwan, Optimal battery energy storage system charge scheduling with dynamic programming, Proc. Sci. Meas. Technol. 142 (1995) 453–458.

[19] T.-Y. Lee, N. Chen, Optimal capacity of the battery energy storage system in a power system, IEEE Trans. Energy Convers. 8 (1993) 667–673.

[20] Kyung-Hee Jung, Hoyong Kim, Daeseok Rho, Determination of the installation site and optimal capacity of the battery energy storage system for load leveling, IEEE Trans. Energy Convers. 11 (1996) 162–167. doi:10.1109/60.486591.

[21] M. Gitizadeh, H. Fakharzadegan, Effects of electricity tariffs on optimal battery energy storage sizing in residential PV/storage systems, in: 2013 Int. Conf. Energy Effic. Technol. Sustain., IEEE, 2013: pp. 1072–1077. doi:10.1109/ICEETS.2013.6533536.

[22] A. Nottrott, J. Kleissl, B. Washom, Storage dispatch optimization for grid-connected combined photovoltaic-battery storage systems, in: 2012 IEEE Power Energy Soc. Gen. Meet., IEEE, 2012: pp. 1–7. doi:10.1109/PESGM.2012.6344979.

[23] S.X. Chen, H.B. Gooi, M.Q. Wang, Sizing of Energy Storage for Microgrids, IEEE Trans. Smart Grid. 3 (2012) 142–151. doi:10.1109/TSG.2011.2160745.

[24] A. Oudalov, R. Cherkaoui, A. Beguin, Sizing and Optimal Operation of Battery Energy Storage System for Peak Shaving Application, in: 2007 IEEE Lausanne Power Tech, IEEE, 2007: pp. 621–625. doi:10.1109/PCT.2007.4538388.

[25] E. Oh, S.-Y. Son, Electric energy storage design decision method for demand responsive buildings, Energy Build. 126 (2016) 139–145. doi:10.1016/j.enbuild.2016.05.048.

[26] D. Wu, M. Kintner-Meyer, T. Yang, P. Balducci, Analytical sizing methods for behind-the-meter battery storage, J. Energy Storage. 12 (2017) 297–304. doi:10.1016/j.est.2017.04.009.

[27] C.E. Borges, Y.K. Penya, I. Fernandez, Optimal combined short-term building load forecasting, 2011 IEEE PES Innov. Smart Grid Technol. (2011) 1–7. doi:10.1109/ISGT-Asia.2011.6167091.

[28] A. Khosravi, S. Nahavandi, D. Creighton, A.F. Atiya, Comprehensive Review of Neural Network-Based Prediction Intervals and New Advances, IEEE Trans. Neural Networks. 22 (2011) 1341–1356. doi:10.1109/TNN.2011.2162110.

[29] Tesla Motors, Tesla Power System Specifications, (2016). https://www.teslamotors.com/powerpack (accessed June 5, 2016).

[30] B. Nykvist, M. Nilsson, Rapidly falling costs of battery packs for electric vehicles, Nat. Clim. Chang. 5 (2015) 329–332. doi:10.1038/nclimate2564.

Appendix C: Additional Modelling Details

Coefficient Estimates and Prediction Intervals

Coefficient estimates in the following tables can be used in equation 1 from the main paper to recreate the prediction curve for a particular demand charge / duration scenario. The prediction interval column can be used to recreate the 95% prediction interval by both adding and subtracting the listed value from the prediction curve. While the true prediction interval is slightly wider near the endpoints of the threshold ratio range, the difference in interval width between the mean threshold ratio and the endpoints is only 0.1% of the mean width. The value reported in the prediction interval column represents half of the mean width.

Table C-1: Coefficient estimates for 0.5hr duration

Demand Charge ($/kW)	coef_a	coef_b	coef_c	±Prediction Interval (95% PI)
10	-192.9	-1.728	213.9	25.7
15	-289.8	-1.726	323.3	37.1
20	-385.9	-1.725	431.8	48.6
25	-481.7	-1.727	539.9	60.3
30	-577.9	-1.725	648.4	72.2
35	-674.0	-1.724	756.6	84.1
40	-770.3	-1.723	865.0	96.0

Table C-2: Coefficient estimates for 1hr duration

Demand Charge ($/kW)	coef_a	coef_b	coef_c	±Prediction Interval (95% PI)
10	-110.6	-1.301	119.7	13.9
15	-164.8	-1.332	179.9	19.1
20	-219.0	-1.343	240.2	24.3
25	-273.0	-1.349	300.2	29.6
30	-327.4	-1.348	360.6	35.0
35	-382.1	-1.345	421.2	40.5
40	-436.7	-1.343	481.9	46.2

Table C-3: Coefficient estimates for 2hr duration

Demand Charge ($/kW)	coef_a	coef_b	coef_c	±Prediction Interval (95% PI)
10	-56.7	-1.167	60.5	9.1
15	-84.5	-1.235	91.0	12.5
20	-111.5	-1.279	120.9	15.7
25	-138.6	-1.300	150.9	18.8
30	-165.6	-1.311	180.9	22.0
35	-192.6	-1.317	210.8	25.2
40	-219.8	-1.317	241.1	28.5

Table C-4: Coefficient estimates for 3hr duration

Demand Charge ($/kW)	coef_a	coef_b	coef_c	±Prediction Interval (95% PI)
10	-36.1	-1.238	37.3	6.7
15	-55.0	-1.311	57.4	9.5
20	-73.3	-1.369	76.9	12.0
25	-91.5	-1.402	96.3	14.4
30	-109.7	-1.422	115.8	16.8
35	-127.5	-1.436	134.9	19.2
40	-145.4	-1.441	154.3	21.7

Table C-5: Coefficient estimates for 4hr duration

Demand Charge ($/kW)	coef_a	coef_b	coef_c	±Prediction Interval (95% PI)
10	-28.3	-1.100	28.6	5.1
15	-43.2	-1.191	44.0	7.4
20	-57.7	-1.267	58.9	9.5
25	-71.9	-1.328	73.4	11.5
30	-85.8	-1.375	87.7	13.5
35	-99.4	-1.410	101.7	15.5
40	-113.2	-1.430	116.0	17.5

Additional Results

Any building with a spike-to-battery ratios of 1 or lower (corresponding to a threshold ratio of 1) was removed for model fitting purposes. There is no clear relationship between spike-to-battery ratios below 1 and revenue, and thus predictive modelling breaks down. However, these building face the lowest need for modelling – their revenue is generally clustered above the curve followed by the rest of the data (Figure C-1). Located far from the mean threshold ratio, these buildings held very high influence in parameter estimates, and were raising modelling error for the rest of the dataset. In practice, it should be sufficient to know that if a building has a threshold ratio of 1, its normalized revenue is likely above the model prediction.

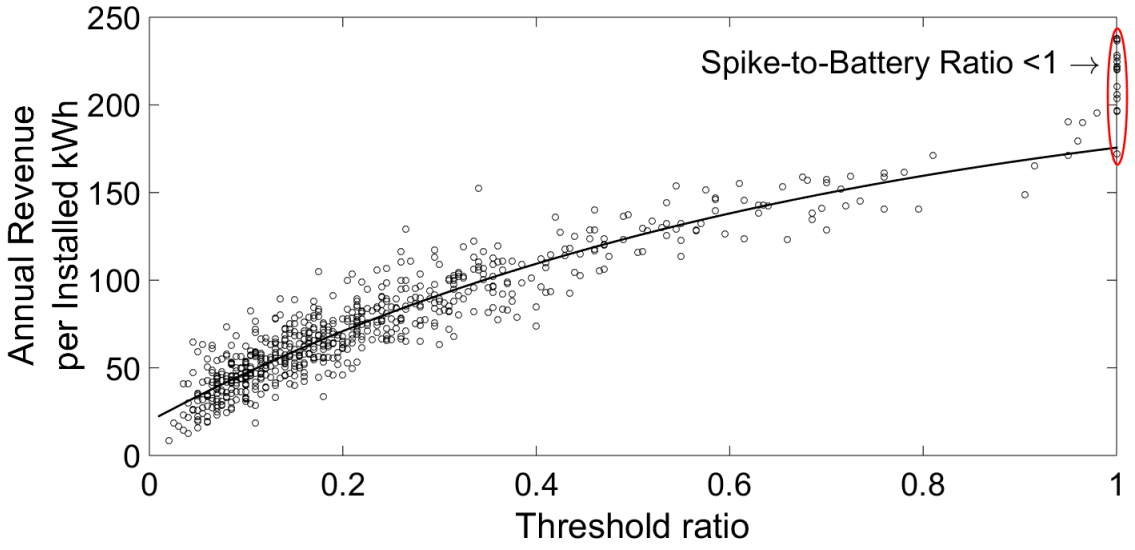

Figure C-1: Buildings with spike-to-battery ratios equal to or less than 1 do not follow the prevailing revenue trend. These buildings were removed for modelling purposes.

The following figures show the independence of revenue predictions to battery power capacity at a number of battery durations. Recall equation 1 is as follows:

$$y = a * e^{b*THRESH} + c \quad (1)$$

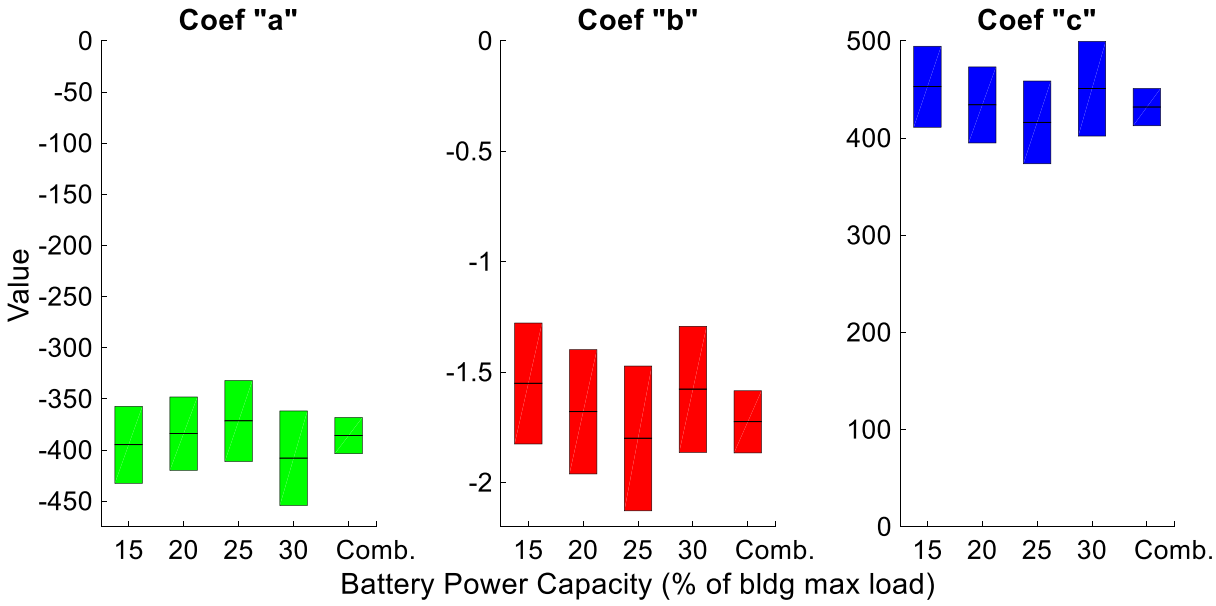

Figure C-2: Coefficient estimates (horizontal black line) with 95% uncertainty range (colored bars) across battery power capacities. Assumed $20/kW demand charge, 0.5hr duration, and 83% round-trip efficiency.

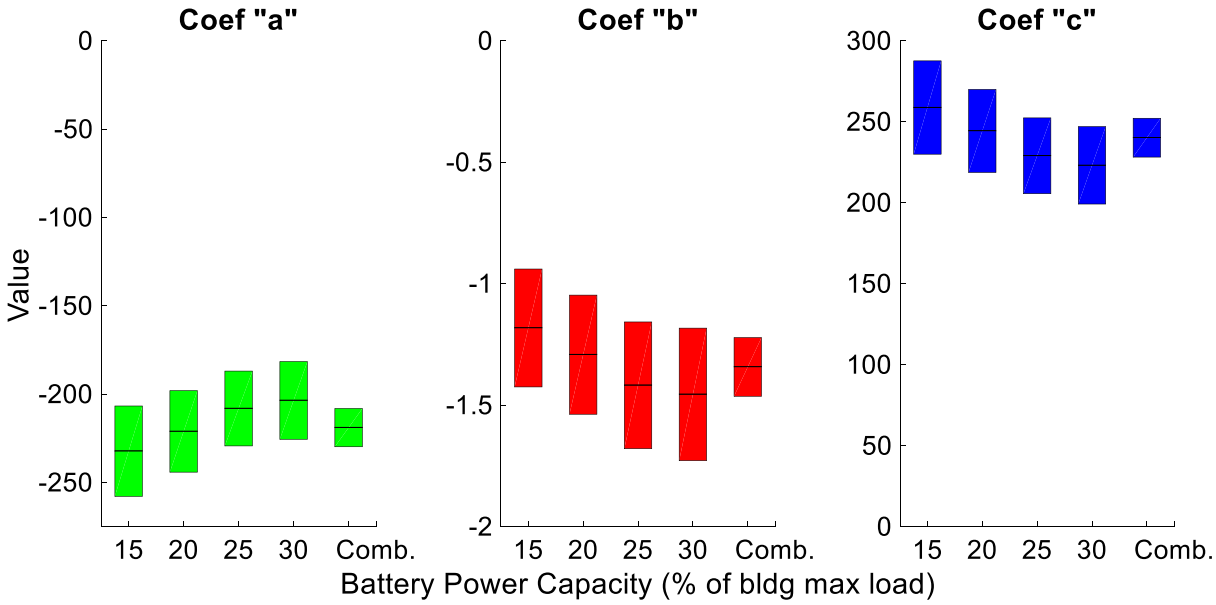

Figure C-3: Coefficient estimates (horizontal black line) with 95% uncertainty range (colored bars) across battery power capacities. Assumed $20/kW demand charge, 1hr duration, and 83% round-trip efficiency.

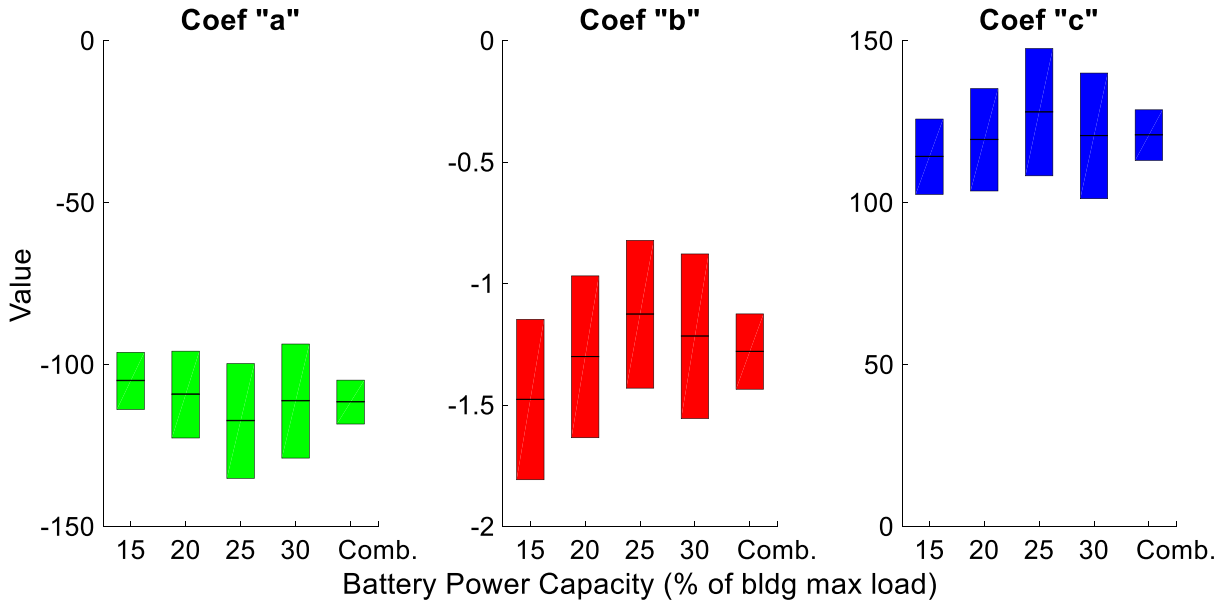

Figure C-4: Coefficient estimates (horizontal black line) with 95% uncertainty range (colored bars) across battery power capacities. Assumed $20/kW demand charge, 2hr duration, and 83% round-trip efficiency.

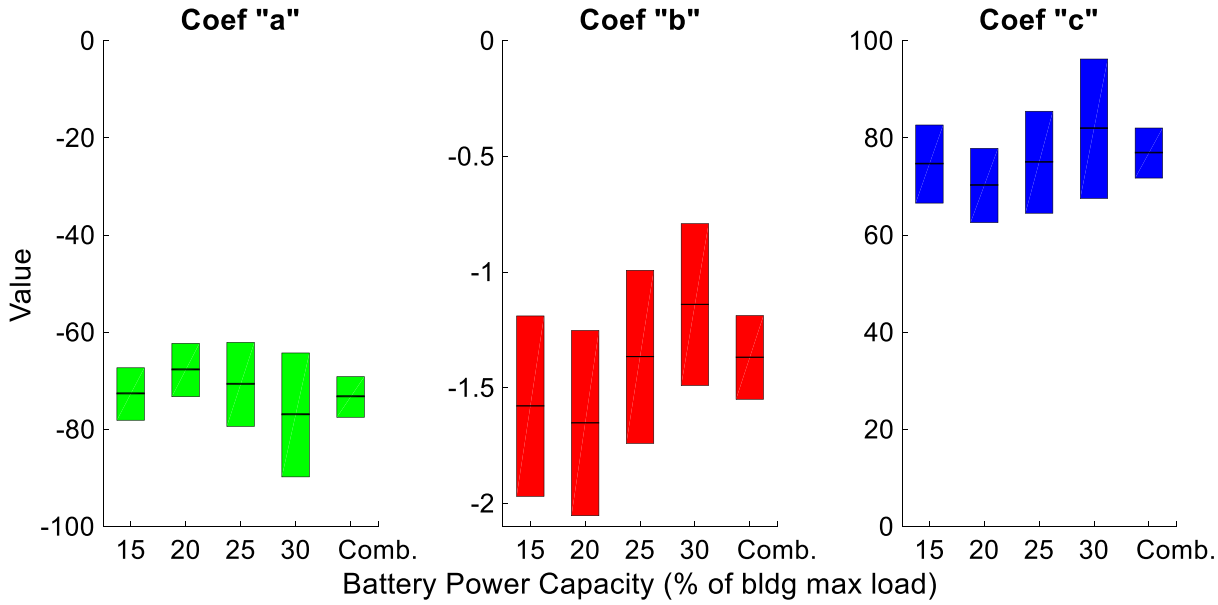

Figure C-5: Coefficient estimates (horizontal black line) with 95% uncertainty range (colored bars) across battery power capacities. Assumed $20/kW demand charge, 3hr duration, and 83% round-trip efficiency.

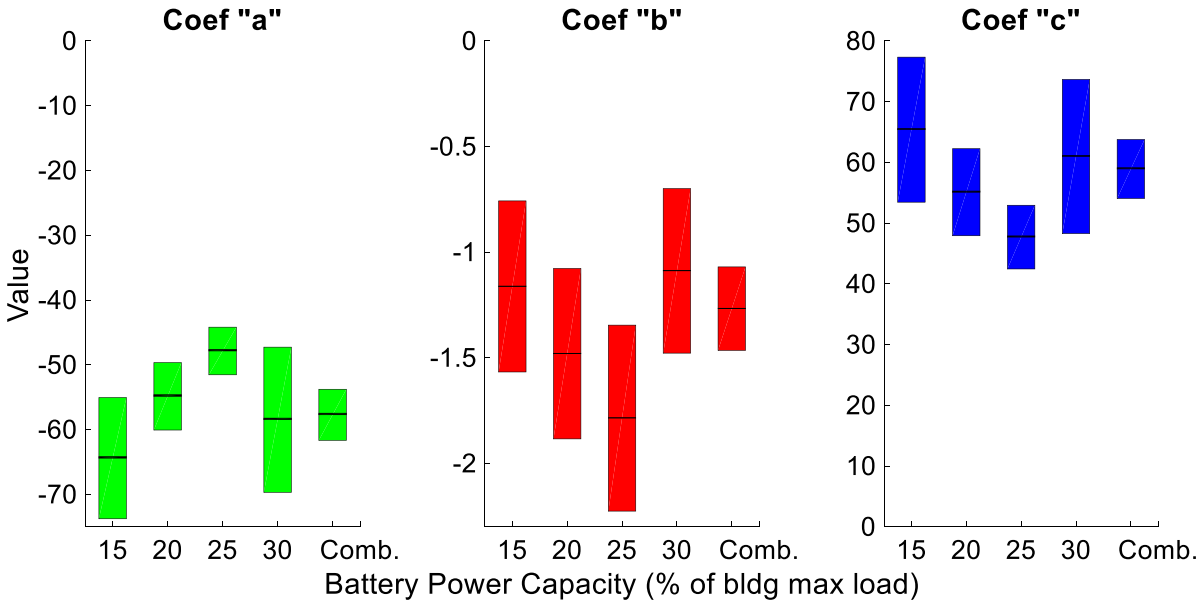

Figure C-6: Coefficient estimates (horizontal black line) with 95% uncertainty range (colored bars) across battery power capacities. Assumed $20/kW demand charge, 4hr duration, and 83% round-trip efficiency.

Figure C-7 shows the changes in round-trip efficiency do not significantly affect revenue predictions. While this makes sense for a peak-shaving application where the battery is not used very often, other applications such as daily price arbitrage or renewable energy shifting will face a much higher sensitivity to efficiency.

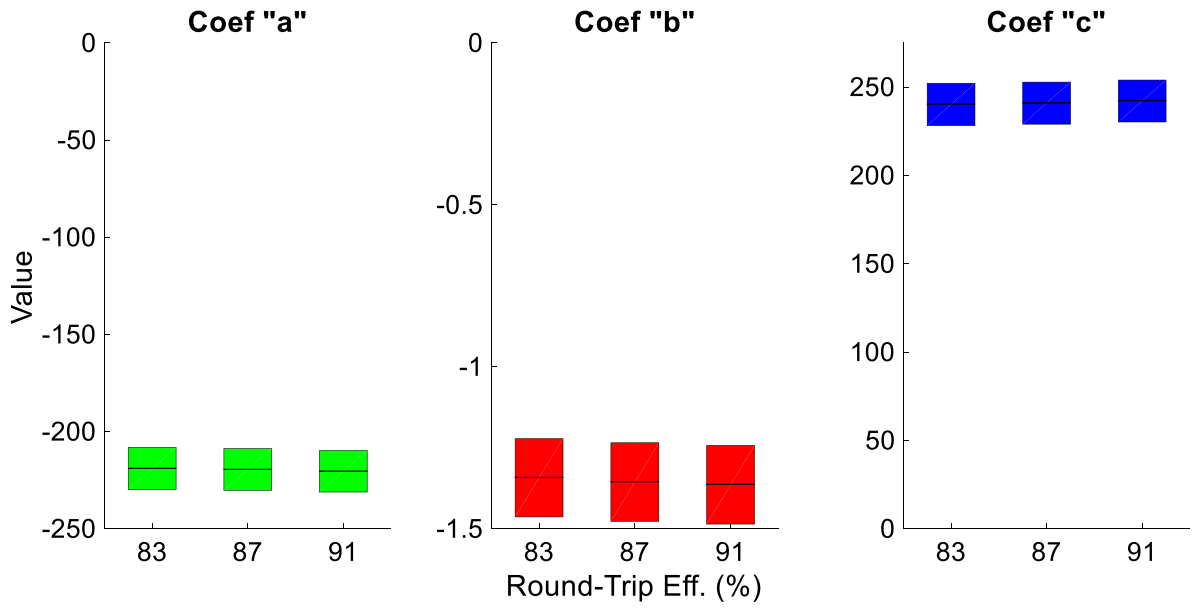

Figure C-7: Comparison of coefficient estimates across round-trip efficiency. The parameters show that as efficiency gets higher, the revenue prediction slope does not change significantly.

External Validity

We use a building load dataset from one geographical region, implicitly assuming that these data are representative of other regions which may or may not have different load characteristics. Average customer type (e.g., manufacturing vs. service), weather, and energy costs may cause differences in load profiles that are masked by using data from a single region. We cannot comment on the size and direction of bias introduced by these threats. However, when we compare the results from our main dataset from the Carolinas to the results from a geographically diverse set of 100 buildings made public by EnerNOC [1], we arrive at the same conclusions. Figure C-8 shows the locations of the 100 buildings in the EnerNOC dataset. Figure C-9 compares the prediction curve from the Carolinas dataset to the EnerNOC dataset, which shows nearly identical results. Figure C-10 compares coefficient estimates for the Carolina and EnerNOC datasets, showing statistically indistinguishable differences.

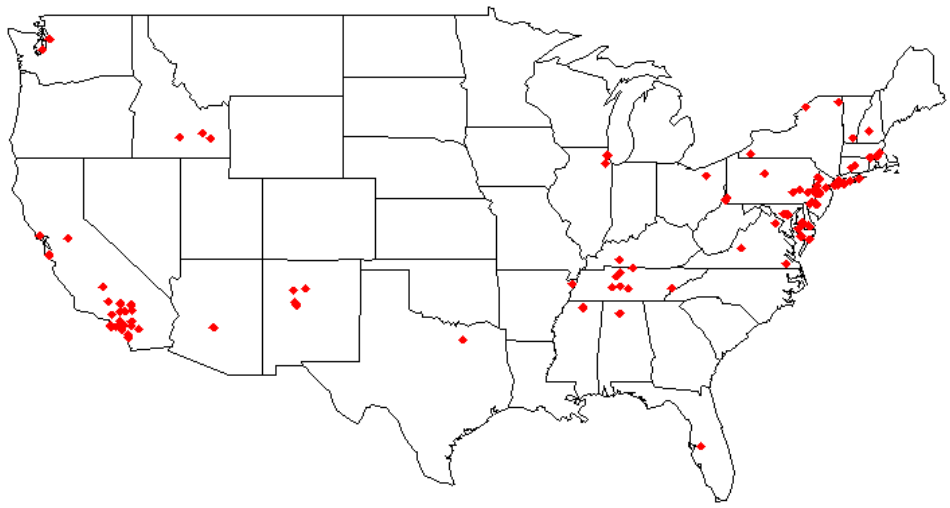

Figure C-8: Approximate location of 100 buildings in EnerNOC building dataset.

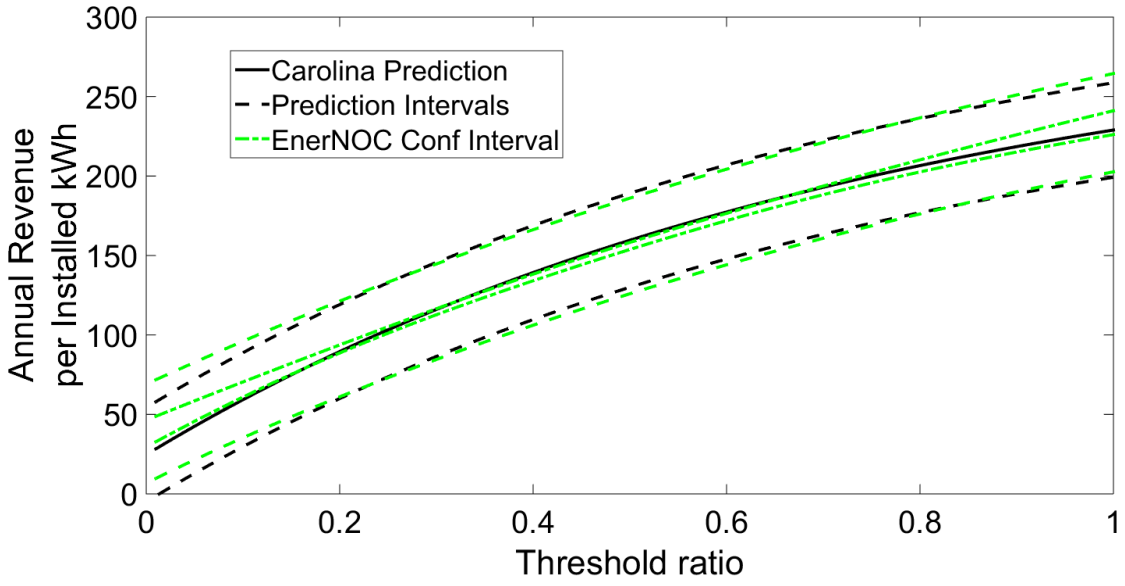

Figure C-9: Comparison of Carolina and EnerNOC predictions for data combined across battery power capacity scenarios. Black solid line represents the prediction for the Carolinas dataset; the dashed black lines represent the 95% prediction interval. The green dash-dot line represents the 95% confidence interval for the EnerNOC fit; the green dashed line represents the 95% prediction interval for the EnerNOC dataset. The EnerNOC revenue prediction is slightly flatter than the Carolina's prediction, but the

EnerNOC confidence interval nearly encompasses the prediction for the Carolina's dataset.

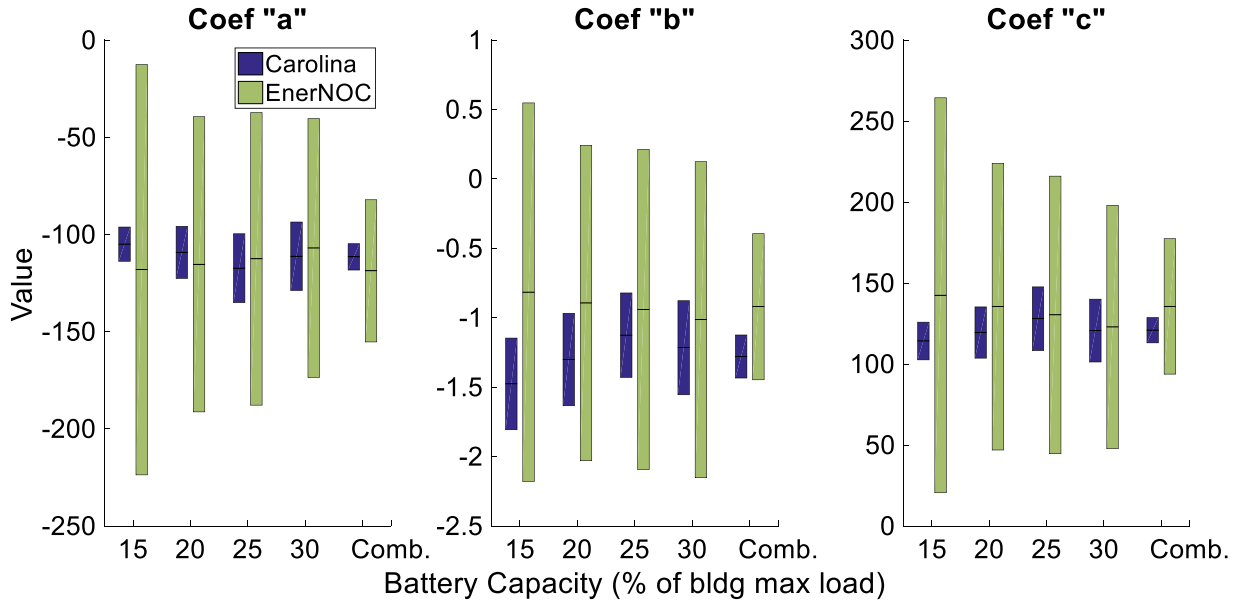

Figure C-10: Comparison of Carolina and EnerNOC coefficient estimates. Coefficients are statistically indistinguishable across datasets, but the EnerNOC dataset does not contain enough data to characterize the non-linear model for individual battery power capacity scenarios. When combining data across battery power capacity scenarios, the non-linear relationship becomes significant.

Optimization Model

Constants

$\overline{SoC}$	Max state of charge of battery (kWh)
$\bar{P}$	Rated power of battery (kW)
η	round-trip efficiency of battery (%)
BL(t)	building load at time t (kW)
EC(t)	Energy cost at time t ($/kWh)
DC_k	Demand charge for demand period k ($/kW)

BRC	Battery Replacement Cost ($)

Variables

c(t)	battery charging at time t (kW)
d(t)	battery discharge at time t (kW)
pd_k	peak demand during demand period k (kW)
soc(t)	state of charge of battery at time t (kWh)
nl(t)	net load at time t (kW)
deg(t)	battery degradation cost at time t ($)

Sets

T	Set of 15-minute time periods
K	Set of demand periods (e.g. peak, mid-peak and off-peak - depends on tariff), each of which is a subset of T

Objective Function

$$\min \sum_{t \in T} [EC(t) * nl(t) + deg(t)]/4 + \sum_{k \in K} DC_k * pd_k \quad (2)$$

Equation 2 represents the objective function of a retail customer. We divide the building power by 4 to convert kW to kWh for a 15-minute time-step to match the units of energy cost ($/kWh). This initial portion of the objective function represents real costs/revenues to the battery owner. Degradation is an amortization of the assumed replacement cost into the use phase of the battery; it prevents the use of the battery to perform services when those services have low value.

The last term in the objective functions sums demand charges over each demand period k; the form of this portion of the equation will change depending on the structure of demand charges in each utility tariff. In our model we assume a flat demand charge, so there is only one demand period.

$$nl(t) = BL(t) + c(t) - d(t) \quad (3)$$

$$deg(t) = \frac{\sqrt{\eta} * c(t) + \frac{d(t)}{\sqrt{\eta}}}{4 * \overline{SoC} * 4598} * BRC \quad (4)$$

Equation 3 calculates the net load of the building at time t (the load seen by the meter) from the underlying building load and the charging or discharging of the battery.

Equation 4 calculates degradation cost at time t as the product of the replacement capital cost and the fraction of total lifetime energy processed by a lithium-ion phosphate battery at time t. As determined by experimental results in Peterson, et al. [2], we account only for amp-hours processed by the battery, not depth of discharge, when calculating battery degradation for lithium-ion phosphate batteries. Based on data in Peterson, et al., we assume that the energy consumed to reach the end of battery lifetime (80% of initial battery capacity) is 4,598 times the maximum SOC. We derive this number from an average of the model coefficients reported in the paper. To express the energy processed by the battery at time t in fractions of lifetime energy, we divide the energy processed (sum of charging, discharging, and regulation energy) by the lifetime energy capacity of the battery (4,598 times maximum SOC). We divide by 4 to convert charge and discharge kW to kWh. Battery replacement cost is assumed to be 70% of the current system cost. Battery behavior is relatively insensitive to the replacement cost assumption.

The problem is initialized with a 90% SOC at t = 0.

Constraints

$$soc(t+1) = soc(t) + \frac{\sqrt{\eta} * c(t) - \frac{d(t)}{\sqrt{\eta}}}{4} \quad (5)$$

Equation 5 is an intertemporal constraint to track changes in SOC. Charging and discharging power is modified by internal energy loss, which is characterized by the round-trip efficiency (η). We divide by 4 to convert charge and discharge kW to kWh. We ignore standby losses as they are small (~1-2% per month) [3], which causes us to slightly overestimate revenues to the owner.

$$0 \leq c(t) \leq \bar{P} \quad (6)$$

$$0 \leq d(t) \leq \bar{P} \quad (7)$$

Equations 6 and 7 restrict the charging and discharging power to the rated power of the battery.

$$0.2 \leq soc(t) \leq \overline{SoC} \quad (8)$$

The state of charge (SOC), expressed as a fraction of total charge carrying capacity, is restricted to values between 20% and 100% in Equation 8. The lower limit of 20% is imposed to prevent degradation at low voltages. Lithium-ion batteries in electric vehicles have similar constraints imposed by car manufacturers [4].

Our model does not implement a constraint specifically to restrict simultaneous charging and discharging, which is functionally impossible, but could be economic in certain circumstances. This type of constraint is difficult to implement in a linear program. In practice, our results contain no instances of simultaneous charging and discharging, obviating the need for this constraint.

Spike-to-Battery Ratio for Low Variation Load Profiles

In Figure C-11, we explore what happens when the battery power capacity becomes very large relative to the variance of the load profile. As battery capacity increases, the spike-to-battery ratio asymptotes at the width of the load shape time window divided by the duration of the battery. In our example, the width of the time window is 5hrs and the battery duration is 1 hr.

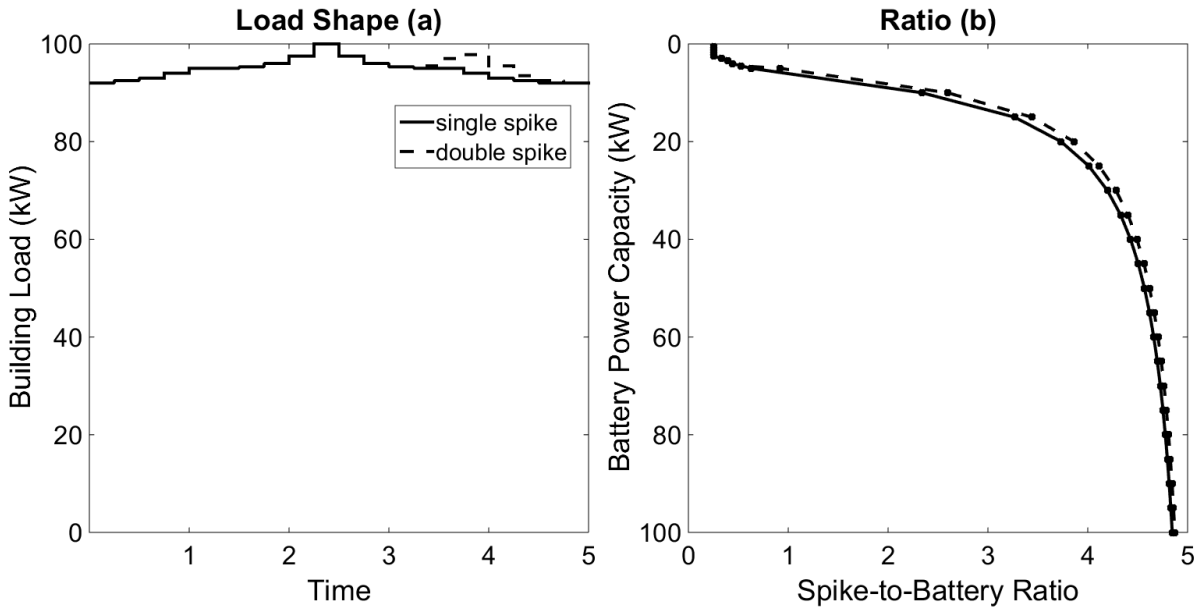

Figure C-11: Behavior of Spike-to-Battery Ratio when the battery power capacity becomes large relative to the load shape variance (a). The ratio will asymptote at the width of the load shape time window divided by the duration of the battery (b). In our example, this is 5hrs:1hr.

References

[1] EnerNOC Open Data, (2013). https://open-enernoc-data.s3.amazonaws.com/anon/index.html (accessed January 1, 2016).

[2] S.B. Peterson, J. Apt, J.F. Whitacre, Lithium-ion battery cell degradation resulting from realistic vehicle and vehicle-to-grid utilization, J. Power Sources. 195 (2010) 2385–2392. doi:10.1016/j.jpowsour.2009.10.010.

[3] M. Broussely, S. Herreyre, P. Biensan, P. Kasztejna, K. Nechev, R.. Staniewicz, Aging mechanism in Li ion cells and calendar life predictions, J. Power Sources. 97–98 (2001) 13–21. doi:10.1016/S0378-7753(01)00722-4.

[4] M. Eberhard, A Bit About Batteries, Tesla Mot. Blog. (2006). https://www.teslamotors.com/blog/bit-about-batteries (accessed January 1, 2016).

Chapter 5: Flow Batteries are Uncompetitive in the Commercial and Industrial Market

Abstract

Commercial and industrial customers represent a large potential market for energy storage technologies because storage allows customers to reduce energy costs and provide wholesale market services. While flow batteries have existed for decades, they have recently received significant investor interest as a storage solution that can provide multiple simultaneous services to markets newly opened to storage, such as renewable generation time-shifting and frequency regulation. Flow batteries are operationally quite different from established storage technologies like lithium-ion and lead-acid, and thus have different performance characteristics. We model advanced lead-acid, lithium-ion, and flow batteries under various tariff scenarios providing retail and wholesale market services to determine if flow batteries can compete in the retail market. We find that flow batteries are uncompetitive with lithium-ion and lead-acid batteries across a range of use cases and modelling assumptions. Flow batteries at a 4-hour duration must be less expensive than their competitors on a dollar per installed kWh basis, often by 20-30%, to break even with shorter duration li-ion or lead-acid despite allowing for deeper depth of discharge and superior cycle life. Our results are robust to assumptions of tariff rates, battery round-trip efficiencies, amount of solar generation and whether the battery can participate in the wholesale energy and ancillary services markets.

5.1 Introduction

Commercial and industrial behind-the-meter (BTM) electricity storage is growing rapidly [1] as a way for customers to offset utility demand charges, participate in demand response programs, and for utilities to procure distributed capacity resources [2]. Storage technologies have proliferated in response to the opportunity in these markets and to federal research funding [3]. Lead-acid batteries have dominated the market for decades, and lithium-ion (li-ion) chemistries have recently gained significant market share, but flow batteries have attracted considerable investor interest [4,5] with the promise of attractive performance characteristics that cannot be matched by competing technologies. This suite of characteristics has become attractive as enabling technologies and changes in regulations have opened new markets for energy storage.

While conventional batteries store energy in the solid electrode, flow batteries store energy in soluble chemicals in liquid electrolyte. Two separate redox couples are pumped on either side of an ion-selective membrane, where they undergo oxidation or reduction reactions [6] that charge or discharge the cell. Adjusting the energy capacity of a flow battery is as easy as changing the volume or concentration of the electrolyte [7], which often does not require design changes in the battery cell where the reactions take place. For li-ion batteries, the electrode thickness must be decided at the time of manufacturing, and governs whether the battery should be used in energy or power focused applications. Thinner electrodes allow for higher power output at a given energy capacity, but increase manufacturing costs [8]. The “de-coupling” of energy and power in flow batteries allows for significant design latitude in situations that require simultaneous energy and power services, and reduces the risk of investing in a long-lived asset under regulations, incentives, and market structures that change frequently.

Flow batteries suffer very little capacity degradation when cycled to full depth of discharge, whereas lithium-ion and lead-acid batteries cannot cycle to such depths without substantial degradation [9]. A larger effective energy capacity can be useful in applications that require deep discharges, such as demand charge mitigation. Cycle life is extremely long in comparison to li-ion and lead-acid [10], with typical warranties at 20 years versus 10 for li-ion. However, round-trip efficiency (RTE) is much lower in flow batteries. Typical flow battery AC-AC conversion efficiencies are 60-70% [11,12], while li-ion batteries are reaching 90% [6]. A review of commercialized products also reveals that there are no flow batteries on the market with a rated discharge duration at full power of less than 3 hours. Most products are rated at 4 or 5 hours. Longer duration storage assets will have lower capacity utilization than short duration assets in many commercial applications, which leads to lower cost effectiveness.

Technology characteristics are very important for consumers looking to invest in such long-lived assets. To date there has not been a comprehensive comparison of economic performance across storage technologies and use cases in the retail and/or wholesale space. Some have explored using electric vehicle batteries for reducing energy costs and emissions [13,14], but the use constraints imposed by mobile storage are severe. Studies of behind-the-meter stationary storage have focused on only one storage technology [15–18]. While they may vary certain storage performance characteristics for sensitivity analyses, none examine realistic changes along multiple performance dimensions. Recent studies have examined the practicality of using of stationary storage in conjunction with solar, but examined only one storage technology [19–21]. Leadbetter and Swan [10] examined storage technology choice in the context of grid-level renewable generation integration, but did not consider behind-the-meter storage.

We compare revenue generation from advanced lead-acid, li-ion, and flow batteries across many metered commercial building and solar load profiles while applying different retail and wholesale market conditions. The batteries are allowed to perform arbitrage, demand charge mitigation and provide ancillary services in the wholesale market. We examine whether the effective capacity and cycle life advantages of flow batteries outweigh their inefficiency and make them cost competitive with the market incumbents. When li-ion and lead-acid battery operations are restricted in order to ensure the same 20-year lifetime as a flow battery, flow batteries earn slightly more revenue due to their greater effective energy capacity. However, applying more realistic assumptions around battery sizing, lifetime, and operations we find that flow batteries are not competitive with li-ion or lead-acid in a wide range of scenarios.

5.2 Data and Revenue Model

We formulate a mathematical program to minimize energy costs and maximize revenue to a battery owner using metered data from multiple buildings and solar installations in southern California. By varying the model parameters, we can assess the relative economic advantages or disadvantages of each storage technology to determine the best choice for the desired application. Our results show the costs flow batteries must achieve relative to li-ion and lead-acid to break even from an economic standing. Table 5-1 shows the applications we consider here.

Table 5-1: Storage applications examined here

Solar/Tariff	Retail*	Retail + Wholesale**
No Solar	✓	✓
Solar w/Net Metering	✓	✓
Solar w/Value of Solar Tariff (see Tariff section below)	✓	✓

*Retail = energy arbitrage + demand charge mitigation
**Wholesale = wholesale energy arbitrage + spinning reserve + frequency regulation

5.2.1 Data

The building data used for this analysis come from southern California and were published as part of a larger dataset by EnerNOC [22]. The energy (kWh) data have a 5-minute sample rate for 1 calendar year, which were aggregated (summed) to 15-minute blocks to fit the time period over which demand charges are typically measured. There are 18 commercial buildings in this data set. We recognize that 18 buildings does not represent a large sampling of the population. However, there is significant load diversity inherent in this sample. Figure D-1 in Appendix D shows considerable variation in profitability of equal sized batteries across each of the buildings.

One of the major use cases for storage is to shift solar generation to periods of peak load. We obtained 16 metered solar generation profiles from commercial buildings in California covering all of 2015. The solar arrays ranged in size from 90-500 kW. The computational expense of running our model over all building and solar profiles, however, was prohibitive. We instead chose to run an average solar profile for our analysis. This average was taken across all 16 profiles for each 15-minute period. Figures in Appendix D show that the majority of the variation in storage profitability across building and solar profiles is captured by sampling over buildings alone. To ensure our conclusions are robust to the choice of solar profile, we also ran our model using the solar profile with the highest variation in power output. The results were nearly identical to those presented here.

Real-time wholesale market data for calendar year 2015 were downloaded from the California system operator (CAISO) [23].

5.2.2 Tariffs

We chose utility tariffs from Southern California Edison (SCE) to match the location of our building and solar profiles. California is an appropriate location in which to explore storage technology choice because of large differences in peak and off-peak energy costs, high demand charges, and a well-developed solar market.

Table 5-2: Solar and non-solar tariffs from Southern California Edison (as of July 2017) [24]

Utility Tariff: **Southern California Edison (SCE) – CA**	**Demand Charges ($/kW)** **Summer / Winter**	**Energy Charges ($/kWh)** **Summer / Winter**
Non-solar: General Service – Large; TOU-8, Option B (under 2kV)	$15.57 – all periods + $22.95 / 0 – peak + $6.49 / 0 – mid-peak	$0.14202 / 0.08899 – peak $0.08749 / 0.08899 – mid-peak $0.06288 / 0.0681 – off-peak
Solar Net Metered: General Service – Large; TOU-8, Option R (under 2kV)	$16.23 – all periods	$0.30854 / 0.07836 – peak $0.10962 / 0.07836 – mid-peak $0.06396 / 0.06883 – off-peak

As behind-the-meter solar generation grows rapidly in many western states, rate design for solar customers has evolved. Some states are exploring value-of-solar (VOS) tariffs that compensate customers at a reduced rate for any energy exported to the grid. Nevada's proposed excess energy credit is only 25% of the retail rate in 2028 [25]. We created a hypothetical VOS tariff for southern California by applying a single factor to the prevailing time-of-use tariff in any period where energy is exported to the grid. For example, if we apply a 50% factor to the net metering tariff in Table 5-2, a solar customer would be compensated at $0.15/kWh during summer peak periods, $0.05/kWh mid-peak, and $0.03/kWh during off-peak periods for any

energy exported to the grid. We explored a -5%, 0%, 50% and 75% factor for energy exports to the grid.

5.2.3 Storage Characteristics

Storage performance characteristics are given in Table 5-3. A consistent 80kW maximum rated power was used across all scenarios to ease comparison across scenarios and buildings. We vary the flow battery rated duration to recognize both the current production landscape and hypothetical capabilities. An online survey of commercialized flow batteries reveals that there are no flow batteries on the market with a rated discharge duration at full power of less 3 hours. Most are rated at 4 hours or longer. While we recognize that costs for equipment such as pumps make longer duration flow batteries more economic than short duration flow batteries, to understand how shorter duration flow batteries would fare in comparison to their competitors, we ran some scenarios with 2 hour duration for all batteries.

Table 5-3: Storage performance characteristics

	Lithium-ion	Advanced Lead Acid	Flow
Round-trip efficiency	90%	90%	65%
Lifetime	10-20yr	10-20yr	20yr
Capacity degradation	See appendix	See appendix	None
Maximum rated power	80kW	80kW	80kW
Duration (at max power)	2hr	2hr	2-4hr
Current installed cost	$750/kWh[1]	$600/kWh[2]	Treated parametrically

[1] Middle of the range given by Lazard [26].
[2] 20% less than li-ion as assumed in Ciez and Whitacre [27].

We did not include self-discharge rates or other parasitic loads in our analysis. They would not significantly change the results of our analysis, and would not be large enough to change our conclusions.

5.2.4 Model

Each building in our dataset is given a simulated battery. We formulate a mathematical program to minimize energy costs and maximize revenue to the battery owner over 20 years. The 1-year building, solar, and market price profiles are repeated in each of the 20 years. Lead-acid and li-ion batteries are replaced at the end of 20 years in scenarios that put them on an equal footing with flow batteries, and at the end of 10 years in more realistic scenarios. In scenarios with solar generation, the nameplate capacity of the solar array can be varied to reach a certain goal (e.g., 50% of annual load). The revenue calculated in these scenarios is the difference between the building with solar and storage, and the building with solar only.

The battery is able to perform energy arbitrage, reduce demand charges, and, depending on the ability to participate in wholesale markets, provide frequency regulation or spinning reserve. The optimization is conducted at 15-minute intervals to reflect the typical structure of demand charges and the sampling rate of many meters. We assume that the storage system is too small to affect market prices. The optimization model minimizes retail energy costs to the customer, maximize revenue from wholesale market participation, and considers battery degradation in making decisions.

We perform daily optimizations in which costs are minimized over a 36-hour horizon. The extra 12 hours in the optimization horizon ensures that the battery does not discharge all of its energy at the end of each day. We assume perfect foresight of building load, which will somewhat overestimate revenue to the battery. In reality, building load forecasts would be used in the battery optimization. Short-term building load forecasting algorithms are an active area of research, and average forecast errors of 5-10% are routinely feasible [28,29]. Hence, we do not

believe the perfect foresight assumption distorts our conclusions. Detailed information about the optimization model can be found in Appendix D.

The economic incentives facing the battery owner will affect battery operations. In addition to a retail-only customer facing retail rates, an "aggregator" can pool retail resources for participation in wholesale markets. We examine both ownership perspectives by varying the components of the objective function and constraints (Table 5-4). Both perspectives consider the economic tradeoff between battery use and degradation by multiplying the calculated capacity degradation by the estimated replacement cost of the battery. This acts as a kind of "hurdle rate" for the performance of any service, and by adjusting this rate we can ensure each battery lasts for its intended lifetime. We calculate capacity degradation according to the formulae in Ciez and Whitacre [27] (see appendix), and reduce available capacity in our model on a monthly basis. We assume the battery is replaced after it reaches 80% of its original capacity. We assume a 10% discount rate for valuing future cash flows.

Table 5-4: Components of total energy cost minimization

Perspective	Customer Energy Cost	Customer Demand Charge	Wholesale Energy Cost	Frequency Regulation Revenue	Spinning Reserve Revenue	Battery Degradation
Retail-only	✓	✓				✓
Retail+Wholesale	✓	✓	✓	✓	✓	✓

In this analysis, we consider only the initial capital costs to install the system. By ignoring other costs in our comparison (e.g., maintenance), we are implicitly assuming these costs are similar across technologies.

5.3 Results

We first examine if flow batteries can compete with equal sized li-ion and lead-acid batteries when the incumbent technologies are forced to last for 20 years. We achieve this lifetime by raising their hurdle rate, effectively restricting their charge/discharge activity. In this scenario, flow batteries produce more revenue than li-ion or lead-acid.

We then create a more realistic comparison by allowing for li-ion and lead-acid replacement after 10 years, and increasing the duration of the flow battery from 2 hours to 4 hours. Flow batteries in all tariff scenarios must be priced less than li-ion and lead-acid on a dollar per installed kWh basis to achieve the same net present value. Under the most optimistic assumptions of improved round-trip efficiency, flow battery prices can be the same as lead-acid but must remain lower than li-ion prices to be competitive.

5.3.1 Common Battery Lifetime and Duration

Given similar lifetimes and discharge durations, flow batteries can generate the same revenue as li-ion and advanced lead-acid despite their round-trip efficiency losses. Figure 5-1 shows that revenue for flow batteries is the same (if not slightly higher) as li-ion and lead-acid across building load profiles. While retail energy costs will be higher for flow batteries due to increased charging energy, their larger effective energy capacity allows for greater demand charge mitigation. Figure 5-2 shows a comparison of revenue by service for a number of different tariff and ownership perspectives.

Despite faster degradation, lead-acid batteries perform nearly as well as li-ion in most scenarios. As expected, lead-acid generates less revenue from retail and wholesale energy arbitrage, but a majority of battery revenue is generated from demand charge mitigation and

ancillary services. These services do not require large amounts of energy and are used infrequently, which is why lead-acid batteries can compete with li-ion.

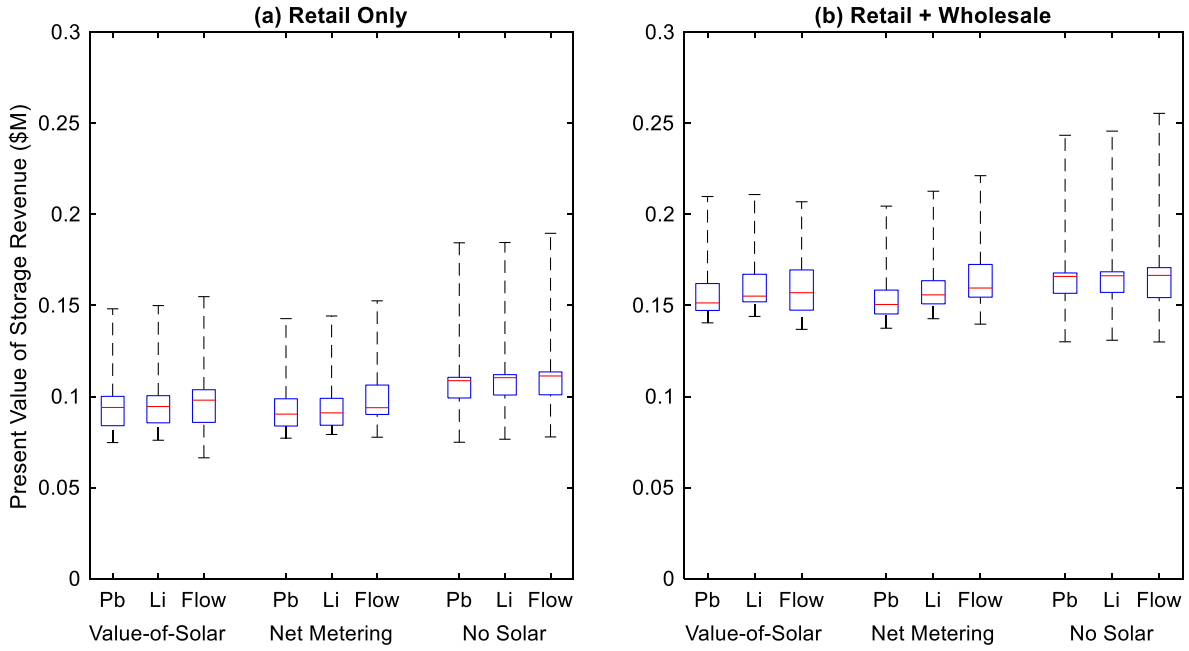

Figure 5-1: Present value of storage revenue under different storage technologies and tariffs for retail-only (a) and retail + wholesale (b) revenue. All batteries have 20yr lifetime, 80kW max power and 2hr duration. An individual boxplot represents the distribution across 18 buildings in the dataset. Value-of-solar and net metering scenarios assume solar delivers 50% of each building's annual energy requirement. Value-of-solar tariff compensates energy exports at 50% of retail tariff. Boxplot whiskers show the maximum and minimum value, the box shows the interquartile range, and the line represents the median value.

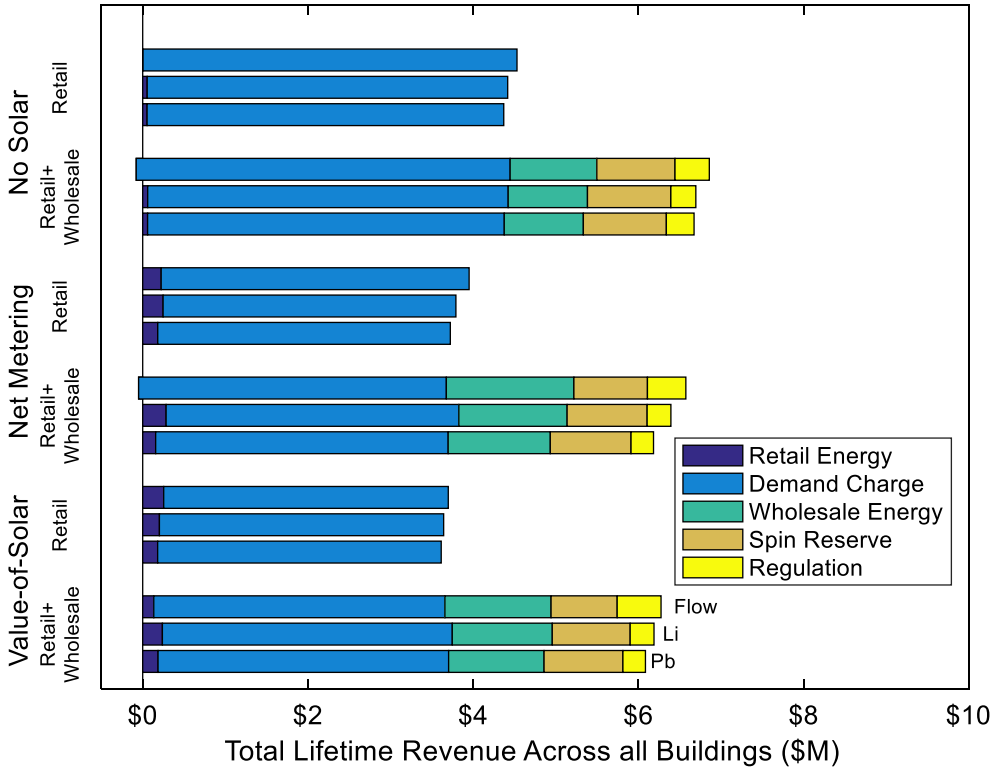

Figure 5-2: Breakdown of revenue by service across tariff and ownership scenarios. All batteries have 20yr lifetime, 80kW max power and 2hr duration.

The installed price needed for flow batteries to break even (achieve the same net present value) with li-ion and lead-acid is favorable, with the median cost relative to li-ion and lead-acid costs above a ratio of 1 (Figure 5-3). This means that flow batteries can be priced more than li-ion or lead-acid and still produce the same net present value. We call this metric the breakeven price ratio. It should be noted that installed flow battery costs on a $/kWh basis for a 2-hr duration battery may be much higher than published costs because most current flow batteries have durations longer than 3 hours.

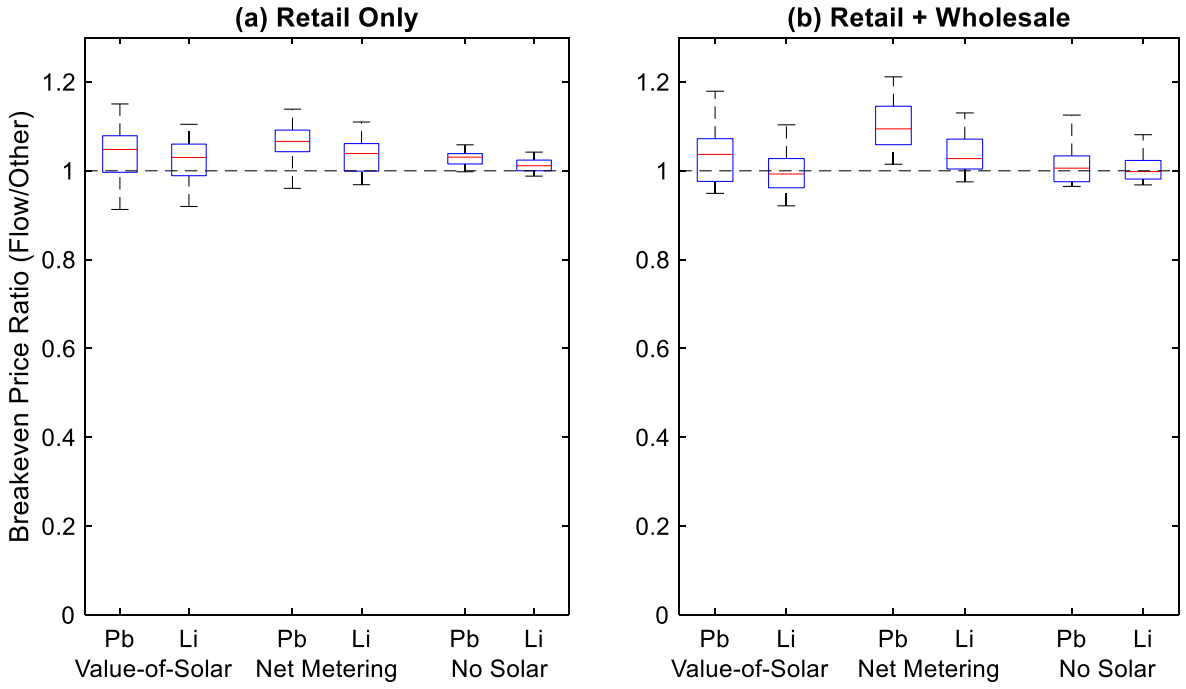

Figure 5-3: Breakeven price ratio under different storage technologies and tariffs for retail-only (a) and retail + wholesale (b) revenue. These scenarios assume equal lifetimes across technologies; a more realistic case is considered in the following section. The breakeven cost ratio is defined as the cost of the flow battery relative to the cost of the comparison battery at which the net present value of the two technologies is equal.

To make this comparison, we adjusted the hurdle rate for li-ion and lead-acid batteries to ensure that each could last for the full 20 year lifetime that flow batteries can achieve. We also assumed a 2 hour duration for all battery technologies. However, this is a somewhat theoretical exercise. Lead-acid and li-ion batteries may not be able to last 20 years, and there are no commercial flow batteries that have a duration at maximum power of 2 hours. This exercise was useful to confirm that flow batteries can produce a similar amount of revenue as li-ion and lead-acid, and we can now make a more realistic comparison.

5.3.2 A More Realistic Comparison

As a first step, we increase flow battery duration to 4 hours to match the duration of most flow batteries now on the market, while keeping li-ion and lead-acid duration at 2 hours. The

scarcity of flow batteries at lower duration is not due to technical challenges [7], but rather economics. Current estimates of installed prices place flow and li-ion batteries at roughly the same price point at a 4-hour duration [26]. However, costs will scale down more quickly for li-ion at lower durations because the need for physical energy storage media and associated equipment is reduced[3]. Reducing flow battery duration is a matter of reducing the volume of electrolyte storage or switching to a less concentrated electrolyte. The associated piping, pumps, and ion exchange cell remain the same, however. This locks in higher fixed costs at a given rated power for flow batteries, likely making a 4-hour duration more economically attractive than a 2-hour duration. It is difficult to accurately quantify how costs scale at different durations for flow batteries given low sales volumes in this technology.

Doubling flow battery duration in our model from 2 to 4 hours will increase revenue in all scenarios (Figure 5-4). However, there are decreasing returns to adding energy capacity. It allows for a small increase in retail and wholesale energy arbitrage, but does not significantly increase demand charge mitigation because the maximum power output remains the same.

[3] This is true for batteries at the low power-to-energy (P/E) ratios considered by this paper. At high P/E ratios (low durations) such as those encountered in some electric vehicles, manufacturing costs may increase due to requirements for thinner electrodes [8].

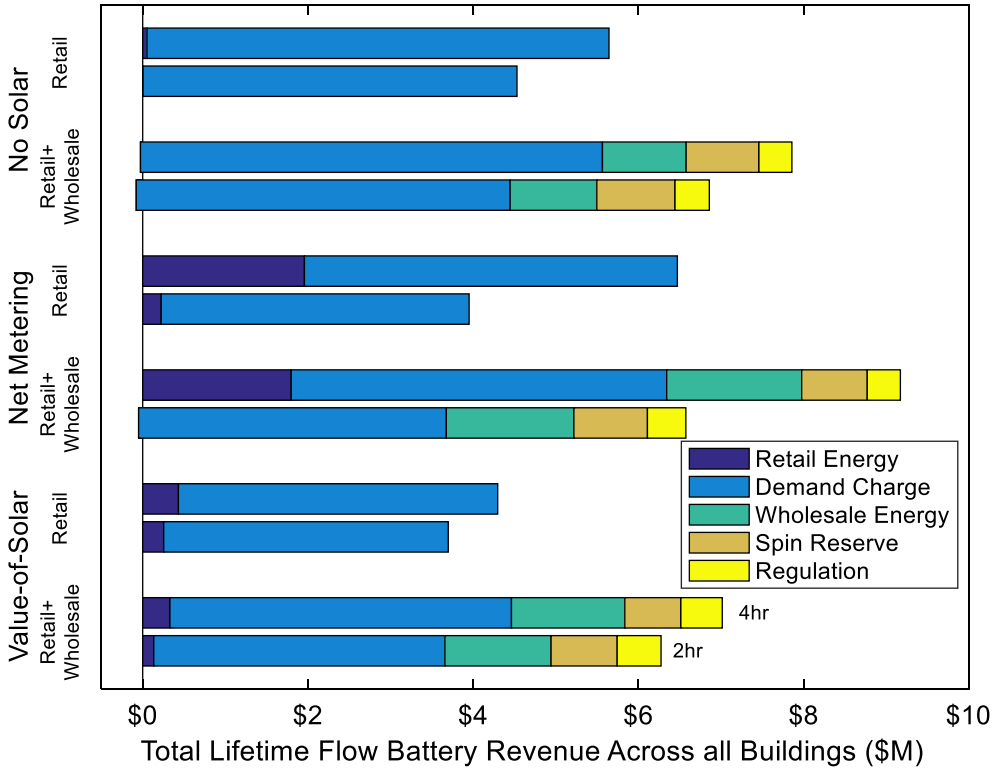

Figure 5-4: Increase in flow battery revenue by increasing duration from 2 to 4 hours.

The final step in making our technology comparison realistic is to assume the li-ion and lead-acid batteries must be replaced at the end of 10 years. We model this as a decrease in the hurdle rate, which encourages the battery to perform more revenue generating activities (Figure 5-5). We ensure that both technologies reach a 10 year lifetime, at which point they are replaced, and then run for another 10 years. This allows us to compare revenue over the same 20 year lifetime as the flow battery.

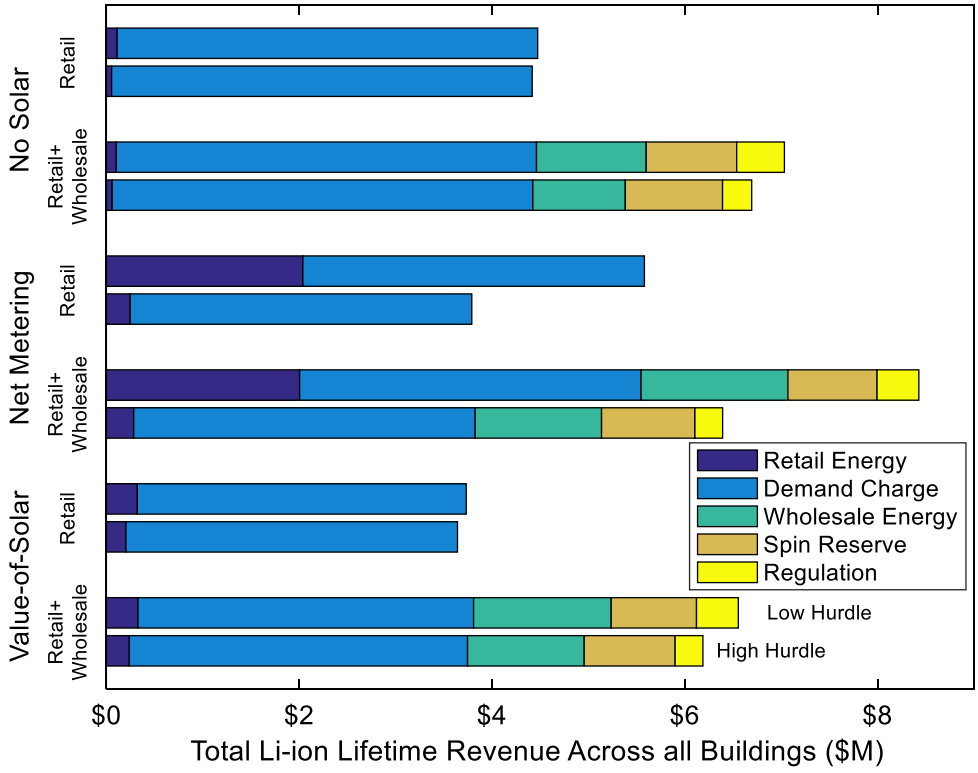

Figure 5-5: Increase in Li-ion revenue from lowering hurdle rate. Battery duration remains at 2 hours.

We can now assess the breakeven cost ratio after making these changes to our model. Revenue has increased for all storage technologies, but costs have increased as well – we have doubled the energy capacity of the flow batteries and required a battery replacement at the end of 10 years for li-ion and lead acid. We assume that li-ion and lead-acid replacement prices are 70% of current prices. Figure 5-6 shows that the entire breakeven cost ratio distribution is below 1 for all tariffs, meaning that flow batteries must be priced less on a $/kWh basis than either li-ion or lead-acid to break even with those technologies.

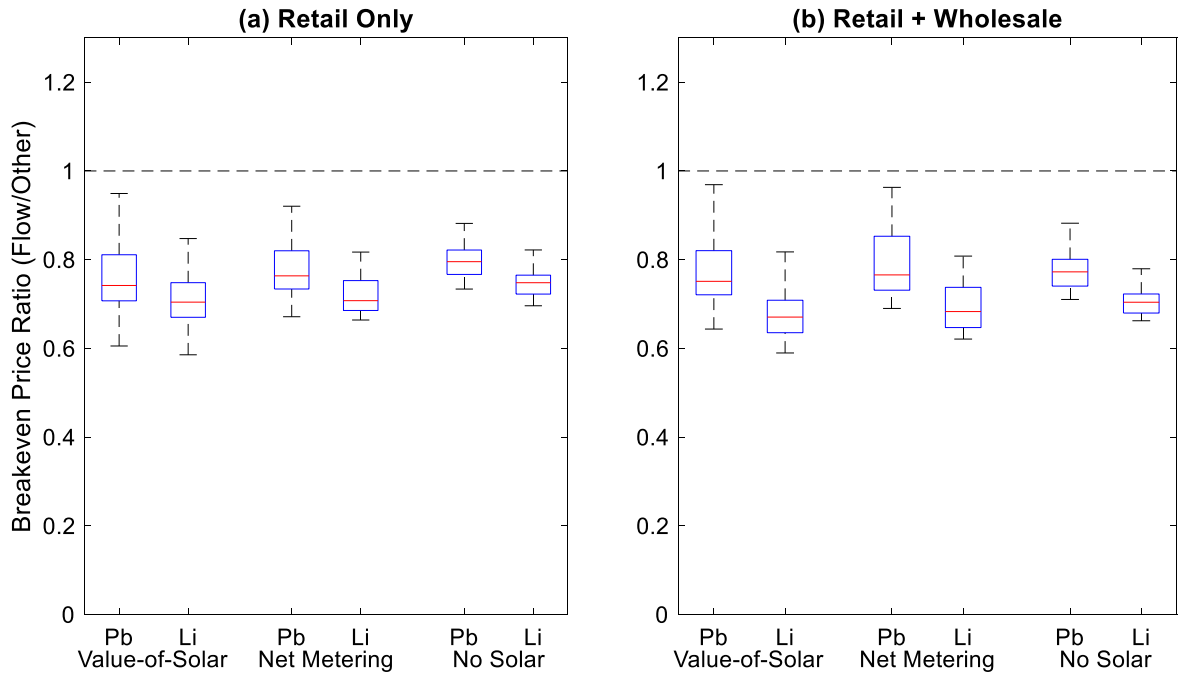

Figure 5-6: Breakeven price ratio under different storage technologies and tariffs for retail-only (a) and retail + wholesale (b) revenue. These scenarios assume a 20yr lifetime / 4hr duration for flow batteries and 10yr lifetime / 2hr duration for li-ion and lead-acid. Value-of-solar and net metering scenarios assume solar delivers 50% of each building's annual energy requirement. Value-of-solar tariff compensates energy exports at 50% of retail tariff.

Figure 5-7 and Figure 5-8 show how the breakeven price ratio distribution changes under different solar generation and energy export compensation assumptions. Most breakeven price distributions remain below 1, indicating that flow batteries must be less expensive than storage competitors on a dollar per installed kWh basis to produce the same net present value.

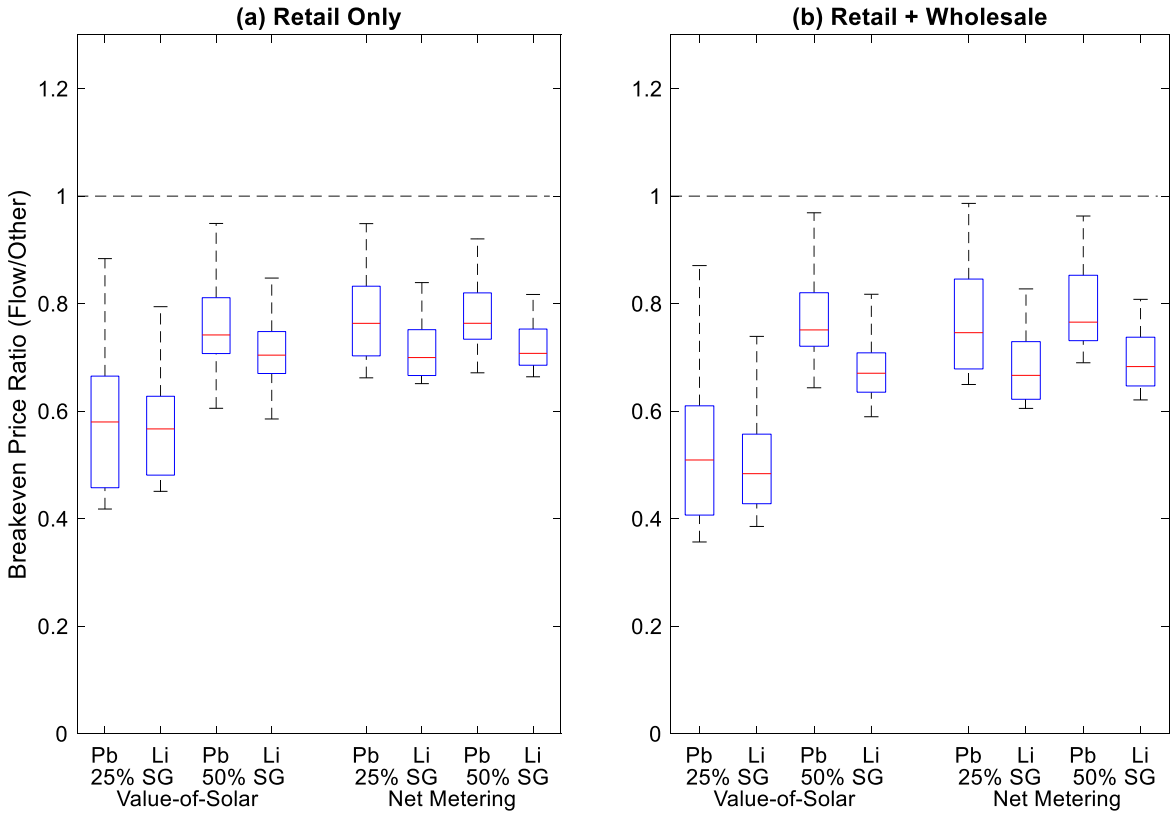

Figure 5-7: Effect of solar generation fraction on breakeven price ratios under different tariffs. We examined two levels of solar generation, 25% and 50% of annual building energy consumption. These scenarios assume a 20yr lifetime / 4hr duration for flow batteries and 10yr lifetime / 2hr duration for li-ion and lead-acid.

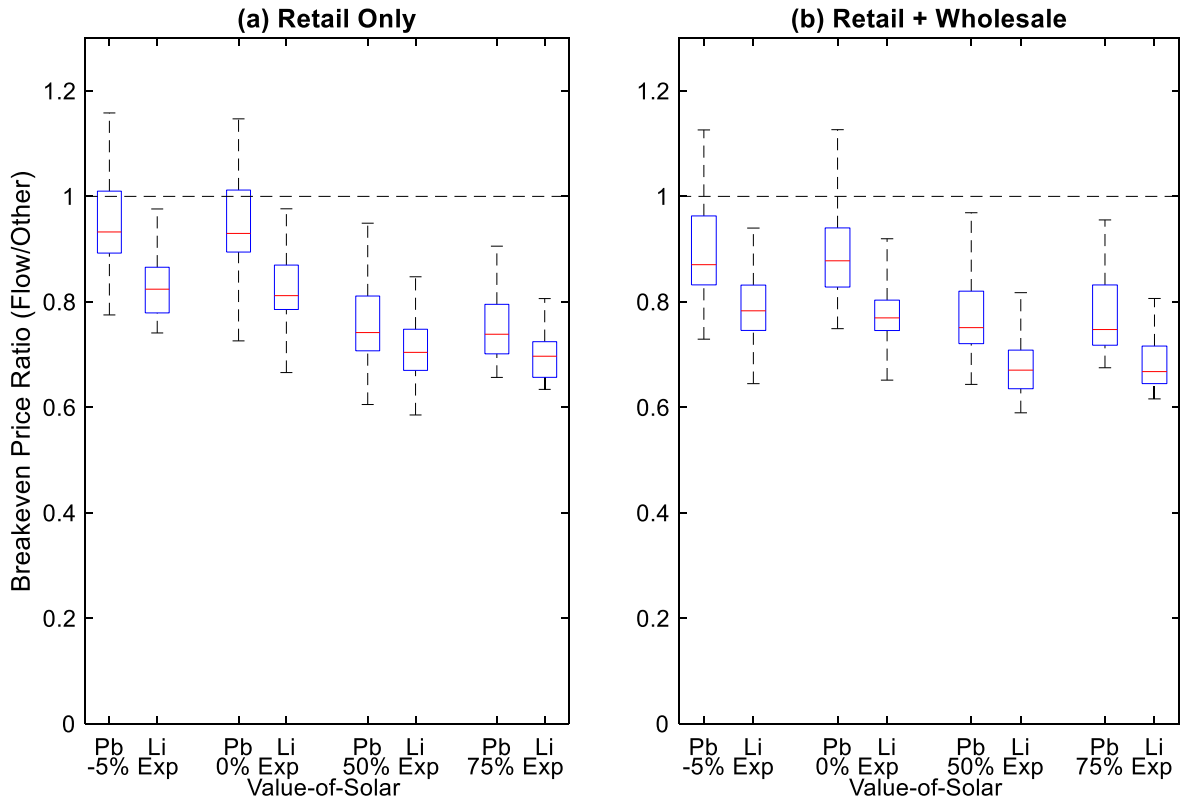

Figure 5-8: Effect of energy export compensation fraction on breakeven price ratios for the value-of-solar tariff. We examined four levels of energy export compensation fraction, -5%, 0%, 50% and 75% of the retail tariff. These scenarios assume a 20yr lifetime / 4hr duration for flow batteries and 10yr lifetime / 2hr duration for li-ion and lead-acid.

We included -5% and 0% export tariffs in Figure 5-8 to mimic the effects of policies in Europe and Hawaii that encourage self-consumption of solar generation. Even in these extreme scenarios, flow batteries do not have breakeven price ratios above 1 when compared with li-ion. A simple multiplier is an imperfect method to replicate these tariffs, but we believe it is an appropriate qualitative proxy that supports our conclusions.

Figure 5-9 shows how breakeven price distributions improve if flow batteries become more efficient. In the extreme case that flow batteries achieve 90% RTE (about as efficient as current li-ion RTE), then breakeven flow battery prices are roughly equal to lead-acid prices, but still must be less expensive than li-ion.

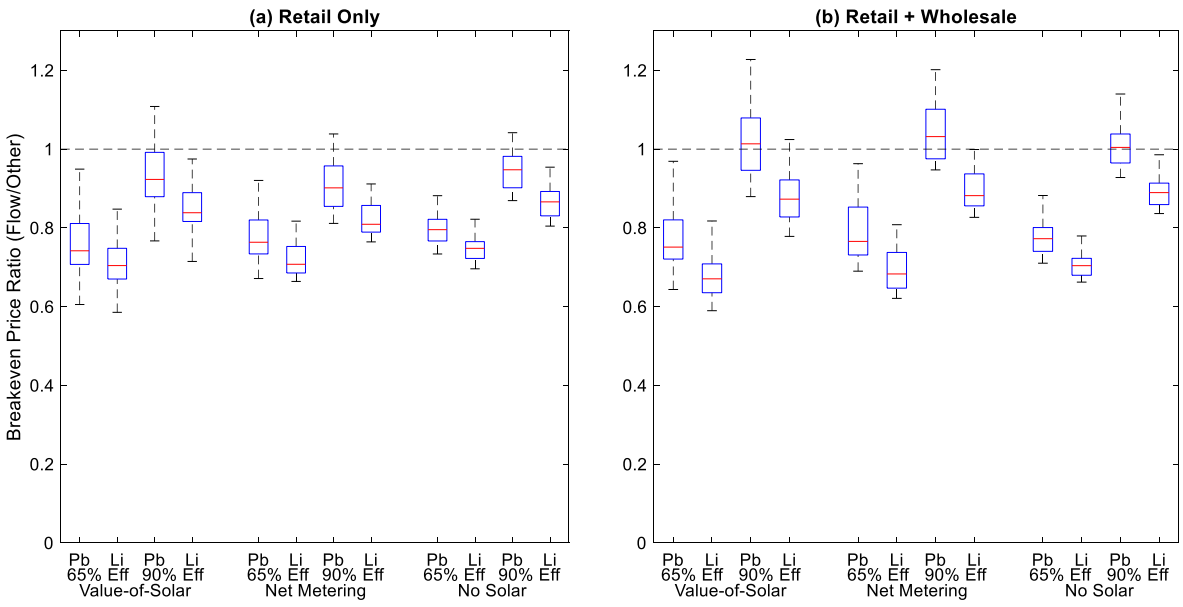

Figure 5-9: Effect of flow battery round-trip efficiency on breakeven price ratios across tariffs and technologies. We examined two levels of round-trip efficiency, 65% in the baseline and 90% to examine what would happen if flow batteries became as efficient as li-ion. These scenarios assume a 20yr lifetime / 4hr duration for flow batteries and 10yr lifetime / 2hr duration for li-ion and lead-acid.

5.4 Discussion

Our analysis indicates that flow batteries are uncompetitive with li-ion or even with advanced lead-acid batteries in the commercial and industrial market. Flow batteries at a 4-hour duration must be less expensive on a dollar per installed kWh basis, often by 20-30%, to break even with shorter duration li-ion or lead-acid despite allowing for deeper depth of discharge and superior cycle life. Our results are robust to assumptions of tariff rates, battery round-trip efficiencies, amount of solar generation and whether the battery can participate in the wholesale energy and ancillary services markets.

The ability of flow battery manufacturers to significantly reduce cost is questionable. Cost reduction requires economies of scale and research funding [30], which may not materialize if sales do not increase. The disparity between flow batteries and li-ion will only widen as

manufacturing capacity for li-ion expands. Cost projections for li-ion battery packs suggest at least a 30% reduction within 5 years [30,31].

We are not asserting that flow batteries have no place in the storage market, only that they will not likely be competitive in the commercial and industrial space. Their larger effective energy capacity allows for deeper demand reductions. This may be useful at the distribution level to utilities that need to offset infrequent peaks in feeder load or shift large amounts of distributed renewable generation. Flow batteries may also be useful at the transmission level to relieve congestion from the production of renewable energy or to shift that energy to more lucrative times of the day. Though, again, if li-ion costs drop significantly, it may be less expensive to simply install a larger lithium battery if more energy capacity is required. Very long duration applications (8+ hours) in microgrids or off-grid systems may be the best use of flow batteries because cost scaling in energy capacity is relatively small when compared to li-ion.

Using less efficient flow batteries would also raise grid-level emissions rates, assuming the current grid fuel mix in most regions. Grid-level net emissions will depend on the timing and total amount of charging energy versus the timing and total amount of discharge energy, and the emissions rate of the marginal generators. Lower storage efficiency leads to higher overall energy consumption via increased charging. This has implications for indirect emissions rates attributable to each storage technology. In conventional grid systems with lower penetrations of renewable generators, more efficient storage devices have significantly lower net emission rates [16,32]. We did not attempt to calculate the impact of using flow batteries instead of more efficient li-ion batteries at the grid-level for high renewable scenarios due to the lack of emissions modelling accuracy. Many of the studies of storage net emission rates rely on marginal emissions factors [33] that have an important limitation; they do not include renewable

generators. This requires the use of a full production cost model, which is outside the scope of this study.

5.5 References

[1] U.S. Energy Storage Monitor, GTM Research & Energy Storage Association, Boston, MA, 2014.

[2] J. Eyer, G. Corey, Energy Storage for the Electricity Grid: Benefits and Market Potential Assessment Guide, Sandia National Laboratories, Albuquerque, NM, 2010. http://www.sandia.gov/ess/publications/SAND2010-0815.pdf.

[3] ARPA-E, Grid-Scale Rampable Intermittent Dispatchable Storage, (n.d.). https://arpa-e.energy.gov/?q=programs/grids (accessed February 7, 2017).

[4] C. Roselund, Flow battery maker Primus Power raises $32 million, PV Mag. (n.d.). https://pv-magazine-usa.com/2017/03/24/flow-battery-maker-primus-power-raises-32-million/ (accessed January 1, 2017).

[5] A. Colthorpe, Flow batteries, energy storage system companies attracted most VC funding in 2015, says Mercom, Energy Storage News. (n.d.). https://www.energy-storage.news/news/flow-batteries-energy-storage-system-companies-attracted-most-vc-funding-in (accessed January 1, 2017).

[6] B. Dunn, H. Kamath, J.-M. Tarascon, Electrical Energy Storage for the Grid: A Battery of Choices, Science (80-.). 334 (2011) 928–935. doi:10.1126/science.1212741.

[7] M. Skyllas-Kazacos, M.H. Chakrabarti, S.A. Hajimolana, F.S. Mjalli, M. Saleem, Progress in Flow Battery Research and Development, J. Electrochem. Soc. 158 (2011) R55. doi:10.1149/1.3599565.

[8] A. Sakti, J.J. Michalek, E.R.H. Fuchs, J.F. Whitacre, A techno-economic analysis and optimization of Li-ion batteries for light-duty passenger vehicle electrification, J. Power Sources. 273 (2015) 966–980. doi:10.1016/j.jpowsour.2014.09.078.

[9] A.Z. Weber, M.M. Mench, J.P. Meyers, P.N. Ross, J.T. Gostick, Q. Liu, Redox flow batteries: a review, J. Appl. Electrochem. 41 (2011) 1137–1164. doi:10.1007/s10800-011-0348-2.

[10] J. Leadbetter, L.G. Swan, Selection of battery technology to support grid-integrated renewable electricity, J. Power Sources. 216 (2012) 376–386. doi:10.1016/j.jpowsour.2012.05.081.

[11] Primus Power - Energy Pod Specifications, (2017). http://primuspower.com/en/product/ (accessed July 21, 2017).

[12] Vionx Energy Specifications, (2017). http://vionxenergy.com/wp-content/uploads/2016/08/Vionx-Technology-Specifications.pdf (accessed July 21, 2017).

[13] S.B. Peterson, J.F. Whitacre, J. Apt, The economics of using plug-in hybrid electric vehicle battery packs for grid storage, J. Power Sources. 195 (2010) 2377–2384. doi:10.1016/j.jpowsour.2009.09.070.

[14] M. Stadler, M. Kloess, M. Groissböck, G. Cardoso, R. Sharma, M.C. Bozchalui, C. Marnay, Electric storage in California's commercial buildings, Appl. Energy. 104 (2013) 711–722. doi:10.1016/j.apenergy.2012.11.033.

[15] J. Neubauer, M. Simpson, Deployment of Behind-The-Meter Energy Storage for Demand Charge Reduction, National Renewable Energy Laboratory, Golden, CO, 2015. http://www.nrel.gov/docs/fy15osti/63162.pdf.

[16] M.J. Fisher, J. Apt, Emissions and Economics of Behind-the-Meter Electricity Storage, Environ. Sci. Technol. 51 (2017) 1094–1101. doi:10.1021/acs.est.6b03536.

[17] K. Zheng, Z. Zheng, H. Jiang, J. Ren, Economic analysis of applying the used EV battery to commercial electricity customer, in: 2015 5th Int. Conf. Electr. Util. Deregul. Restruct. Power Technol., IEEE, 2015: pp. 2100–2103. doi:10.1109/DRPT.2015.7432593.

[18] R.T. de Salis, A. Clarke, Z. Wang, J. Moyne, D.M. Tilbury, Energy storage control for peak shaving in a single building, in: 2014 IEEE PES Gen. Meet. | Conf. Expo., IEEE, 2014: pp. 1–5. doi:10.1109/PESGM.2014.6938948.

[19] R.L. Fares, M.E. Webber, The impacts of storing solar energy in the home to reduce reliance on the utility, Nat. Energy. 2 (2017) 17001. doi:10.1038/nenergy.2017.1.

[20] P. Hanser, R. Lueken, W. Gorman, J. Mashal, The practicality of distributed PV-battery systems to reduce household grid reliance, Util. Policy. 46 (2017) 22–32. doi:10.1016/j.jup.2017.03.004.

[21] R. Hanna, J. Kleissl, A. Nottrott, M. Ferry, Energy dispatch schedule optimization for demand charge reduction using a photovoltaic-battery storage system with solar forecasting, Sol. Energy. 103 (2014) 269–287. doi:10.1016/j.solener.2014.02.020.

[22] EnerNOC Open Data, (2013). https://open-enernoc-data.s3.amazonaws.com/anon/index.html (accessed January 1, 2016).

[23] CAISO Oasis, (2017). http://oasis.caiso.com (accessed February 1, 2017).

[24] Southern California Edison Historical Prices and Rate Schedules, (2017). https://www.sce.com/wps/portal/home/regulatory/tariff-books/historical-rates/ (accessed March 1, 2017).

[25] Nevada Energy, Net Metering, (2017). https://www.nvenergy.com/renewablesenvironment/solar/netmetering.cfm (accessed January 1, 2017).

[26] Lazard's Levelized Cost of Storage Analysis - Version 2.0, Lazard, 2016. https://www.lazard.com/media/438042/lazard-levelized-cost-of-storage-v20.pdf.

[27] R.E. Ciez, J.F. Whitacre, Comparative techno-economic analysis of hybrid micro-grid systems utilizing different battery types, Energy Convers. Manag. 112 (2016) 435–444. doi:10.1016/j.enconman.2016.01.014.

[28] C.E. Borges, Y.K. Penya, I. Fernandez, Optimal combined short-term building load forecasting, 2011 IEEE PES Innov. Smart Grid Technol. (2011) 1–7. doi:10.1109/ISGT-Asia.2011.6167091.

[29] A. Khosravi, S. Nahavandi, D. Creighton, A.F. Atiya, Comprehensive Review of Neural Network-Based Prediction Intervals and New Advances, IEEE Trans. Neural Networks. 22 (2011) 1341–1356. doi:10.1109/TNN.2011.2162110.

[30] N. Kittner, F. Lill, D. Kammen, Energy storage deployment and innovation for the clean energy transition, Nat. Energy. 2 (2017). doi: 10.1038/nenergy.2017.125.

[31] B. Nykvist, M. Nilsson, Rapidly falling costs of battery packs for electric vehicles, Nat. Clim. Chang. 5 (2015) 329–332. doi:10.1038/nclimate2564.

[32] E.S. Hittinger, I.M.L. Azevedo, Bulk energy storage increases United States electricity system emissions., Environ. Sci. Technol. 49 (2015) 3203–10. doi:10.1021/es505027p.

[33] K. Siler-Evans, I.L. Azevedo, M.G. Morgan, Marginal Emissions Factors for the U.S. Electricity System, Environ. Sci. Technol. 46 (2012) 4742–4748. doi:10.1021/es300145v.

Appendix D: Additional Modelling Details

Variation in Solar Profiles

Performing sensitivity analysis across all buildings and solar profiles is computationally prohibitive. We reduced the computational resources required for our analysis by using a single solar profile. This profile is the average of the 16 solar profiles in our dataset for each 15-minute period after being normalized to the rated capacity of the system. Using a geographically smoothed solar profile reduces power variability in the solar system [1]. In a solar and storage system, solar variability may be compensated by the storage system. Thus we need to understand how the reduced variability of solar power in our averaged solar profile affects the profitability of the storage system.

The figures below investigate the distribution of storage profitability across all solar profiles. We find that the distribution of profit across solar profiles is much less variable than the distribution of profit across buildings, and below the level that would change the conclusions of our work.

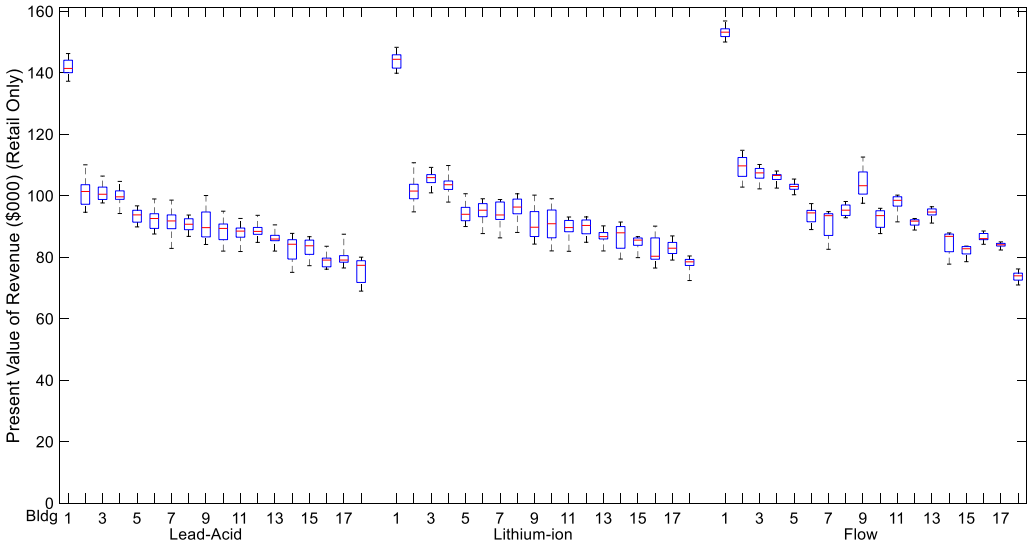

Figure D-1: Distribution of revenue across solar profiles by building and storage technology (25% solar generation). An individual boxplot represents the distribution across 16 solar profiles for an individual building in the dataset. All batteries are rated at 80kW max power and 2-hr duration. A net metering tariff was used. We assume solar delivers 25% of each building's annual energy requirement. Boxplot whiskers show the maximum and minimum value, the box shows the interquartile range, and the line represents the median value.

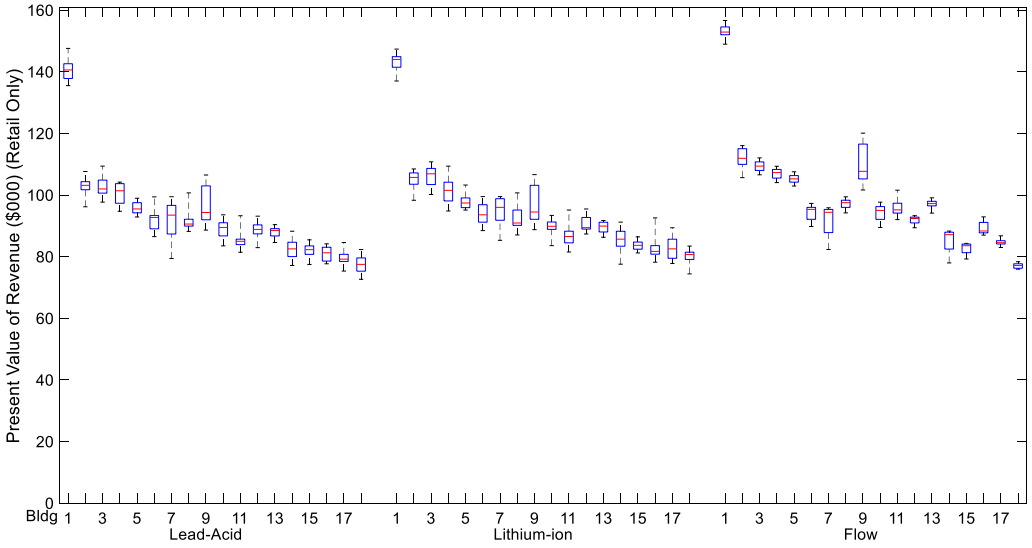

Figure D-2: Distribution of revenue across solar profiles by building and storage technology (50% solar generation). An individual boxplot represents the distribution across 16 solar profiles for an individual building in the dataset. All batteries are rated at

80kW max power and 2-hr duration. A net metering tariff was used. We assume solar delivers 50% of each building's annual energy requirement. Boxplot whiskers show the maximum and minimum value, the box shows the interquartile range, and the line represents the median value.

Optimization Model

Constants

$\overline{SoC}$	Max state of charge of battery (kWh)
$\underline{SoC}$	Minimum state of charge of battery (kWh)
SoC(0)	Initial state of charge of battery (kWh)
$\bar{P}$	Rated power of battery (kW)
η	round-trip efficiency of battery (%)
BL(t)	building load at time t (kW)
EC(t)	Energy cost at time t ($/kWh)
EX(t)	Price paid by utility for energy exported to the grid at time t ($/kWh)
DC_k	Demand charge for demand period k ($/kW)
BRC	Battery Replacement Cost ($)
LMP(t)	Wholesale energy cost at time t ($/kWh)
M	Large positive number used with mixed integer non-linear programs
REGP(t)	Wholesale regulation market price at time t ($/kWh)
SPINP(t)	Wholesale spinning reserve market price at time t ($/kWh)

RDNE Regulation Down Net Energy (kWh/kW) – maximum amount of net energy charge during a typical hour of frequency regulation. Expressed as a fraction of the regulation capacity offered.

RUNE Regulation Up Net Energy (kWh/kW) – maximum amount of net energy discharge during a typical hour of frequency regulation. Expressed as a fraction of the regulation capacity offered.

ABSE Absolute Energy (kWh/kW) – total energy processed by a battery during frequency regulation. Expressed as a fraction of the regulation capacity offered.

Variables

c(t) battery charging at time t (kW)

d(t) battery discharge at time t (kW)

reg(t) frequency regulation capacity participation at time t (kW)

spin(t) spinning reserve participation at time t (kW)

pd_k peak demand during demand period k (kW)

soc(t) state of charge of battery at time t (kWh)

nl(t) net load at time t (kW)

deg(t) battery degradation cost at time t ($)

capdeg battery capacity degradation (unitless, fraction of total capacity)

soc_{swing} average SOC swing in given month (unitless)

u(t) binary variable to indicate positive or negative net load. Equal to 1 if positive net load; 0 if negative net load

Sets

T Set of 15-minute time periods

K Set of demand periods (e.g. peak, mid-peak and off-peak - depends on tariff), each of which is a subset of T

Objective Functions

Customer (Retail-only) Perspective

$$\min \sum_{t \in T} [EC(t) * nl(t) + deg(t)]/4 + \sum_{k \in K} DC_k * pd_k \quad (1)$$

$$\min \sum_{t \in T} \left[EC(t) * nl(t) * u(t) + EX(t) * nl(t) * \left(1 - u(t)\right) + deg(t)\right]/4 + \sum_{k \in K} DC_k * pd_k \quad (2)$$

Aggregator (Retail+Wholesale) Perspective

$$\min \sum_{t \in T} [(LMP(t) + EC(t)) * nl(t) - REGP(t) * reg(t) - SPINP(t) * spin(t)]/4 + deg(t) + \sum_{k \in K} DC_k * pd_k \quad (3)$$

$$\min \sum_{t \in T} \left[\left(LMP(t) + EC(t) * u(t)\right) * nl(t) + EX(t) * nl(t) * \left(1 - u(t)\right) - REGP(t) * reg(t) - SPINP(t) * spin(t)\right]/4 + deg(t) + \sum_{k \in K} DC_k * pd_k \quad (4)$$

Equations 1 and 2 are the objective functions for the customer ownership perspective. Equations 3 and 4 are from the aggregator perspective. Equations 2 and 4 are used in scenarios with “value-of-solar” tariffs, where energy exported to the grid is compensated at a different rate

than the prevailing retail rate. Here we employ a binary variable *u(t)* to track when building net load is positive or negative (negative means energy is exported to the grid). Tariffs with net metering, where energy exported to the grid is compensated at the retail rate, will use equations 1 and 3 because we do not need to use a different cost structure with negative net load. We divide the energy cost and ancillary service revenue by 4 to convert kW to kWh for a 15-minute time-step to match the units of market clearing prices ($/kWh). This initial portion of the objective function represents real costs/revenues to the battery owner. Degradation is an amortization of the assumed replacement cost into the use phase of the battery; it prevents the use of the battery to perform services when market prices are low.

The last term in the customer and aggregator objective functions sums demand charges over each demand period k; the form of this portion of the equation will change depending on the structure of demand charges in each utility tariff. Southern California Edison (SCE) has a flat-rate charge for all hours of a month, as well as time-of-day adders that depend on the month. In this case, there are 4 different demand periods to track in any given month. The implementation of tracking peak demand in each demand period in the GAMS software, while maintaining a linear programming problem, warrants some discussion. The use of a maximum function (MAX) common to many software packages is not a linear function, and therefore would necessitate the use of a non-linear solver in the optimization calculations. This would drastically slow the solution time. Fortunately, there is an equivalent method to a MAX function that maintains a linear programming problem. We create a number of extra variables equal to the number of demand periods we need to track (for SCE, this was 4). The variables will track the peak demand in each of these periods. We then add an equivalent number of constraints at each time step to our problem (again, 4 for SCE at each time step) that force the variable to assume the maximum

load experienced during that period. These take the form $nl(t) \leq pd_k \ \forall t \in k$ where *nl(t)* is the net load at time *t* where *t* falls in demand period *k* and pd_k is the variable that holds the max load for demand period *k*. A similar method is used in the imperfect information scenarios to provide "memory" of the previous demand peak across each rolling-horizon optimization in a given month.

$$nl(t) = BL(t) + c(t) - d(t) \quad (5)$$

$$nl(t) < M * u(t) \quad (6)$$

$$nl(t) \geq -M * \big(1 - u(t)\big) \quad (7)$$

Equation 5 calculates the net load of the building at time t (the load seen by the meter) from the underlying building load and the charging or discharging of the battery. Equations 6 and 7 force the binary variable *u(t)* to track whether net load is positive or negative. The scalar M is a large positive number. We want *u(t)* to equal 1 when net load is greater than or equal to 0, and *u(t)* to equal 0 when net load is negative. If net load is positive, then equation 6 forces *u(t)* to be 1. If net load is negative, then equation 7 forces *u(t)* to be 0.

$$deg(t) = \frac{\sqrt{\eta} * c(t) + \frac{d(t)}{\sqrt{\eta}} + reg(t) * ABSE}{4 * \overline{SoC}} * BRC * CapDeg \quad (8)$$

$$CapDeg = \left(\frac{SOC_{swing}}{12.838}\right)^{1.838} \quad \text{(Lead-Acid)} \quad (9)$$

$$CapDeg = \left(\frac{SOC_{swing}}{1307.4}\right)^{0.95} \quad \text{(Lithium-ion)} \quad (10)$$

Equation 8 calculates degradation cost at time t as the product of the replacement capital cost and the fraction of total capacity degraded by actions taken at time t. This acts as a "hurdle rate" for any potential service the battery is to provide. If the service is not sufficiently lucrative

to overcome the hurdle rate, the mathematical program will not instruct the battery to take action. Equation 9 is the capacity degradation for lead-acid batteries and equation 10 is for lithium-ion batteries, as outlined in Ciez and Whitacre [2]. These two equations rely on the average SOC swing, which is the average depth of discharge reached by the battery in all previous months over all discharging events. In equation 8, we divide by 4 to convert charge and discharge kW to kWh. Dividing regulation energy by 4 converts the hourly Absolute Energy (ABSE) metric into a 15 minute metric (see paragraph below for more on ABSE). The battery replacement cost assumption is adjusted in each model scenario to ensure that the battery lasts for the intended lifetime (e.g., 10 or 20 years).

ABSE, used in equation 8, is the total amount of energy processed by the battery during 1 hour of frequency regulation, both by charging and discharging, expressed as a fraction of the regulation capacity offer (kWh/kW). In other words, it's the integral of the absolute value of the regulation signal with respect to time. We derive a single value for ABSE (0.26 kWh/kW) from 1 year of PJM regulation D signal [3] (2 second sample rate). For each hour of the dataset, we calculate the integral as described above. A period of one hour was chosen to match the period over which PJM attempts to maintain energy neutrality in the regulation signal. The final parameter value is calculated as the mean of the distribution of hourly energy values.

Equation 8 does not have a term addressing the provision of spinning reserve. We assume that the battery clears its idle capacity in the wholesale market, and therefore receives payment for that capacity, but is never actually called to provide spinning reserve. We make this simplification because spinning reserve is called infrequently and for relatively short periods of time. Using PJM as an example, spinning reserve events were called 18 times in 2013, 37 times in 2014, and 21 times in 2015 where the average length of an event was 15 minutes [4].

Attempting to model spinning reserve in a probabilistic manner (reserve events typically occur as a result of the unforeseen loss of a power plant or transmission line) would increase computational complexity with little change in the overall results. As a test, we modelled spinning reserve events at the exact times they occurred during 2013 in PJM and found overall revenue decreased by 0.01% under the base case assumptions. The one constraint we do place on spinning reserve in our model is limiting the capacity offer by the capacity used for other services (equation 16).

The problem is initialized with a 50% SOC at t = 0.

Constraints

$$soc(t+1) = soc(t) + \frac{\sqrt{\eta} * c(t) - \frac{d(t)}{\sqrt{\eta}} - reg(t) * ABSE * (1-\eta)}{4} \quad (11)$$

Equation 11 is an intertemporal constraint to track changes in SOC. Charging and discharging power is modified by internal energy loss, which is characterized by the round-trip efficiency (η). The frequency regulation service does not directly affect SOC changes because we assume the regulation signal is designed to be energy neutral, as with PJM's dynamic signal for fast-responding resources [5]. However, frequency regulation causes rapid charging/discharging and therefore internal energy losses. ABSE is used to calculate the amount of energy processed while providing frequency regulation and the round-trip efficiency is used to convert this value into energy losses. Again, we assume that the battery is never called to provide spinning reserve, and thus does not suffer any energy losses for this service. We divide by 4 to convert charge and discharge kW to kWh. Dividing regulation energy by 4 converts the hourly ABSE metric into a 15 minute metric. We ignore standby losses as they are small (~1-2% per month) [6], which causes us to slightly overestimate revenues to the owner.

$$0 \leq c(t) \leq \bar{P} \quad (12)$$

$$0 \leq d(t) \leq \bar{P} \quad (13)$$

Equations 12 and 13 restrict the charging and discharging power to the rated power of the battery.

$$\underline{SoC} \leq soc(t) \leq \overline{SoC} \quad (14)$$

The state of charge (SOC) is restricted between a minimum and maximum threshold, as determined by the battery technology employed. For lead-acid and lithium-ion technology, we restrict SOC between to values between 20% and 95% of maximum charge (Equation 14). For flow batteries, the technology permits SOC to vary between 0% and 100% of maximum charge. The lower limit of 20% and upper limit of 95% for lead-acid and lithium-ion is imposed to prevent degradation at low and high voltages, respectively. Lithium-ion batteries in electric vehicles have similar constraints imposed by car manufacturers [7].

$$reg(t) \leq \bar{P} - c(t) - d(t) - spin(t) \quad (15)$$

Equation 15 limits the amount of regulation capacity the battery can offer to the rated power of the battery minus any net charging or discharging of the battery and the capacity held for spinning reserve. In the customer ownership case where participation in ancillary service markets is not allowed, this equation is still valid and simply limits the charging and discharging of the battery.

$$\overline{SoC} \geq soc(t) + RDNE * reg(t)/4 \quad (16)$$

$$\underline{SoC} \leq soc(t) - RUNE * reg(t)/4 \quad (17)$$

Equations 16 and 17 constrain the amount of regulation capacity the battery can offer based on the state of the charge of the battery. Equation 16 prevents the SOC from exceeding the upper

limit imposed in equation 14 while Equation 17 ensures SOC does not fall below the lower limit imposed in equation 14. The frequency regulation signal will cause the battery to temporarily charge and/or discharge. We do not want the battery to violate the state of charge constraints at any time during regulation participation so we must adjust the regulation capacity offer to account for the maximum amount of net energy charge/discharge typically experienced while providing frequency regulation. We derive the values for RDNE (0.1 kWh/kW) and RUNE (0.2 kWh/kW) from 1 year of PJM regulation D signal [3] and express the value as a fraction of the regulation capacity offer. These parameters are set at the 97.5% percentile of the distribution of net energy charge/discharge during each hour of regulation signal, as opposed to the 100% percentile, to not overly constrict frequency regulation participation due to a few hours of atypical regulation signal patterns. The resulting values for RDNE and RUNE are very similar to the values of corresponding parameters used in EPRI's battery storage modelling for California (0.13 and 0.11, respectively) [8]. We then divide by 4 to convert RDNE and RUNE from hourly metrics to 15-minute metrics.

Our model does not implement a constraint to restrict simultaneous charging and discharging, which is functionally impossible, but could be economic in certain circumstances. In practice, our results contain no instances of simultaneous charging and discharging, obviating the need for this constraint.

References

[1] K. Klima, J. Apt, M. Bandi, P. Happy, C. Loutan, R. Young, Geograhpic Smoothing of Solar Photovoltaic Electric Power Production, Pittsburgh, PA, 2017. http://ceic.tepper.cmu.edu/publications/working-papers.

[2] R.E. Ciez, J.F. Whitacre, Comparative techno-economic analysis of hybrid micro-grid systems utilizing different battery types, Energy Convers. Manag. 112 (2016) 435–444. doi:10.1016/j.enconman.2016.01.014.

[3] PJM RTO Regulation Signal Data, PJM Ancillary Serv. (2015). http://www.pjm.com/markets-and-operations/ancillary-services.aspx (accessed January 10, 2015).

[4] PJM Ancillary Services, (n.d.). http://www.pjm.com/markets-and-operations/ancillary-services.aspx (accessed January 1, 2016).

[5] Order on Compliance Filing, Washington, D.C., 2012. https://www.ferc.gov/whats-new/comm-meet/2012/051712/E-4.pdf.

[6] M. Broussely, S. Herreyre, P. Biensan, P. Kasztejna, K. Nechev, R.. Staniewicz, Aging mechanism in Li ion cells and calendar life predictions, J. Power Sources. 97–98 (2001) 13–21. doi:10.1016/S0378-7753(01)00722-4.

[7] M. Eberhard, A Bit About Batteries, Tesla Mot. Blog. (2006). https://www.teslamotors.com/blog/bit-about-batteries (accessed January 1, 2016).

[8] B. Kaun, S. Chen, Cost-Effectiveness of Energy Storage in California: Application of the EPRI Energy Storage Valuation Tool to Inform the California Public Utility Commission Proceeding R. 10-12-007, Palo Alto, CA, 2013. http://www.epri.com/abstracts/Pages/ProductAbstract.aspx?ProductId=000000003002001162.